JOURNAL OF THE AERONAUTICAL SCIENCES

UNI... OF MICHIGAN
OCT 21 1952
ENGINEERING LIBRARY

VOLUME 19 OCTOBER, 1952 NUMBER 10

CONTENTS

A Mixing Theory for the Interaction Between Dissipative Flows and Nearly Isentropic Streams.....LUIGI CROCCO AND LESTER LEES 649

A Method for Reducing the Analysis of Complex Redundant Structures to a Routine Procedure.....L. B. WEHLE, JR., AND WARNER LANSING 677

A Second-Order Solution for an Oscillating Two-Dimensional Supersonic Airfoil.....ALEXANDER WYLLY 685

Partially Plastic Rotating Discs.....MELVIN ZAID 697

On Heat Transfer over a Sweat-Cooled Surface in Laminar Compressible Flow with a Pressure Gradient.....MORRIS MORDUCHOW 705

Readers' Forum: "On the Lift and Circulation of Airfoils in Some Unsteady-Flow Problems," by Nelson H. Kemp; "Note on Creep Buckling of Columns," by George Gerard; "Transonic Flow Past a Wedge with Detached Shock Wave," by A. H. Armstrong, M. Holt, and C. K. Thornhill; "Remarks on 'An Analytical Approach to the Fuel Sloshing and Buffeting Problems of Aircraft,'" by M. Z. Krzywoblocki; "Supersonic Nozzles with Continuous Wall Curvature," by R. C. Frost and H. P. Liepman; "Direct Measurement of Supersonic Skin Friction," by Donald Coles; "On Theodorsen Function in Incompressible Flow and C-Function in Supersonic Flow," by Chieh-Chien Chang; "Radii of Gyration of Aircraft," by J. P. Chawla; "On Folds Occurring in the Mapping from the Physical Plane to the Hodograph Plane," by Keith C. Harder and E. B. Klunker; "Determination of Modes and Frequencies Above the Fundamental by Matrix Iteration," by P. Cicala.....713–720

Published by the

INSTITUTE OF THE AERONAUTICAL SCIENCES, INC.

JOURNAL OF THE AERONAUTICAL SCIENCES

Editor: HUGH L. DRYDEN, *Director, N.A.C.A.*

Associate Editor: ROBERT R. DEXTER *Managing Editor:* BERNEICE H. JARCK

Editorial Committee

Aerodynamics

Francis Clauser
Howard Emmons
Alexander Flax
R. Paul Harrington
R. T. Jones
Carl Kaplan
H. W. Liepmann
C. C. Lin
H. F. Ludloff
Harold Luskin
John R. Markham
Clark B. Millikan
Shatswell Ober
W. Bailey Oswald
Allen E. Puckett
Elliott G. Reid
H. J. E. Reid
Russell Robinson
G. B. Schubauer
W. R. Sears
John Stack
Theodore von Kármán
Richard von Mises

Air Transport

Charles Froesch
J. A. Herlihy
R. D. Kelly
Otto E. Kirchner
Jerome Lederer
John C. Leslie
R. Dixon Speas

Flight Testing

W. K. Ebel
R. R. Gilruth
Melvin N. Gough
E. G. Stout

Structures and Materials

W. B. Bleakney
E. W. Conlon
L. H. Donnell
E. C. Hartmann
N. J. Hoff
Samuel Levy
E. E. Lundquist
Alfred S. Niles
W. Ramberg
E. Reissner
F. R. Shanley
H. W. Sibert
C. R. Strang
S. Timoshenko
H. S. Tsien
Chi-Teh Wang

Rotating Wing Aircraft

F. B. Gustafson
K. H. Hohenemser
Bartram Kelley
R. B. Maloy
Ralph McClarren
R. H. Miller
R. H. Prewitt
Igor I. Sikorsky

Vibration and Flutter

Lee Arnold
M. A. Biot
R. L. Bisplinghoff
William Bollay
Chieh-Chien Chang
I. E. Garrick
Martin Goland
J. P. Den Hartog

Aircraft Design

W. E. Beall
W. K. Ebel
Hall L. Hibbard
Richard Hutton
C. L. Johnson
A. A. Kartveli
C. J. McCarthy
Fred E. Weick
Robert J. Woods

Electronics in Aviation

K. C. Black
E. F. Herzog
David S. Little
D. K. Martin
George Rappaport
Paul Rosenberg
L. M. Sherer

Physiologic Problems

H. G. Armstrong
Louis H. Bauer
Robert J. Benford
Eugene Du Bois
W. Randolph Lovelace, II
Ross A. MacFarland

Fuels and Oils

D. P. Barnard
J. H. Doolittle
Graham Edgar
R. T. Goodwin
S. D. Heron
A. M. Rothrock

Flight Propulsion

George W. Brady
Frank W. Caldwell
L. S. Hobbs
E. E. Johnson
Joseph Keenan
R. P. Kroon
Hans Reissner
Abe Silverstein
C. Fayette Taylor
E. S. Taylor
P. Taylor
E. S. Thompson
H. S. Tsien

Instruments

Allan G. Binnie
J. R. Bradburn
Charles H. Colvin
C. S. Draper
S. G. Eskin
O. E. Esval
H. W. Holzapfel
W. L. Howland
George H. Purcell
C. F. Savage
O. Hugo Schuck
C. L. Seward, Jr.
L. D. Statham
R. C. Sylvander
D. K. Warner

Meteorology

C. F. Brooks
D. M. Little
E. J. Minser
F. W. Reichelderfer
H. C. Willett

SUBSCRIPTION RATES

JOURNAL OF THE AERONAUTICAL SCIENCES, Published Monthly.—United States and Possessions: 1 Year, $12.00; Single Copies, $1.50. Foreign Countries Including Canada (American Currency Rates): 1 Year, $13.00; Single Copies, $1.50.

AERONAUTICAL ENGINEERING REVIEW, Published Monthly.—United States and Possessions: 1 Year, $3.00; Single Copies, $0.50. Foreign Countries Including Canada (American Currency Rates): 1 Year, $3.50; Single Copies, $0.50.

Notices of change of address should be sent to the Institute at least 30 days prior to actual change of address.

Manuscripts for publication, proofs, and all correspondence should be addressed to the Editorial Office of the JOURNAL.

Correspondence regarding subscriptions may be addressed to Publication Office, 20th and Northampton Sts., Easton, Pa., or to the Editorial Office of the JOURNAL OF THE AERONAUTICAL SCIENCES, 2 East 64th Street, New York 21, New York.

Copyright, 1952, by the Institute of the Aeronautical Sciences, Inc.

Entered as Second Class Matter at the Post Office, Easton, Pa., May 1, 1937. Acceptance for mailing at a special rate of Postage provided for in the Act of August 24, 1912. Authorized April 29, 1937.

10

JOURNAL OF THE AERONAUTICAL SCIENCES

VOLUME 19 OCTOBER, 1952 NUMBER 10

A Mixing Theory for the Interaction Between Dissipative Flows and Nearly Isentropic Streams*

LUIGI CROCCO† AND LESTER LEES‡

Princeton University

SUMMARY

By means of a simplified theoretical "model," the present paper treats the general class of flow problems characterized by the interaction between a viscous or dissipative flow near the surface of a solid body, or in its wake, and an "outer" nearly isentropic stream. For the present, the external flow is taken to be a plane, steady, supersonic flow, which makes a small angle with a plane surface or plane of symmetry, although the methods used can be extended to curved surfaces, to axially symmetric supersonic flows, and also to subsonic flows. The internal dissipative flow is regarded as quasi-one-dimensional and parallel to the surface on the average, with a properly defined mean velocity and mean temperature. The nonuniformity of the actual velocity distribution is taken into account only approximately by means of a relation between mean temperature and mean velocity. Mixing, or the transport of momentum from outer stream to dissipative flow, is considered to be the fundamental physical process determining the pressure rise that can be supported by the flow. With the aid of this concept, a large number of flow problems is shown to be basically similar, such as boundary-layer-shock-wave interaction, wake flow behind blunt-based bodies (base pressure problem), flow separation in overexpanded supersonic nozzles, separation on wings and bodies, etc.

When the mixing rate is taken to be proportional to the mass flux density of the isentropic stream, the equations of motion are reduced to a single nonlinear ordinary differential equation that can be integrated numerically. An important property of this equation is the existence of a "critical point" for supersonic wake flows and, also, under certain conditions, for supersonic flows directed toward a solid surface. This critical point acts much like the "throat" of a nozzle in determining the base pressure, for example, or in some cases the surface pressure distribution in a boundary-layer-shock-wave interaction. One important reason for the marked difference between laminar and turbulent flows is the fact that the turbulent mixing rates are from five to ten times larger than the laminar mixing rates.

By introducing several reasonable physical assumptions, a "simplified" form of the mixing theory is developed particularly for separated and reattaching flows and wake flows. Separating flows, as well as reattaching flows, are found to be capable of supporting considerable pressure increases at high velocities. The maximum compression, as measured by the isentropic flow deflection, is roughly proportional to the square root of the mixing coefficient and also to $(M^2 - 1)^{1/4}$, where M is some average Mach Number. Thus, the pressure ratio increases rapidly with Mach Number, or the base pressure ratio, for example, decreases rapidly with increasing Mach Number. In separated flows, the pressure gradient along the surface is a maximum at separation and drops off steeply downstream; in reattaching flows, or wake flows, the pressure gradient is negligible some distance upstream of the "reattachment point" and increases rapidly toward a maximum as this point is approached. The inflected surface pressure distribution observed in laminar boundary-layer-shock-wave interactions with flow separation is now understandable, and the distribution itself can be calculated approximately.

When the present mixing theory is applied to the problem of determining the base pressure for a supersonic airfoil with a blunt trailing edge, it gives the correct fluid-mechanical explanation of the observed phenomena. Qualitative agreement is found between the theoretical calculations of the curve of base pressure versus Reynolds Number and the data of Chapman and Bogdonoff on bodies of revolution and Chapman's data on blunt trailing-edge airfoils. The theory is now being extended to axially symmetric supersonic flows.

Received February 25, 1952.

* A major portion of the support for the present study was furnished jointly by the Office of Naval Research (U.S.N.), Mechanics Branch, and by the U.S.A.F. Research & Development Command, as part of a broad program of theoretical and experimental research on viscous effects in supersonic flow being conducted by the Department of Aeronautical Engineering, Princeton University. The authors are grateful for the valuable assistance of C. E. Cohen, Daniel and Florence Guggenheim Fellow in Jet Propulsion. The numerical computations were carried out by Mrs. Alberta J. Mozley and Misses Carol Knoderer, Margaret Liptak, and Shirley Itter, Assistants in Research.

† Robert H. Goddard Professor, Jet Propulsion Center.

‡ Associate Professor of Aeronautical Engineering.

The results obtained in the base pressure problem for a supersonic airfoil with a blunt trailing edge open the way for application of the mixing theory to boundary-layer-shock-wave interactions, boundary-layer separation, and many other phenomena. However, the dependence of the mixing rate and the mean velocity-mean temperature relation for the dissipative flow region on the flow parameters must be carefully investigated experimentally and theoretically and the results incorporated into the analysis.

List of Symbols

The subscript e denotes quantities in the nearly isentropic flow; the subscript 1 denotes mean quantities for the dissipative flow; the subscript cr signifies values taken at the critical point of the basic differential equation. Except where otherwise noted, the subscript s denotes stagnation conditions. In addition, the subscript i applies to quantities of the equivalent incompressible flow in the Stewartson transformation; the subscript b denotes quantities in the airfoil boundary layer just upstream of the trailing edge; the subscript b' denotes quantities evaluated in the mixing zone just aft of the trailing edge, while the subscript j applies to the mixing zone in general.

x, y = coordinates parallel and normal to surface, or plane of symmetry
δ = thickness of dissipative flow region
p = pressure
ρ = density
T = temperature
h = enthalpy
a = speed of sound
μ = ordinary coefficient of viscosity
γ = ratio of specific heats, c_p/c_v
R = gas constant
u_e = magnitude of local velocity of nearly isentropic stream at $y = \delta$
M = Mach Number, u_e/a_e
θ = local angle between external stream and x-axis at $y = \delta$
ν = characteristic angle variable of plane, isentropic supersonic flow
$\bar{p}, \bar{M}, \bar{w}_e, \bar{\nu}$, etc. = "free-stream" pressure, Mach Number, reduced velocity, etc., far from body
u = component of velocity parallel to surface in internal flow
$\bar{m}$ = mass flux, $\int_0^\delta \rho u \, dy$
$\bar{I}$ = momentum flux, $\int_0^\delta \rho u^2 \, dy$
δ^* = displacement thickness, $\int_0^\infty \left(1 - \frac{\rho}{\rho_e}\frac{u}{u_e}\right) dy$
δ^{**} = momentum thickness, $\int_0^\infty \frac{\rho}{\rho_e}\frac{u}{u_e}\left(1 - \frac{u}{u_e}\right) dy$†
u_1 = mean velocity of internal flow, $\bar{I}/\bar{m}$
T_1 = mean temperature of internal flow, defined by $\bar{m} = (pu_1\delta/RT_1)$
w_1 = u_1/a_s
w_e = u_e/a_s
$\bar{m}$ = $\bar{m}/a_s$
φ_e = $\frac{T_e}{T_s}\frac{1}{\gamma w_e} = \frac{1 - [(\gamma - 1)/2]w_e^2}{\gamma w_e}$
φ_1 = $(T_1/T_s)(1/\gamma w_1)$
κ = $u_1/u_e = w_1/w_e$
f = parameter appearing in mean temperature-mean velocity relation $T_1/T_e = f - [(\gamma - 1)/2]w_1^2$
F = $(f/\kappa^2) - 1$
k = mixing coefficient, defined by relation $d\bar{m}/dx = k\rho_e u_e$
τ_W = viscous shear stress at solid surface
c_f = local skin-friction coefficient, $\tau_W/(1/2)\rho_e u_e^2$
C_f = total skin-friction coefficient, $\frac{1}{x}\int_0^x c_f \, dx$
σ = $c_f/2k\,(1 - \kappa)$
$\delta_s, \theta_s, X_s, \delta_{R_i}, \theta_{R_i}, X_R$ = thickness of dissipative flow, local angle of inclination of external stream, and coordinate of separation point (s) or reattachment point (R)
$\bar{X}$ = x/δ_R or x/δ_s
δ = $\frac{\delta - \kappa_j(\delta_j - \delta_j^*)}{\delta_R}$ or $\frac{\delta - \kappa_j(\delta_j - \delta_j^*)}{\delta_s}$
δ_R or δ_s = $1 - \kappa_j[1 - (\delta^*/\delta)]_j$
θ_w = flow deflection across incident oblique shock
c = airfoil chord
h = airfoil thickness at trailing edge
Re_c = Reynolds Number, $\bar{\rho}_e\bar{u}_e c/\bar{\mu}_e$
Re_{tr} = transition Reynolds Number, $\rho_e u_e x_{tr}/\mu_e$, where x_{tr} is defined in the text where needed
Re_{x_s} = $\rho_e u_e x_s/\mu_e$, Reynolds Number based on location of separation point

† The symbol δ^{**} is used in order to avoid confusion with the local angle, θ.

(1) Introduction

One of the least understood phenomena in fluid mechanics is the interaction between a viscous or dissipative flow near the surface of a solid body, or in its wake, and an "outer" nearly isentropic stream with varying static pressure. This phenomenon is observed in all types of boundary-layer-shock-wave interactions, in the wake behind blunt-based bodies and airfoils with blunt trailing edges at supersonic speeds (base pressure problem), in flow separation associated with recompression in an overexpanded supersonic nozzle, in flow separation from the surface of airfoils and bodies at high angles of incidence, etc. Apart from its theoretical interest, the problem is of considerable technical importance because of the widespread occurrence of such interactions in compressors, in rocket nozzles, in supersonic and subsonic diffusers, and on supersonic wings and bodies.

In all these interactions, the "external flow" cannot be regarded as a known datum for the calculation of the "internal" dissipative flow. In contrast to the usual Prandtl boundary-layer theory and its extension to wakes and jets, the development of the dissipative flow itself helps to determine the external flow, and it is now generally recognized that this interplay must be made the basis of any valid theoretical treatment. It is the aim of this paper to bring out the importance of the transport of momentum from outer stream to dissipative flow (turbulent "mixing" or laminar diffusion) in determining the flow pattern and pressure rise in these interactions and to formulate this concept in quantitative terms. By means of this concept a large number

of seemingly diverse flow problems are shown to be basically similar and therefore capable of being treated by one general theory.

Previous theoretical treatments of the interaction between an internal dissipative flow and an outer nearly isentropic stream do not seem to have recognized the importance of mixing. For example, in the case of the boundary-layer-shock-wave interaction problem, Tsien and Finston,[1] Lighthill,[2] and others regard the interaction between the subsonic flow field adjacent to the surface and the outer supersonic stream as paramount and treat the problem by means of a linearized nonviscous flow theory. Their calculations show only a negligible upstream spreading of the interaction near the surface, and this result corresponds to the facts only for a turbulent boundary layer and a weak shock. Even in this case the mechanism is not correct, because it does not include the mixing between external and internal flows and does not take into account the nonlinear character of the external flow and of the interaction. The importance of mixing in determining the pressure rise that can be supported by the turbulent boundary layer in an adverse pressure gradient has already been recognized by Schubauer and Klebanoff[3] for low-speed flows.

Treatments of the boundary-layer-shock-wave interaction problem which regard viscous effects as important, such as those of the junior author,[4] utilize the ordinary Prandtl boundary-layer theory to determine the rate of growth of the displacement thickness, $d\delta^*/dx$, in terms of the (unknown) pressure variation in the external stream. (Here, mixing is taken into account approximately.) The wall is then replaced by a stream line of slope $d\delta^*/dx$, and the pressure variation in the external stream is obtained in terms of the curvature $d^2\delta^*/dx^2$ by means of the Prandtl-Meyer relation. The solution obtained for the laminar boundary layer shows an extensive region of upstream influence and an exponential decay of the upstream pressure rise along the surface away from the shock, and predicts separation of the boundary layer ahead of the shock. While these predictions now seem to be qualitatively correct, the theory is unable to deal with the flow downstream of separation and tells us nothing about the subsequent reattachment of the flow downstream of the reflected expansion fan, where most of the pressure rise along the surface apparently occurs. Ritter[5] recently attempted to improve upon this treatment, but the basic difficulty has not been overcome because of the inability of the usual boundary-layer theory to deal with this type of dissipative flow. Since the characteristics of the compressible turbulent boundary layer in an adverse pressure gradient are largely unknown, this technique has not been applied to the turbulent layer at all.

In the case of the base pressure problem, it has long been recognized that mixing in the wake just aft of the body must determine the amount of recompression that can be supported by the flow and, hence, the base pressure, but this concept has never been precisely formulated. Chapman[6] recently reviewed the entire problem and found that existing data on base pressure could be correlated in terms of the ratio of the boundary-layer thickness at the base to the base diameter. No mechanism is advanced to explain the correlation. The ordinary theory of wakes and jets, which is usually restricted to uniform pressure, is of little assistance in this problem.

Another important phenomenon involving the interaction between a dissipative flow near a surface and an "external" flow with increasing pressure in the flow direction is observed in an overexpanded supersonic nozzle. When the ratio of chamber pressure to receiver pressure is reduced below a certain critical value, it is observed experimentally[7, 8] that the oblique shocks at the nozzle exit move upstream into the nozzle. The stream lines near the nozzle wall are deflected through these shocks, and the flow separates from the wall. For the conditions investigated, the flow deflection angle is remarkably constant ($\approx 14°$), and the pressure ratio across the shock is about 3.0, virtually independent of nozzle divergence half-angle, in the range from 5° to 30°. The flow deflection and pressure ratio lie well below the possible maxima corresponding to the local Mach Number ahead of the shock. Nonviscous flow theory establishes certain limits for the flow deflection angle and shock pressure ratio, but otherwise the problem is indeterminate without the introduction of viscosity. No theoretical explanation of this phenomenon has as yet been advanced.

It seems hopeless to attempt to solve the complete Navier-Stokes equations in detail, or these equations including the Reynolds stresses, for these interactions between an internal dissipative flow and an external nearly isentropic stream. What is required is a generalization of the concept of the von Kármán momentum integral for the dissipative flow region, where, however, this internal flow is treated as quasi-one-dimensional with properly defined mean velocity and mean temperature. It is essential to retain the nonlinear character of the external flow and of the interaction itself. The nonuniformity of the actual velocity distribution across the internal flow is taken into account only approximately by means of a relation between mean temperature and mean velocity. Mixing between the external and internal streams is admitted as a fundamental physical process, which will furnish the mechanism for the pressure rise. While some of the details of the flow are undoubtedly lost, it is believed that this simplified theoretical "model" preserves the main features of the interaction with the external stream. The loss of detail is outweighed for the present by the generality of the results and by the fact that flows are treated which cannot be analyzed at all by the classical boundary-layer theory.

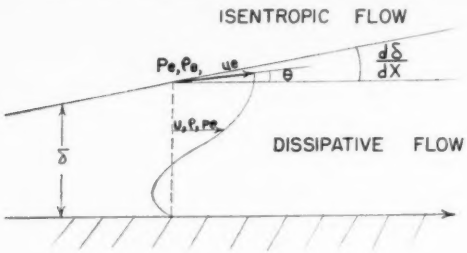

FIGURE 1. THE TWO DISTINCT FLOW REGIONS.

(2) General Theory

(2.1) *Basic Equations of Motion*

Suppose that the flow along a plane surface or a plane of symmetry (x-axis) is characterized by two more or less distinct regions (Fig. 1):† Region (1), an internal dissipative region of local thickness δ, in which the nonuniform velocity u is essentially parallel to the x-axis, on the average; and Region (2), an external isentropic flow, making the local angle θ with the x-axis at $y = \delta$. For the moment, θ is assumed to be sufficiently small so that $\tan\theta \approx \theta$ and $\cos\theta \approx 1$. Because of the mass transfer, or "mixing," between the external and internal streams, $d\delta/dx > \theta$.

In order to bring out the main aspects of the theory without becoming too involved in mathematical difficulties, the treatment is restricted for the present to plane, steady, isentropic, supersonic external flows, for which the Prandtl-Meyer relation

$$dp/p = (\gamma M^2/\sqrt{M^2 - 1})\, d\theta$$

holds. Actually, the analysis can be extended to axially symmetric supersonic flows by the method of characteristics, and shock-wave losses in the external flow can also be taken into account. In principle, subsonic external flows can also be treated by conformal mapping techniques.

The following assumptions are introduced:

(i) The static pressure p is constant across the internal flow and equal to the local pressure p_e in the external stream at $y = \delta$.

(ii) Heat transfer between the fluid and surface (if a solid surface is present) is zero, and the stagnation enthalpy h_s is constant across the flow and equal to h_{se} at $y = \delta$. The applicability of these assumptions will be discussed later in brief (see Section 6).

For the internal stream, the mass flux is given by

$$\bar{m} = \int_0^\delta \rho u\, dy$$

the momentum flux is

$$I = \int_0^\delta \rho u^2\, dy$$

and the flux of enthalpy is

$$H = \int_0^\delta h_s \rho u\, dy = \bar{m} h_{se}$$

By referring to Fig. 1, one sees that the angle between the stream line and the outer boundary of the dissipative flow at $y = \delta$ is $(d\delta/dx) - \theta$; therefore, the rate at which mass is transported to the internal flow is

$$d\bar{m}/dx = \rho_e u_e[(d\delta/dx) - \theta] \tag{2.1}$$

A momentum balance yields

$$\frac{dI}{dx} = u_e \frac{d\bar{m}}{dx} - \delta \frac{dp}{dx} - \tau_w \tag{2.2}$$

where τ_w is the frictional stress at the surface (if a surface is present). Since h_{se} is constant, the energy equation is automatically satisfied under the assumption (ii) above.

The momentum equation [Eq. (2.2)] represents the integral of the exact equations of motion across the flow, except that the gradients of the viscous or Reynolds stresses in the flow direction are considered to be negligible in comparison with the pressure gradient. Up to this point the approach does not differ essentially from the von Kármán momentum integral method of ordinary boundary-layer theory.

Let an average velocity of the internal flow be defined by the relation

$$u_1 = I/\bar{m} \tag{2.3}$$

i.e., the ratio of the momentum flux to the mass flux. Let us also define, without attributing any particular physical meaning to the definition, a mean density ρ_1, or a mean temperature T_1, through the mass flow relation

$$\bar{m} = \rho_1 u_1 \delta = (p u_1 \delta)/RT_1 \tag{2.4}$$

Introducing the displacement and momentum thicknesses of ordinary boundary-layer theory‡

$$\delta^* = \int_0^\delta \left(1 - \frac{\rho u}{\rho_e u_e}\right) dy = \delta - \int_0^\delta \frac{\rho u}{\rho_e u_e}\, dy = \delta - \frac{\bar{m}}{\rho_e u_e} \tag{2.5a}$$

$$\delta^{**} = \int_0^\delta \frac{\rho u}{\rho_e u_e}\left(1 - \frac{u}{u_e}\right) dy = \delta - \delta^* - \int \frac{\rho u^2}{\rho_e u_e^2}\, dy = \delta - \delta^* - \frac{I}{\rho_e u_e^2} \tag{2.5b}$$

From these equations, $\bar{m}$ and I can be derived and replaced in Eqs. (2.3) and (2.4) to obtain the following

† The treatment can be extended to the more general case of a curved surface.

‡ δ^{**} has been used here to indicate the momentum thickness in order to avoid confusion with the angle of flow, θ.

expressions for the mean quantities in terms of the thicknesses:

$$u_1/u_e = \kappa = (\delta - \delta^* - \delta^{**})/(\delta - \delta^*) \quad (2.6a)$$

$$\rho_1/\rho_e = T_e/T_1 = (\delta - \delta^*)^2/\delta(\delta - \delta^* - \delta^{**}) \quad (2.6b)$$

where $\kappa = I/\bar{m}u_e$ is an important parameter always less than 1. The definition of the thickness δ will be discussed in Section (2.2).

Nondimensional reduced velocities $w = u/a_s$ are now introduced by dividing through by the stagnation speed of sound a_s. The auxiliary quantities

$$\left.\begin{aligned} \varphi_1 &= T_1/T_s(1/\gamma w_1) \\ \varphi_e &= \frac{T_e}{T_s}\frac{1}{\gamma w_e} = \frac{1 - [(\gamma - 1)/2]w_e^2}{\gamma w_e} \end{aligned}\right\} \quad (2.6c)$$

are defined, in terms of which the Bernoulli equation can be written as

$$dp/p = -\frac{dw_e}{\varphi_e} \quad (2.6d)$$

Useful relations are, also,

$$\rho_e u_e a_s = \frac{p}{\varphi_e}; \qquad \rho_e u_e^2 = \frac{pw}{\varphi_e} \quad (2.6e)$$

The reduced mass flow is then given by

$$m = \bar{m}a_s = p\delta/\varphi_1 = I/w_1 \quad (2.7)$$

and Eqs. (2.1) and (2.2) become

$$\frac{dm}{dx} = \rho_e u_e a_s\left(\frac{d\delta}{dx} - \theta\right) = \frac{p}{\varphi_e}\left(\frac{d\delta}{dx} - \theta\right) \quad (2.8)$$

$$\frac{d}{dx}(mw_1) = w_e\frac{dm}{dx} - \delta\frac{dp}{dx} - \tau_W = w_e\frac{dm}{dx} - \delta\frac{dp}{dx} - \frac{pw_e c_f}{\varphi_e}\frac{2}{} \quad (2.9)$$

where the wall friction $\tau_W = (1/2)\rho_e u_e^2 c_f$ has been expressed through the friction coefficient c_f. Suppose now that c_f can be related directly to the unknowns m, δ, w_e, and w_1. Suppose also that T_1/T_s can be expressed explicitly in terms of the unknowns through a more general formula than the ordinary one-dimensional energy relation $T_1/T_s = 1 - [(\gamma - 1)/2]w_1^2$ (correct for a uniform velocity distribution *only*). Then, since $p = p(w_e)$ and $\theta = \theta(w_e)$ are known by the Prandtl-Meyer relation, Eqs. (2.7), (2.8), and (2.9) furnish three relations between the four variables m, δ, w_e, and w_1. An additional relation between these variables is introduced by means of an assumption regarding the mixing rate dm/dx, which will be discussed in Section (2.3). It is at this point, with the introduction of an approximate expression for the mean temperature and for the mixing rate, that the present approach departs from the usual boundary-layer theory.

(2.2) *Expression for the Mean Temperature: The F-κ Curve*

In any given flow the mean temperature can be computed from the defining relations, Eqs. (2.6) and (2.7). However, since the solution is not known, the exact evaluation cannot be obtained *a priori*. Therefore, if any progress is to be made toward a solution of the equations, an approximate relationship must be introduced, which depends on some average properties of the flow and involves the minimum possible number of parameters.

Laminar Flow.—In the laminar case, such a relationship can be established from the following considerations: Stewartson[9] has shown that, for Prandtl number unity, $\mu \sim T$, and an insulated wall, any compressible boundary-layer flow with prescribed variation of external velocity can be reduced to an equivalent incompressible boundary-layer flow with a transformed external velocity distribution. This means that, from a given incompressible flow, a family of compressible flows can be generated whose solutions are related in a simple way to the incompressible solution. The Stewartson transformation is represented completely by the relations

$$\left.\begin{aligned} &\rho_0 a_0\, d\eta = \rho a_e\, dy; \quad p_0 a_0\, d\xi = p_e a_e\, dx \\ &\frac{\rho}{\rho_0}u = \psi_y; \quad \frac{\rho}{\rho_0}v = -\psi_x; \quad u_i = \psi_\eta; \quad v_i = -\psi_\xi \end{aligned}\right\} \quad (2.10)$$

where the subscript 0 denotes some fixed reference condition and the subscript i denotes the quantities of the equivalent incompressible flow with the constant density ρ_0, with coordinates ξ, η, and with the same stream function ψ as in the compressible case. From the relations (2.10), the two following additional relations can be written:

$$\frac{u_i}{a_0} = \frac{u}{a_e}; \quad \rho_0 u_i\, d\eta = \rho u\, dy \quad (2.10a)$$

It follows that at corresponding stations the relative velocities in the compressible and incompressible flows coincide.

$$u_i/u_{ie} = u/u_e \quad (2.11)$$

By utilizing the first two relations in Eq. (2.10), the expressions corresponding to Eqs. (2.5a) and (2.5b) can be written as follows:

$$\delta_i - \delta_i^* = \int_0^{\delta_i}\frac{u_i}{u_{ie}}\,d\eta = \frac{\rho_e a_e}{\rho_0 a_0}\int_0^{\delta}\frac{\rho u}{\rho_e u_e}\,dy = \frac{\rho_e a_e}{\rho_0 a_0}(\delta - \delta^*) \quad (2.12)$$

$$\delta_i - \delta_i^* - \delta_i^{**} = \int_0^{\delta_i}\frac{u_i^2}{u_{ie}^2}\,d\eta = \frac{\rho_e a_e}{\rho_0 a_0}\int_0^{\delta}\frac{\rho u^2}{\rho_e u_e^2}\,dy = \frac{\rho_e a_e}{\rho_0 a_0}(\delta - \delta^* - \delta^{**}) \quad (2.13)$$

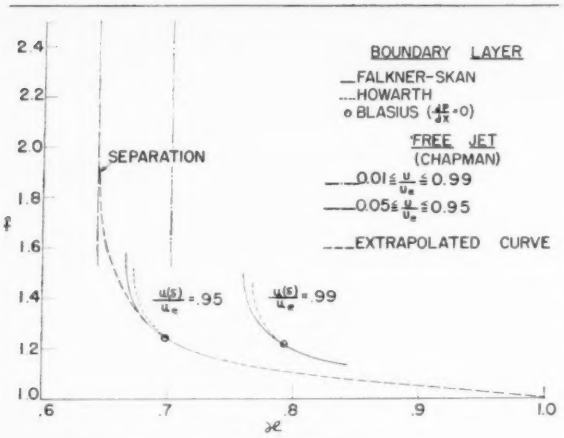

FIGURE 2a. LAMINAR FLOWS.

Also,

$$\delta = \int_0^{\delta} dy = \int_0^{\delta_i} \frac{\rho_0}{\rho}\frac{u_i}{u}\, d\eta = \frac{\rho_0 a_0}{\rho_e a_e}\int_0^{\delta_i} \frac{T}{T_e}\, d\eta = \frac{\rho_0 a_0}{\rho_e a_e}\frac{T_s}{T_e}\int_0^{\delta_i} \frac{T}{T_s}\, d\eta \quad (2.14)$$

However, from the constancy of the stagnation enthalpy,

$$T/T_s = 1 - [\gamma - (1/2)]w^2$$

Therefore, utilizing Eqs. (2.11) and (2.13), one finds

$$\int_0^{\delta_i} \frac{T}{T_s}\, d\eta = \int_0^{\delta_i} \left(1 - \frac{\gamma - 1}{2}\, w_e^2 \frac{u_i^2}{u_{ie}^2}\right) d\eta = \delta_i - \frac{\gamma - 1}{2} w_e^2(\delta_i - \delta^* - \delta^{**}) \quad (2.15)$$

Finally, by employing Eqs. (2.12) and (2.13), Eq. (2.6a) can be written as follows:

$$\kappa = \frac{u_1}{u_e} = \frac{\delta_i - \delta_i^* - \delta_i^{**}}{\delta_i - \delta_i^*} \quad (2.16)$$

By means of Eqs. (2.14) and (2.15), Eq. (2.6b) is transformed into

$$\frac{T_1}{T_s} = \frac{\delta_i - \delta_i^* - \delta_i^{**}}{(\delta_i - \delta_i^*)^2}\left[\delta_i - \frac{\gamma - 1}{2} w_e^2 (\delta_i - \delta_i^* - \delta_i^{**})\right]$$

or, utilizing Eq. (2.16), into

$$\frac{T_1}{T_s} = f - \frac{\gamma - 1}{2}\kappa^2 w_e^2 = f - \frac{\gamma - 1}{2} w_1^2 \quad (2.17)$$

where

$$f = (\delta_i - \delta_i^* - \delta_i^{**})\delta_i/(\delta_i - \delta_i^*)^2 \quad (2.18)$$

This mean temperature-mean velocity relationship differs from that for a one-dimensional isoenergetic flow only in that the quantity f appears rather than unity. It is to be observed that, for every incompressible boundary-layer flow, f [Eq. (2.18)] and κ [Eq. (2.16)] can be related to each other, so that the given incompressible flow and the corresponding complete family of compressible boundary layer flows obtained through the Stewartson transformation are characterized by a certain $f(\kappa)$ relation. All the effects of Mach Number for the compressible family are contained in the second term of the right-hand side of Eq. (2.17). Of course, in general, this $f(\kappa)$ relation is different for every flow. However, at this point it should be observed that certain classes of low-speed laminar boundary-layer flows, such as those investigated by Falkner and Skan[10, 11] ($u_{ie} = C\xi^s$), are described completely in terms of a single parameter. Each flow corresponds to a point in the f-κ plane, and the whole class of flows is represented by a *single* f-κ curve. By means of the Stewartson transformation this one-parameter description is extended to the corresponding compressible flows as well.

The $f(\kappa)$ relation can be evaluated for known incompressible solutions once the thickness δ_i of the dissipative region is suitably defined. Now the thickness of a laminar boundary layer is not a sharply defined quantity, because of the asymptotic transition from dissipative to nondissipative conditions. Too large a value of δ_i would result in the inclusion of too much of the nearly isentropic flow in the dissipative region, while for too small δ_i appreciable viscous effects could be lost. Clearly, the choice of δ_i is influenced by the relative importance of the transversal pressure variations in the flow [see Section (6)]. For comparison two different values of δ_i are employed in what follows, corresponding to $u(\delta)/u_e = 0.99$ and 0.95. Once δ_i is defined, κ and f can be obtained from Eqs. (2.16) and (2.18) by utilizing the ordinary values of δ_i^* and δ_i^{**} computed for $y \to \infty$, which corresponds to concentrating all of the actual mass and momentum defect of the boundary layer in the conventionally defined dissipative region. Observe that the definition of δ follows immediately from that of δ_i because of Eq. (2.11).

In Fig. 2a the f-κ curves are shown for two laminar incompressible boundary-layer solutions: the Howarth[12] solution for a linearly decelerated velocity distribution, and the Falkner-Skan[10, 11] family ($u_{ie} = C\xi^s$) of solutions. The first curve corresponds to the development of a specific boundary-layer flow, with κ going from an initial maximum value to a final minimum value where separation occurs; this curve passes through the f-κ point corresponding to the Blasius solution on a flat plate, which is characterized by constant values of f and κ. On the other hand, each point of the second curve corresponds to a different boundary-layer flow, evolving in such a way that f and κ remain constant and the "position" of the flow with respect to separation remains fixed. Here, again, the Blasius solution is included; all the points on the right of the Blasius point correspond to acceleration; those on the left, to deceleration. The minimum κ corresponds to a flow that is continuously on the verge of separation.

All of the curves show a common qualitative behavior: going toward separation κ decreases and f increases steadily, the slope becoming steeper and steeper until, at separation, the slope is practically vertical—i.e., κ varies but little as f increases. This fact has a clear physical interpretation. The increase in thickness near separation is caused mainly by an increase in the extent of the low-velocity portion of the boundary layer, the high-velocity region being pushed away from the wall, while the velocity distribution in the high-velocity region remains approximately similar to itself. In the extreme case, when the velocities near the wall are very low, the effect of this region on I and $\bar{m}$ is negligible, and κ is nearly constant at the value computed from the high-velocity region alone. On the other hand, f increases steadily because of the increase in total thickness of the dissipative flow. This fact can also be expressed in the following way: With approaching separation, the effect of the wall on the high-velocity portion becomes less and less marked, and the conditions in this portion, which determines the value of κ, become more and more similar to those of a "free" half-jet with a constant κ value. This physical picture is essential, since it gives a clue to the qualitative prediction of what happens after separation, where no theoretical solutions are known. It is to be expected that in the separated region the jetlike behavior is still more pronounced, and therefore κ undergoes only small variations, while all the variations in the flow will be reflected in f. The f-κ curve will have therefore a nearly vertical extension beyond the separation point.

An interesting case is one of a flow that, after having undergone separation in the way just described, is brought to reattach itself to the wall and to build up a regular boundary layer again. A compressible flow of this type is observed, for example, in the laminar boundary-layer-shock-wave interaction. Again, despite the absolute lack of theoretical information on flows of this kind, the qualitative behavior of a "reattaching" flow in the f-κ plane can be predicted to follow a path analogous to the one observed for separating and separated flows, but in the opposite direction. The f-κ curve, after having described some loop with small κ variation and large f-variation, reaches a reattachment point, generally distinct from the separation point, after which κ starts increasing again. If, for instance, the conditions are uniform after reattachment, a Blasius flow will finally be reached, and the f-κ curve again passes through the Blasius point.

Consider finally the case of a wake formed behind a body, where the velocity distribution across the dissipative flow region passes from a typical boundary-layer profile just upstream of the base of the body to a necessarily uniform distribution in the wake far behind the body (e.g., Fig. 7). Far beyond the body, $\delta_i^* = \delta_i^{**} = 0$ and $\kappa = f = 1$. In the f-κ plane the path of the flow will be represented by a smooth line connecting the initial f-κ point (say the Blasius point) with the point $\kappa = f = 1$. For a blunt-based body, as in the compressible base pressure problem, conditions in the wake just aft of the body are similar to those of a separated flow, the low-velocity region being in this case represented by the "dead-water" region. The path in the f-κ plane will be developed at first as in the case of reattachment (where, however, the wall influence is negligible) through a line of nearly constant κ. Then κ will start increasing, until far beyond the body κ and $f \to 1$. The f-κ curve for this flow does not necessarily pass through the Blasius point, but it is not likely to pass too far from it.

From this discussion it follows that every incompressible dissipative flow involving separating, separated, reattached regions and wakes can be described as a particular curve in the f-κ plane having qualitatively the shape just discussed. Supposing that the Stewartson transformation still holds in the separated regions, the family of corresponding compressible dissipative flows is described by the same curve. The exact determination of this curve requires the complete solution of the flow, which can be obtained only in the case of unseparated flows, since no known method is available for the other cases. The next step is therefore to replace the exact curve with a suitable approximation.

Based on the preceding qualitative considerations, it appears that the loop characterizing the separation-reattachment case can be replaced with a single representative mean curve, extended vertically (κ = constant) beyond the separation point (jetlike behavior in separated region). For instance, the single mean curve can be the theoretical f-κ curve for the Falkner-Skan solutions. Moreover, this curve can be extended up to $f = \kappa = 1$, and in this way it includes also the wakelike flows. However, the value of κ at separation given by the Falkner-Skan solutions does not coincide with the κ_j value for the free jet given by Chapman's solution,[13] as shown in Fig. 2a. One could neglect this small difference in κ and extend the Falkner-Skan curve vertically or, as we have done in Fig. 2a for $u(\delta)/u_e = 0.95$, utilize an extrapolation between the Falkner-Skan $f(\kappa)$ curve and the line $\kappa = \kappa_j$ given by Chapman's solution. [In order not to complicate the figure, we have not included the curve for $u(\delta)/u_e = 0.99$.]

With the assumption of this general relation between f and κ, the character of the flow, even if slightly distorted, is certainly preserved. Thus, $f(\kappa)$ in Eq. (2.17) becomes a general function† for all types of incompressible flows and therefore for all types of compressible flows covering the cases of separation, reattachment, and wake flow. In other words, the assumption is made that a single parameter, κ (or, better, f), is sufficient to characterize the state of the flow through all its possible development. Of course, all the assumptions and

† This procedure may recall to a certain extent the method of Thwaites,[14] who used a single mean function derived by comparison between known solutions in his successful treatment of incompressible laminar boundary layers with a pressure gradient

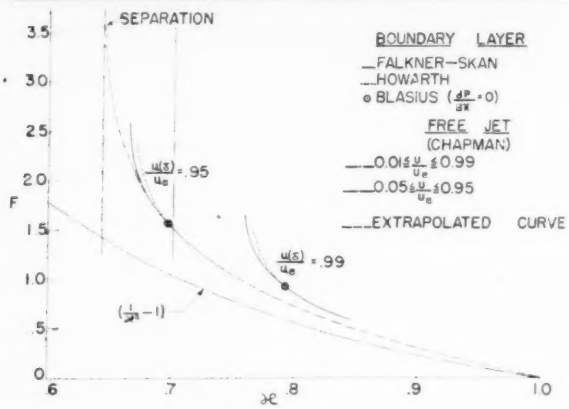

FIGURE 2b. LAMINAR FLOWS

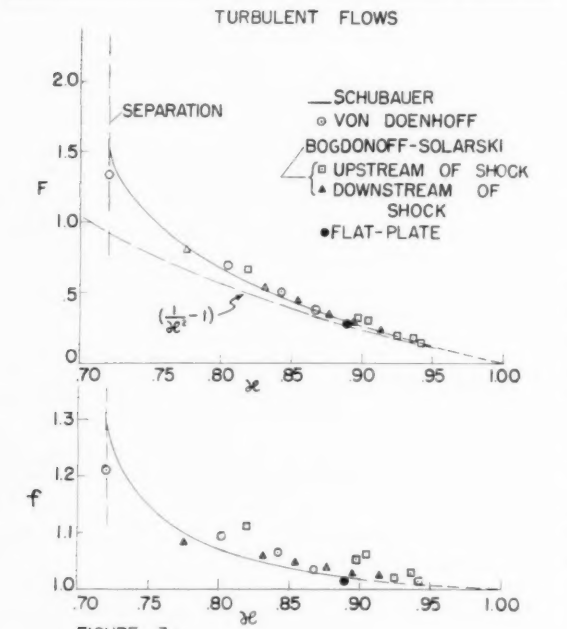

FIGURE 3a.

quantitative considerations regarding the f-κ curve should be thought of as preliminary and may be subject to some revisions after analysis of existing (and new) experimental data.

It proves to be more convenient later to work with the quantity F, which is related to f by

$$F = \frac{f}{\kappa^2} - 1 = \frac{\delta_i^* + \delta_i^{**}}{\delta_i - \delta_i^* - \delta_i^{**}} \qquad (2.19)$$

In Fig. 2b the corresponding F-κ curves for laminar flows are shown. (Note that, in wakelike flows, when f and $\kappa \to 1$, $F \to 0$.)

Turbulent Flows.—While the laminar case gives the possibility of determining the important relation (2.17) and the approximate behavior of the quantities involved from theoretical considerations, nothing of this kind can be done in the turbulent case because of the almost complete lack of theoretical knowledge on the effect of compressibility and because even the empirical information in the incompressible case is meager. The possibility of considering the velocity profiles for an incompressible boundary layer as a one-parameter family has been discussed many times, but it is not yet clear whether this assumption is even approximately correct in general. If the velocity profile is not changing too fast, then this assumption may be correct. In that case the quantity κ defined by Eq. (2.16) can again be chosen as the parameter representing the state of the flow, and the function f is computed from Eq. (2.19) by using known incompressible values of δ_i^* and δ_i^{**}. The curve of Fig. 3a has been computed from the low-speed data of Schubauer and Klebanoff.[3] [It should be observed that in the turbulent case it is possible to take δ such that $u(\delta)/u_e = 1.0$, because the thickness is a sharply defined quantity.] Points calculated from the von Doenhoff-Tetervin semiempirical relation[15] are also shown. The behavior of this f-κ curve, which corresponds to boundary layers going toward separation, is similar to that of the laminar case, and the same qualitative discussion can be applied. The f-κ path corresponding to any given low-speed case involving separation, reattachment, or wakes can be represented approximately by a single curve, consisting of the curve just described extended vertically beyond separation ($\kappa = \kappa_j$),† and extrapolated toward $f = \kappa = 1$ to cover the case of wakes. The curve passes through the point corresponding to zero pressure gradient (flat plate).

Finally, the additional bold assumption is made that the effect of compressibility can be taken into account exactly as in the laminar case by utilizing Eq. (2.17). As a preliminary test of this assumption, good qualitative correlation is observed between the Schubauer low-speed f-κ curve and the points calculated from turbulent boundary-layer profiles measured through a shock-wave interaction region at $M = 3.0$ by Bogdonoff and Solarski[16] in this laboratory (Fig. 3a). Some of these points correspond to the region preceding the incident shock wave, where κ is decreasing, and some to the region downstream of the incident shock, where the velocity profile is gradually returning to its undisturbed form.

(2.3) *Mixing Rate and Friction Coefficient*

Again, the laminar case can be treated by eliminating compressibility effects with the aid of the Stewartson transformation and examining known incompressible solutions. By integrating the second relation of Eq.

† For a semi-infinite "half-jet" at constant pressure, $\kappa_j = 0.720$ by direct calculation from the theoretical (Tollmien) velocity distribution. So little is known about turbulent flows after separation that the vertical extension of the f-κ curve at this value of κ should be regarded only as a first approximation

(2.10a) across the boundary layer, it appears that $\bar{m}_i = \bar{m}$. Therefore, using the second relation of Eq. (2.10), the compressible and the incompressible mixing rates are connected by the following equation:

$$d\bar{m}/dx = (a_e p_e / a_0 p_0)(d\bar{m}_i/d\xi) \tag{2.20}$$

Now, for an incompressible flow [Eq. (2.5a)],

$$\bar{m}_i = \rho_0 u_{i_e}(\delta_i - \delta_i^*) \tag{2.21}$$

and on a flat plate

$$\delta_i - \delta_i^* = \left(\frac{2C\mu_0\xi}{\rho_0 u_{i_e}}\right)^{1/2} \tag{2.21a}$$

where C is a constant whose value depends on the definition of δ_i. The expression for $d\bar{m}_i/d\xi$ can be found from Eqs. (2.21) and (2.21a) and substituted into Eq. (2.20) to obtain the value of $d\bar{m}/dx$. If a mixing coefficient k is introduced such that

$$d\bar{m}/dx = k\rho_e u_e \tag{2.22}$$

the result for the flat plate is $k = C(\mu_e/\bar{m})$. The analogous expression for the incompressible case is $k_i = C(\mu_0/\bar{m}_i)$, and the nondimensional expression $\bar{m}_i/\mu_0$ here replaces the square root of the Reynolds Number [see Eqs. (2.21) and (2.21a)]. The quantity k_i can also be evaluated for various other solutions of the laminar boundary layer; the form of the relation giving k_i remains the same, except that C is now a function of the parameter determining the conditions of the boundary layer. If the parameter κ is chosen, then $C = C(\kappa)$ is the same for the incompressible case and for the corresponding compressible family, and therefore the mixing rate is given by Eq. (2.22) with

$$k = (\mu_e/\bar{m})C(\kappa) \tag{2.23}$$

The values of $C(\kappa)$ depend, of course, on the definition of δ_i; for the theoretical solutions already discussed, $C(\kappa)$ is given in Fig. 4 for the two definitions already used in the f-κ computations.

A similar treatment can be given for the friction coefficient. From Eq. (2.10a), the following relation is derived between the viscous stresses:

$$\tau = \mu u_y = \frac{p_e}{p_0}\frac{T_e}{T_0}\mu_0 u_{i_\eta} = \frac{p_e}{p_0}\frac{T_e}{T_0}\tau_i$$

where the assumption $\mu \sim T$ has been used. On the other hand,

$$\rho_e u_e^2 = (p_e/p_0)\rho_0 u_{i_e}^2$$

therefore,

$$c_f = \frac{2\tau}{\rho_e u_e^2} = \frac{T_e}{T_0}\frac{2\tau_i}{\rho_0 u_{i_e}^2} = \frac{\mu_e}{\mu_0}c_{f_i}$$

Now, for the flat plate, remembering the relations between $\bar{m}_i/\mu_0$ and Reynolds Number, one finds that $c_{f_i} = D(\mu_0/\bar{m}_i)$, with constant D. For the other incompressible solutions, the same relation can be written, with $D = D(\kappa)$, the function being generally different for different solutions. Finally, the relation

$$c_f = (\mu_e/\bar{m})D(\kappa) \tag{2.24}$$

gives the friction coefficient for the corresponding compressible families. $D(\kappa)$ is plotted in Fig. 4 for the Howarth and Falkner-Skan solutions.

The next step now is to replace the particular functions $C(\kappa)$, $D(\kappa)$ representing particular solutions with two general functions, which have to be extended beyond separation and into the wake region and must also cover the reattachment case. *Provisionally*, $C(\kappa)$ and $D(\kappa)$ obtained from the Falkner-Skan solutions are

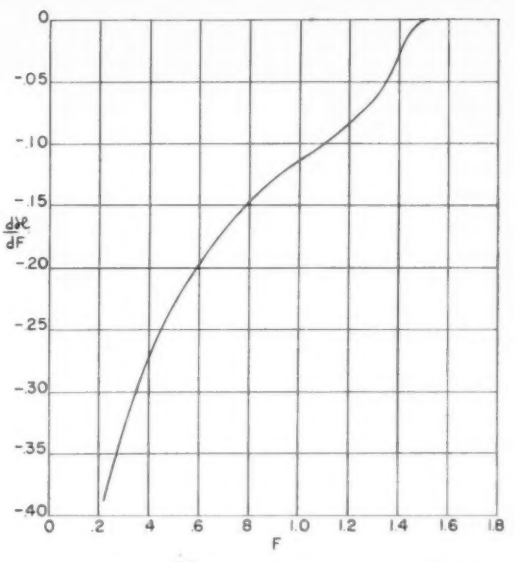

FIGURE 3b. $\frac{d\vartheta c}{dF}$ VS. F FOR TURBULENT FLOWS

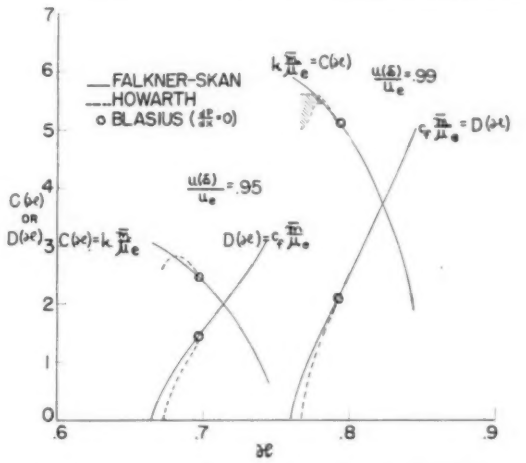

FIGURE 4. MIXING AND SKIN FRICTION COEFFICIENTS FOR LAMINAR FLOWS.

chosen as "universal" functions. However, further study is required to determine the mixing coefficient for the jetlike flow beyond separation and prior to reattachment and also for wake flows with a pressure gradient. Of course, $D(\kappa) = 0$ beyond separation, upstream of reattachment, and in wake flows.

Again the turbulent case can be treated only by analogy. For the flat plate in the incompressible case, the nondimensional expression $\bar{m}_i/\mu_0$ is again a function only of the Reynolds Number. If it is assumed that the $^1/_7$th power law holds for the velocity distribution, then two relations can be written:

$$k_i = C\left(\frac{\mu_0}{\bar{m}_i}\right)^{1/4}; \quad c_{f_i} = D\left(\frac{\mu_0}{\bar{m}_i}\right)^{1/4}$$

with constant values for C and D. Equations analogous to Eqs. (2.23) and (2.24) could be written, where C and D could be considered as functions of κ and $\mu_e/\bar{m}$ would appear to the $^1/_4$th power. However, it is doubtful whether these relations could give a correct answer, including the effects of approaching separation and of Mach Number. For the present, considering that the mass flow variation seems to have but little effect on the turbulent values and that insufficient experimental data are available on the spreading of turbulence with varying pressure, it seems justified to introduce the approximation that k is constant throughout the turbulent region. The skin-friction coefficient c_f is neglected in separated flows or is taken as a simple function of κ in separating or reattached flows. Of course, the same rough assumption could be made in the laminar case, especially when only narrow regions of flow are considered. In physical terms the approximation that k is constant amounts to the assumption that the rate of mass transport from isentropic to dissipative flows is proportional to the mass flux density of the isentropic stream [see Eq. (2.22)].

So far as the order of magnitude of k is concerned, for the boundary layer on a flat plate with zero pressure gradient, Eq. (2.9) yields the relation

$$k_0 = c_{f_0}/2(1 - \kappa_0)$$

where the subscript zero here denotes conditions at zero pressure gradient. At a local Reynolds Number of 10^6 and a Mach Number of 2.0, one finds $k_0 = 1.6 \times 10^{-3}$ for the laminar boundary layer with $u(\delta)/u_e = 0.99$, while $k_0 = 1.5 \times 10^{-2}$ for the turbulent layer. In turbulent separated flows and jets somewhat larger values of k are expected. From the Schubauer and Klebanoff data[3] one finds that $k \to 0.03$ near turbulent boundary-layer separation, and this value is utilized for turbulent flows in the present paper as a first approximation. The fact that the turbulent mixing coefficient k is of the order of ten times the laminar value is largely responsible for the marked difference between turbulent and laminar interaction phenomena.

The constant mixing coefficient introduced in this way should be regarded only as an average value, the introduction of which makes it possible to decide whether mixing furnishes the main mechanism for the pressure rise in interactions between dissipative and isentropic gas streams. Refinements can be introduced later when this mechanism is firmly established and when more experimental data are obtained on the mixing process with varying pressure.

(2.4) *Reduction of Equations of Motion to a Single Equation for Constant Mixing Coefficient*

By introducing the relation (2.17) between mean temperature and mean velocity and the additional Eq. (2.22) for the mixing rate, which can be also written as

$$dm/dx = k(p/\varphi_e) \tag{2.25}$$

the equations describing the flow are completely defined, provided the coefficients k and c_f are known. In what follows, the discussion is restricted to the simplest case of constant k mentioned in the preceding section, which permits a great simplification in the discussion of the important properties of the equations and, moreover, at the present time seems to be the most reasonable assumption in the case of turbulent flow. On the other hand, c_f can be replaced by the quantity

$$\sigma = c_f/2k(1 - \kappa)$$

with the advantage that, even when k and c_f are assumed to depend on m {as, for instance, in the laminar case [Eqs. (2.23) and (2.24)]} the effect of m is eliminated in σ, which is therefore a function of κ alone. For separated flows or wake flows, c_f is negligible or zero and therefore $\sigma = 0$. For the flat plate, $\sigma = 1$.

By utilizing Eq. (2.25), Eq. (2.1) is reduced to the suggestive form

$$d\delta/dx = \theta + k \tag{2.26}$$

The distance x along the surface is now eliminated from Eqs. (2.7), (2.8), and (2.9) with the help of Eq. (2.25), and the momentum and continuity relations are reduced to two simultaneous equations for $d\kappa/d \ln m$ and $dw_e/d \ln m$. These equations furnish a single equation for $d\kappa/dw_e$ or for dF/dw_e.

First, with the aid of Eqs. (2.6c), (2.17), and (2.19), the mass flow equation [Eq. (2.7)] is rewritten in the form

$$m\kappa\left[F + 1 - \frac{\gamma - 1}{2} w_e^2\right] = \gamma p w_e \delta \tag{2.27}$$

By differentiating the value of δ obtained from this equation with respect to x, dividing through by dm/dx, and

using Eq. (2.26), the following equation is obtained:

$$\frac{d}{d\ln m}\left\{\kappa\left[F+1-\frac{\gamma-1}{2}w_e^2\right]\right\}-\kappa\left[F+1-\frac{\gamma-1}{2}w_e^2\right]\frac{d}{d\ln m}(\ln pw_e)=\left(\frac{\theta}{k}+1\right)\times\left(1-\frac{\gamma-1}{2}w_e^2\right)-\kappa\left[F+1-\frac{\gamma-1}{2}w_e^2\right] \quad (2.28)$$

Similarly, the momentum equation [Eq. (2.9)] becomes

$$\frac{d}{d\ln m}(\kappa w_e)-\frac{\kappa\left[F+1-\frac{\gamma-1}{2}w_e^2\right]}{\gamma\varphi_e}\frac{d\ln w_e}{d\ln m}=w_e(1-\sigma)(1-\kappa) \quad (2.29)$$

where the Bernoulli equation [Eq. (2.6d)] has been employed to eliminate the pressure.

So long as the determinant of the simultaneous equations [Eqs. (2.28) and (2.29)] for $d\kappa/d\ln m$ and $dw_e/d\ln m$ does not vanish, these equations yield a single nonlinear first-order equation for

$$(d\kappa/dw_e)=(d\kappa/d\ln m)/(dw_e/d\ln m)$$

or for dF/dw_e if the relation

$$d\kappa/dw_e=(d\kappa/dF)(dF/dw_e)$$

is employed,

$$\frac{dF}{dw_e}=\frac{\left(\frac{\gamma+1}{2}w_e^2-1\right)\left(1-\frac{\gamma-1}{2}w_e^2\right)(1-\sigma)+F\left[\gamma w_e^2(1-\sigma)-\frac{F\kappa}{1-\kappa}+\frac{\theta}{k}\frac{1-\frac{\gamma-1}{2}w_e^2}{1-\kappa}\right]+\frac{\sigma F}{w_e}\left(1-\frac{\gamma-1}{2}w_e^2\right)}{\left(1-\frac{\gamma-1}{2}w_e^2\right)\left\{\left[\frac{1-\frac{\gamma-1}{2}w_e^2}{\kappa(1-\kappa)}\frac{\theta}{k}-\frac{F}{\kappa(1-\kappa)}\right]\frac{d\kappa}{dF}-1+\sigma\left[\frac{F+1-\frac{\gamma-1}{2}w_e^2}{\kappa}\frac{d\kappa}{dF}+1\right]\right\}} \quad (2.30)$$

Since k, $\sigma(\kappa)$, and $F=F(\kappa)$ are presumed known and $\theta(w_e)$ is given by the Prandtl-Meyer relation (or by any other procedure for nonisentropic flows), this equation is integrable by numerical methods.

When $\kappa=$ constant and $\sigma=0$, as in separated flows or wakes, Eq. (2.30) reduces to

$$w_e\frac{dF}{dw_e}=-\left(\frac{\gamma+1}{2}w_e^2-1\right)-\frac{F}{1-\frac{\gamma-1}{2}w_e^2}\left[\gamma w_e^2-\frac{\kappa}{1-\kappa}F+\frac{1-\frac{\gamma-1}{2}w_e^2}{1-\kappa}\frac{\theta}{k}\right] \quad (2.31)$$

which is a Riccati equation. A "simplified" theory has been developed in Section (4) for this important special case.

When the determinant of Eqs. (2.28) and (2.29) vanishes, the numerator and denominator of the right-hand side of Eq. (2.30) also vanish, and the equation for dF/dw_e has a "critical point" that turns out to be significant for the determination of the proper solution.

(2.5) *Critical Point of the Equation for dF/dw_e and Its Significance*

Suppose, for simplicity, that only wake flows or separated flows for which $\sigma=0$ are considered here. (Flows in which skin friction is not negligible can be included in the analysis and will form the subject of a later paper.) Suppose also that the external flow is isentropic. By setting both the numerator and denominator of Eq. (2.30) equal to zero and solving the resultant simultaneous equations for F_{cr} and $w_{e_{cr}}$ with the aid of the Prandtl-Meyer relation, the location of the critical point is determined as a function of $\bar{w}_e$ or $\bar{M}$, where $\bar{M}$ is the Mach Number of the free stream far from the body where $\theta=0$. When the denominator vanishes,

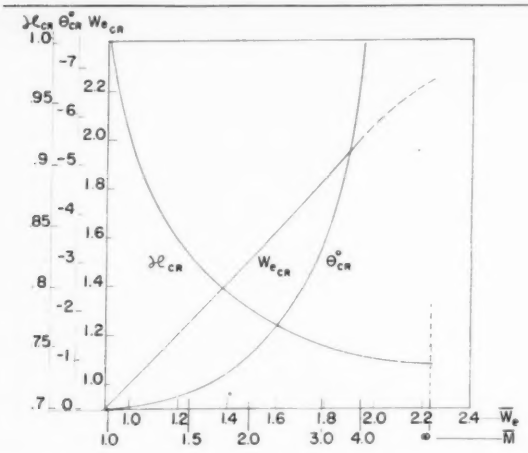

FIGURE 5. VALUES OF $\lambda\ell$, θ, w_e AT CRITICAL POINT FOR TURBULENT FLOW. k=0.03

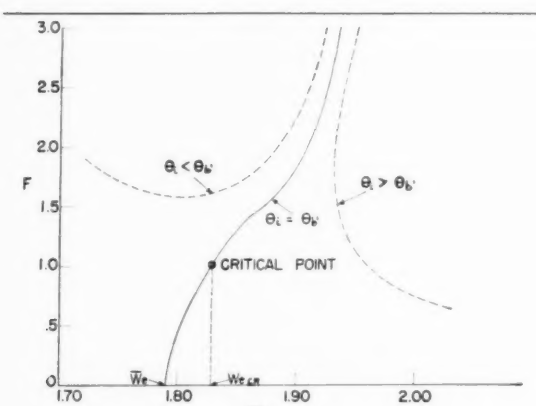

FIGURE 6. SIGNIFICANCE OF CRITICAL POINT, SHOWING INTEGRAL CURVE FOR $\bar{M}$=3.0 k=0.03, TURBULENT FLOW.

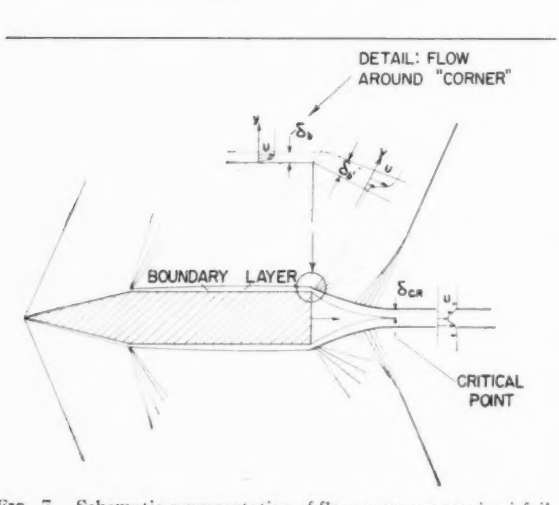

FIG. 7. Schematic representation of flow over supersonic airfoil with blunt trailing-edge.

$$\kappa_{cr}(1 - \kappa_{cr})\left(\frac{dF}{d\kappa}\right)_{cr} + F_{cr} = \left(1 - \frac{\gamma - 1}{2} w_e^2\right)\frac{\theta_{cr}}{k} \tag{2.32}$$

provided $d\kappa/dF \neq 0$. If $d\kappa/dF = 0$ or κ = constant, the denominator never vanishes and no critical point exists. When the numerator also vanishes,

$$F_{cr}\left[\gamma w_{e_{cr}}^2 + F_{cr} + \kappa_{cr}\left(\frac{dF}{d\kappa}\right)_{cr}\right] = -\left(\frac{\gamma + 1}{2} w_{e_{cr}}^2 - 1\right)\left(1 - \frac{\gamma - 1}{2} w_{e_{cr}}^2\right) \tag{2.33}$$

where Eq. (2.32) has already been used to simplify the result. Eqs. (2.32) and (2.33) define θ_{cr}/k and $w_{e_{cr}}$ as functions of κ_{cr}. Since $\theta_{cr}/k = 0(1)$, when k is very small, as in the laminar case, $\theta_{cr} \approx 0$ and $w_{e_{cr}} \approx \bar{w}_e$. In the turbulent case, however, k is not small. For example, choosing $k = 0.03$ on the basis of the Schubauer-Klebanoff data near turbulent separation[3] and utilizing the F-κ curve of Fig. 3a and the $d\kappa/dF$ curve of Fig. 3b, the values of θ_{cr}, κ_{cr}, and w_e shown in Fig. 5 are obtained as functions of $\bar{w}_e$. It appears that θ_{cr} is always negative.

Now, what is the significance of the critical point? Since $\theta_{cr} < 0$, it is necessary to consider only "reattaching flows," such as the flow aft of a supersonic airfoil with a blunt trailing edge or the reattachment of the separated flow downstream of the reflected expansion "fan" in the laminar boundary-layer-shock-wave interaction.

In the first case, for example, κ must increase, or F must decrease and w_e must decrease steadily during the recompression that occurs in the wake after the expansion around the sharp "corner" at the trailing edge. In other words, dF/dw_e is always positive (see Fig. 6). Now, in the separated or "free-jet" region just aft of the base, κ is constant and $d\kappa/dF = 0$, so that the denominator in the expression for dF/dw_e in Eq. (2.30) is initially negative. Therefore, the numerator must also be initially negative. If θ_i, or the flow inclination angle after the expansion around the corner, is *larger* than the proper value $\theta_{b'}$, then the denominator will vanish before the numerator during the recompression (since $d\kappa/dF < 0$), and the slope dF/dw_e will become infinite at some point and negative thereafter. In that case, the $F(w_e)$ integral curve can never represent the actual flow (Fig. 6). On the other hand, if θ_i is *smaller* than the proper value, the numerator vanishes before the denominator, and dF/dw_e passes through zero and becomes negative thereafter. Again, the $F(w_e)$ curve cannot be the correct representation of the flow. Only one value of θ_i, say $\theta_{b'}$, permits the integral curve to pass through the critical point where numerator and denominator vanish simultaneously. Thus, the critical point acts somewhat like the throat of a nozzle in determining $\theta_{b'}$ and the base pressure for the given boundary conditions at the base [Section (3)].

It is an interesting fact that the location of the critical point does not, in general, coincide with the smallest cross section of the mixing region—that is, with the point at which $d\delta/dx = \theta + k = 0$ or $\theta/k = -1$. By referring to Fig. 5, one sees that in the turbulent case $\theta_{cr}/k > -1$ for $1 < \bar{w}_e < 1.61$, so that the critical point lies downstream of the narrowest cross section, while $\theta_{cr}/k < -1$ for $\bar{w}_e > 1.61$, so that the critical point in this range lies upstream of the narrowest cross section. In any case, most of the recompression occurs before the critical point is reached.

Evidently, the mixing plays an essential role here because, for $k = 0$, $w_e(dF/dw_e)$ is negative and no critical point exists. An analysis of compression flows of this type which ignores the mixing process cannot possibly represent the actual conditions.

The discussion of the role of the critical point (when it exists) applies also to the reattaching flow in the boundary-layer-shock-wave interaction phenomenon, even when $\sigma \neq 0$, although the discussion is more complicated and will be given in a later paper. In the case of a turbulent boundary-layer-shock-wave interaction, the flow problem is undoubtedly modified not only by the action of skin friction but also by the penetration of the incident and reflected shock waves through the layer [see Section (6)].

(3) Application to the Base Pressure Problem in Plane Supersonic Flow

In order to illustrate the concepts and methods, the general theory is applied to the problem of the determination of the base pressure for a supersonic airfoil with a blunt trailing edge and a turbulent wake (Fig. 7).† Consider the simplest case in which the airfoil surface is parallel to the flight direction at the trailing edge, and the Mach Number just before the expansion around the "corner" is approximately equal to the free-stream Mach Number. If the recompression in the wake is regarded as isentropic, the Mach Number far downstream is again the free-stream value.‡ The values of κ and F at the critical point are then completely determined once the nondimensional mixing rate, k, is known. Integration of Eq. (2.30) may be started at the critical point and proceeds both downstream in the wake and upstream toward the airfoil trailing edge. Since both numerator and denominator in Eq. (2.30) vanish at the critical point, a parabola, defined by the equation

$$F - F_{cr} = \left(\frac{dF}{dw_e}\right)_{cr}(w_e - w_{e_{cr}}) + \frac{1}{2!}\left(\frac{d^2F}{dw_e^2}\right)_{cr} \times (w_e - w_{e_{cr}})^2$$

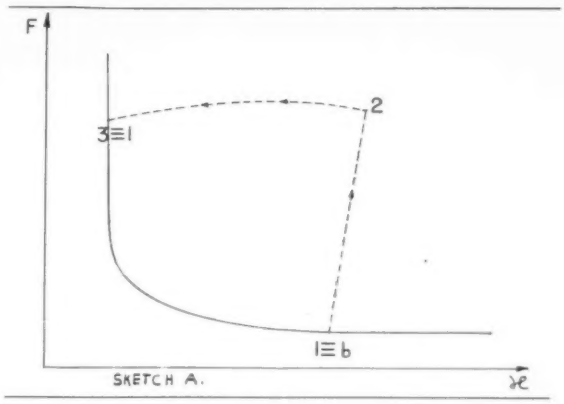

is utilized in the immediate vicinity of this point. [The values of $(dF/dw_e)_{cr}$ and $(d^2F/dw_e^2)_{cr}$ are calculated by substituting the parabolic representation of $F(w_e)$ into Eq. (2.30).] An analytical representation of the F - κ curve of the form

$$\kappa = 0.92954 - 0.10382F - 0.36842F^2 + 0.44575F^3 - 0.09582F^4 - 0.09948F^5 + 0.04505F^6$$

is employed near the critical point, and appropriate polynomial approximations involving fewer terms are utilized away from the critical point, where the integral curve is less sensitive to the function $\kappa = \kappa(F)$. Numerical integration is begun as soon as the slope dF/dw_e can be calculated numerically with sufficient accuracy from Eq. (2.30).††

Far downstream of the airfoil, as already discussed, $\kappa \to 1$ and $F \to 0$. The proper formulation of the boundary condition at the trailing edge, on the other hand, requires a knowledge of the process by which the boundary-layer flow at the body surface just upstream of the trailing edge is transformed to the wake flow downstream of the trailing edge. No similarity parameter exists for this viscous flow, and the problem is further complicated by the interaction between the viscous flow and the "external" isentropic supersonic expansion around the "corner." In the F - κ diagram, the actual transition 1–2–3, indicated by a dotted curve in Sketch A, consists first of the expansion 1–2, in which κ increases because of the uniformizing effect of the expansion and F increases because the dead-water region is now included in the dissipative flow. A subsequent smooth adjustment 2–3 occurs to a condition close to that of a free jet. To be consistent with previous approximations [Section (2.2)], it is assumed that point 3 lies on the vertical extension of the mean F-κ curve (Fig. 3a).

† Extension of the theory to axially symmetric flows and application to the base pressure problem for blunt-based bodies of revolution is now in progress at this Laboratory.

‡ If the oblique shocks in the wake are sufficiently strong, shock-wave losses can also be taken into account in a more exact calculation.

†† It would also be possible to begin the integration just after the expansion at the trailing edge, with various trial values of θ_t (or w_{e_t}), and thus determine the value of θ_t for which the integral curve passes through the critical point (see Fig. 6). In fact, this method is the only feasible one for the general case when k is a function of m and κ, or for axially symmetric supersonic flows where the relation between w_e and θ is not known *a priori*.

A rough calculation indicates that the "free-jet" flow is established in a distance less than one boundary-layer thickness, δ_b. *Provided* that the ratio of boundary-layer thickness to airfoil thickness at the trailing edge is small, it seems justified to treat the problem approximately by assuming that the transition to the "free-jet" flow occurs over a negligible portion of the wake just behind the body and that negligible mixing occurs between stations 2 and 3—i.e., $m_{b'} \approx m_b$. The actual transition 1–2–3 is replaced by a "jump" 1–3 to the free-jet condition. In integrating Eq. (2.30) from the critical point toward the airfoil, the F - κ curve is followed until κ equals κ_j, or the free-jet value, and the value of κ is taken to be constant thereafter and equal to κ_j. Of course, Eq. (2.30) is replaced by Eq. (2.31) in this region.

To this approximation the boundary condition at the trailing edge is $\delta = (h/2) + d$, or

$$\delta/\delta_b = (h/2\delta_b) + (d/\delta_b) \tag{3.1}$$

where h is the airfoil thickness at the trailing edge and the value of d lies somewhere between δ_b, the boundary-layer thickness at the trailing edge, and $\delta_{b'}$, the thickness of the "free-jet" mixing region (point 3) established just aft of the isentropic expansion around the trailing edge (Fig. 7). Since d/δ_b is generally small compared with $h/2\delta_b$, it does not need to be calculated with the same degree of accuracy as δ/δ_b. Therefore, the approximation $d = \delta_{b'}$, which seemed to be a reasonable one, was actually employed in the present calculations. The ratio $\delta_b/\delta_{b'}$ is obtained from the mass flow relation as follows:

$$\bar{m}_{b'} = (\rho_e u_e)_{b'}\delta_{b'}[1 - (\delta^*/\delta)]_{b'} = \bar{m}_b = (\rho_e u_e)_b\delta_b[1 - (\delta^*/\delta)]_b \tag{3.2a}$$

or

$$\frac{\delta_b}{\delta_{b'}} = \frac{[1 - (\delta^*/\delta)]_{b'}}{[1 - (\delta^*/\delta)]_b}\frac{G(M_{b'})}{G(M_b)} \tag{3.2b}$$

where

$$G(M) = M\left(1 + \frac{\gamma - 1}{2}M^2\right)^{-(1/2)[(\gamma+1)/(\gamma-1)]}$$

and $M_b = \bar{M}$, the Mach Number at large distances from the body. For a turbulent boundary layer with a $^1/_7$th power velocity distribution,† zero heat transfer at the surface, and constant stagnation enthalpy, the values of $[1 - (\delta^*/\delta)]_b$ are tabulated below:

M	$[1 - (\delta^*/\delta)]_b$
1.5	0.806
2.0	0.763
3.0	0.669
4.0	0.583
5.0	0.506

The quantity $[1 - (\delta^*/\delta)]_b$ is assumed to have the value corresponding to a turbulent boundary layer right up to the point where transition reaches the trailing edge.

The value of $[1 - (\delta^*/\delta)]_{b'}$, calculated for a low-speed isothermal constant-pressure turbulent half-jet according to Tollmien's theory, is 0.45, and this value is utilized in Eq. (3.2b).

With the aid of the assumption that $m_b = m_{b'}$, the ratio δ/δ_b appearing in the boundary condition [Eq. (3.1)] is obtained as a function of $w_{e_{b'}}$ from Eq. (2.27) as follows:

$$\frac{\delta}{\delta_b} = \frac{\left[\left(1 + F - \frac{\gamma - 1}{2}w_e^2\right)\frac{\kappa}{\rho w_e}\right]_{b'}}{\left[\left(1 + F - \frac{\gamma - 1}{2}w_e^2\right)\frac{\kappa}{\rho w_e}\right]_b} \tag{3.3}$$

Here, $\kappa_{b'} = 0.720$. To be consistent with the previous assumption regarding the effect of compressibility in turbulent flow [Eq. (2.17)], the values of κ_b and F_b at the trailing edge must be taken as identical to the corresponding values for zero pressure gradient at low speeds. Actually, it is believed that the variation of the zero pressure gradient values of F and κ with Mach Number is quite small.

By utilizing the results of the numerical integration of Eq. (2.30) for $F(w_e)$, together with Eqs. (3.2b) and (3.3), both δ/δ_b and $\delta_{b'}/\delta_b$ are determined as functions of $w_{e_{b'}}$. Therefore, to each value of $w_{e_{b'}}$ or $\theta_{b'}$, there corresponds a value of δ_b/h calculated from Eq. (3.1), so that the base pressure ratio

$$p_{b'}/\bar{p} = f(\theta_{b'}, \bar{w}_e)$$

is determined as a function of δ_b/h and the mixing coefficient, k. Chapman's correlation[17] of base pressure data in terms of δ_b/h for an airfoil with a blunt trailing edge and a turbulent wake is now completely understandable. From the nature of the integral curve $F(w_e)$, the relation between δ/δ_b and F [Eq. (3.3)], and the boundary condition at the airfoil trailing edge [Eq. (3.1)], one sees also that, for a given mixing rate in the wake, $w_{e_{b'}}$ is larger and the base pressure ratio $p_{b'}/\bar{p}$ is *lower* the *smaller* the value of δ_b/h.

For any given body shape

$$\frac{\delta_b}{h} = \frac{\delta_b}{c}\frac{c}{h} = \frac{c}{h}\,g\left(Re_c, \bar{M}, Pr, \frac{T_w}{T_1}\right)$$

where the functional relationship for δ_b/c depends on the Reynolds Number range for laminar-turbulent transition on the body. The base pressure is therefore determined as a function of Reynolds Number, Mach Number, Prandtl Number, and thermal conditions at the airfoil surface once the Reynolds Number range for boundary-layer transition on the body is known and once k in the turbulent wake is known. A detailed discussion of the various flow régimes in the base pressure problem will be given in connection with the application of the "simplified" mixing theory in Section (5).

† The meager data available indicate that the $^1/_7$th power velocity distribution is not too far from the truth.

The dependence of boundary-layer thickness δ_b/c on Reynolds Number and Mach Number can be prescribed as follows:

At sufficiently high Reynolds Numbers, boundary-layer transition occurs well forward of the trailing edge, and the turbulent boundary-layer thickness is approximated by the following formula for zero heat transfer to the airfoil surface:

$$\frac{\delta_b}{c} = \frac{0.037}{(Re_c)^{1/5}} \frac{Cf_M}{Cf_i} \frac{1}{(\delta^{**}/\delta)} \tag{3.4}$$

The ratio δ^{**}/δ is evaluated by assuming a $^1/_7$th power velocity distribution and isoenergetic flow,† and the "compressibility correction" Cf_M/Cf_i is taken from Fig. 19 of Van Driest's paper.[18] (The factor $0.037\ Re_c^{-1/5}$ is, of course, the low-speed value of δ^{**}/c.) Values of $Cf_M/Cf_{M=1}$ and δ^{**}/δ are shown in Table 1.

In this so-called "fully turbulent" régime it is clear that the base pressure ratio depends only upon the parameter $Re_c^{1/5}(h/c)$ at a given Mach Number, as found by Chapman.[6,17]

At sufficiently low Reynolds Numbers, on the other hand, the airfoil boundary layer is completely laminar and, for zero heat transfer at the airfoil surface, $Pr = 1$ and $\mu \sim T$,‡

$$\frac{\delta_b}{c} = [5.60 + 1.20(\gamma - 1)M_b^2]/\sqrt{Re_c} \tag{3.5}$$

Two different types of transition between laminar and turbulent flow in the airfoil boundary layer are assumed at intermediate Reynolds Numbers (Fig. 8).

(I) Transition for a smooth body, with the transition point located at the trailing edge when $Re_c = 4 \times 10^6$, and a gradual approach to fully turbulent flow, which is assumed to be attained at the trailing edge when $Re_c = 12 \times 10^6$. Such gradual transitions have been observed experimentally by Wilson,[19] for example.

(II) Transition for a body with some small roughness or external disturbances, with the transition point located at the airfoil trailing edge at $Re_c = 3 \times 10^6$, and fully turbulent conditions approached much more rapidly than in (I), at $Re_c = 6 \times 10^6$.

The transition Reynolds Numbers are assumed to be independent of Mach Number. Values of F_b and κ_b for the boundary layer at the airfoil trailing edge are taken to be those corresponding to a fully turbulent boundary layer until the transition point moves aft to the trailing edge.

TABLE 1

M	δ^{**}/δ	Cf_M/Cf_i
1.5	0.0842	0.870
2.0	0.0773	0.810
3.0	0.0635	0.680
4.0	0.0495	0.600
5.0	0.0395	0.510

Since the wake is turbulent, it is justified to regard k as constant in first approximation [Section (2.3)]. From the Schubauer-Klebanoff data,[3] $k \to 0.03$ near turbulent separation, and this value is utilized in the present computations. With this approximation, the integral curve $F(w_e)$ obtained by numerical integration of Eq. (2.30) is independent of Reynolds Number at a given Mach Number, and this curve is utilized for the calculation of base pressure ratio in the entire Reynolds Number range $Re_c \geqq 4 \times 10^6$ [curve (I)], or $Re_c \geqq 3 \times 10^6$ [curve (II)]. An example of such an integral curve $F(w_e)$ for $\bar{M} = 3.0$ is given in Fig. 6, and the variation of base pressure ratio with Reynolds Number calculated by the methods described above is plotted in Fig. 9 for transition curve (I) and $c/h = 3.0$. {The curve of $p_b'/\bar{p}$ vs. Re_c obtained by the "simplified" mixing theory to be described later [Section (4)] is also shown.}

A comparison between the theoretically predicted variation of base pressure with Reynolds Number in Fig. 9 and the recent experimental data of Bogdonoff[20] on a body of revolution shows excellent qualitative agreement, and it is now clear that the assumption that mixing is the dominant factor is correct. Evidently, the actual values of base pressure depend critically on

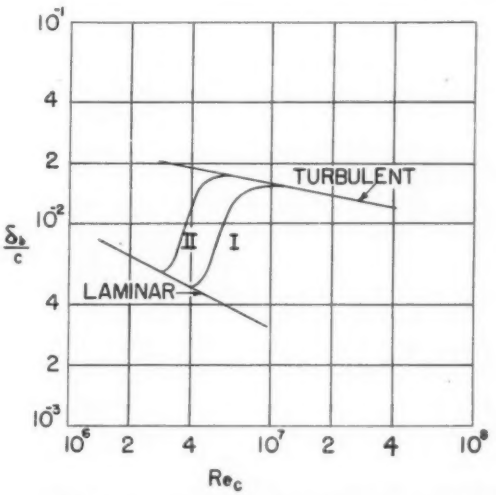

FIGURE 8. BOUNDARY LAYER THICKNESS VS. REYNOLDS NUMBER, SHOWING THE TWO ASSUMED TRANSITION CURVES. M=3.0

† Of course, it is possible to compute δ^{**}/δ also from Van Driest's formulas,[18] but, as no evidence exists that permits us to decide between the Van Driest velocity distribution and the $^1/_7$th power distribution, we have used the latter until reliable data are obtained.

‡ The value 5.60 appearing in Eq. (3.5) corresponds to $u(\delta)/u_e = 0.9975$. To be consistent this value would have to be adjusted to conform to the value of $u(\delta)/u_e$ chosen in calculating the laminar f-κ curve. For example, for $u(\delta)/u_e = 0.99$, the constant is 5.0. Calculations based on 5.60 had already been made before this point was noticed; however, the resulting differences are small, particularly in view of the other approximations introduced in the computations.

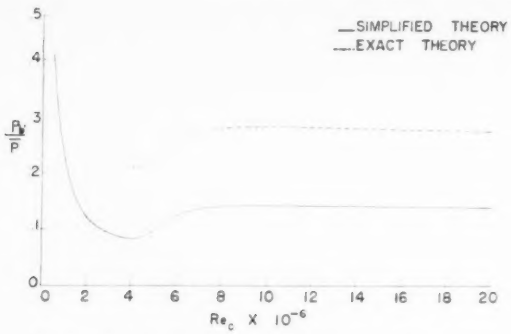

FIGURE 9. BASE PRESSURE RATIO VS. REYNOLDS NUMBER. M=3.0, k_{TURB}=0.03, $\frac{x_t}{l}$=3.0 TRANSITION CURVE I.

the mixing rate, and experimental determinations of the mixing coefficient are now urgently required.

The general theory and methods outlined so far are applicable to any flow régime occurring in the base pressure problem. However, when transition occurs in the wake [$Re_c < 4 \times 10^6$ for curve (I), Fig. 8] a numerical integration of Eq. (2.30) is required for each value of the Reynolds Number, because the laminar mixing rate and location of transition in the wake both depend on the airfoil Reynolds Number. Calculations for this flow régime, and for all flow régimes for Mach Numbers other than 3.0, were therefore carried out by means of a "simplified" form of the mixing theory developed for separated and reattaching flows in general.

(4) "Simplified" Mixing Theory for Separated and Reattaching Flows and Wakes

(4.1) Basic Assumptions and Equations

Certain outstanding characteristics of separated and reattaching flows and wakes behind blunt-based bodies suggest that the treatment of these flows can be somewhat simplified with the aid of a few physical approximations. The aim of such a "simplified" mixing theory is to furnish an approximate description of the main characteristics of separated and reattaching flows, in such a form that some general conclusions can be drawn and a clearer insight gained into the role of the mixing process in these flows. Of course, the results of the simplified approach must be compared with those obtained by the more exact analysis in a few critical cases to test the validity of the approximations employed.

Consider first the flow in the wake behind a supersonic airfoil with a blunt trailing edge (Fig. 7). Two flow regions may be distinguished: (1) a region in which the "external" gas streams from the upper and lower airfoil surfaces are approaching one another, and the "dead-water" area just aft of the body is being obliterated by mixing (most of the flow deflection and recompression occur in this region), (2) a region downstream of (1) in which the "dead-water" region has vanished and the external velocity u_e varies only slightly. Because of the "mixing," the velocity profile across the internal dissipative flow approaches a uniform distribution far behind the body—i.e., $u_1 \to u_e$, or $\kappa \to 1$, while $u_e \to \bar{u}_e$ and $\theta \to 0$.

In Region (1), κ is nearly constant while f is varying; in Region (2), both f and κ vary in general. Suppose now that the actual f-κ curve in Fig. 2a or 3a is replaced by a broken curve, consisting of the extension of the vertical line κ = constant down to $f = 1$ and the horizontal segment $f = 1$ up to $\kappa = 1$. The corresponding curve in the F-κ plane is composed of a vertical line and an arc of the curve $F = (1/\kappa^2) - 1$ as shown, for example, in Fig. 3a. Especially in the turbulent case, this approximation is not too far from the actual F-κ curve.

The two flow regions will now be distinguished more sharply by the conditions κ = constant = κ_j in Region (1), and $f = 1$, $\kappa_j \leqq \kappa \leqq 1$ in Region (2). The differential equation corresponding to the first region is the Riccati equation [Eq. (2.31)], the integration of which gives $F(w_e)$ in Region (1). By integrating Eq. (2.29) with $\kappa = \kappa_j$ and $\sigma = 0$, the mass flux m is obtained as a function of w_e. Finally, Eq. (2.27) gives δ as a function of w_e, and by utilizing Eq. (2.26) both δ and w_e are obtained as functions of x in Region (1).

In Region (2), the governing equation (to be given later) is that corresponding to Eq. (2.30) with $f = 1.0$ and $\sigma = 0$. By properly connecting the solutions for the two regions at the junction point $f = 1$, $\kappa = \kappa_j$, the complete (approximate) solution is obtained.

Actually, a different and somewhat more direct procedure was employed, as follows:

Region (1).—In this region, the mass flux is given approximately by

$$m = \rho\delta/\varphi = (\rho/\varphi_e)(\delta_j - \delta_j^*) \tag{4.1}$$

where δ_j is the thickness of the "jet" or mixing region and δ_j^* is the displacement thickness, corresponding to the velocity and temperature distribution across the jet. In this region κ = constant = κ_j, and by utilizing Eq. (4.1) the momentum equation [Eq. (2.9)] becomes

$$\frac{1}{\varphi_e}\frac{dw_e}{dm}[\delta - \kappa_j(\delta_j - \delta_j^*)] = -\frac{w_e}{p}(1 - \kappa_j) \tag{4.2}$$

where the Bernoulli equation [Eq. (2.6d)] is also employed. Since $d\delta/dx = \theta + k$ and $dm/dx = k(\rho/\varphi_e)$, it follows that

$$d\delta/dm = [(\varphi/k) + 1]/(\rho/\varphi_e) \tag{4.3}$$

When Eq. (4.3) is divided by Eq. (4.2) and the Prandtl-Meyer relation $dw_e/w_e = -d\theta/\sqrt{M^2 - 1}$ for the external flow is introduced, one obtains the relation

$$\frac{d\delta}{d\theta} = \frac{1}{1 - \kappa_j}\frac{(\theta/k) + 1}{\sqrt{M^2 - 1}}[\delta - \kappa_j(\delta_j - \delta_j^*)] \tag{4.4}$$

TABLE 2

The Function $J(M)$ in Radian Measure

M	$J(M)$	M	$J(M)$
1.0	0	2.70	0.16989
1.40	0.01587	2.80	0.18118
1.50	0.02461	2.90	0.19209
1.60	0.03486	3.00	0.20262
1.70	0.04604	3.10	0.21277
1.80	0.05795	3.20	0.22253
1.90	0.07035	3.30	0.23191
2.00	0.08305	3.40	0.24091
2.10	0.09588	3.50	0.24955
2.20	0.10872	3.60	0.25783
2.30	0.12144	3.70	0.26577
2.40	0.13397	3.80	0.27338
2.50	0.14626	3.90	0.28067
2.60	0.15824	4.00	0.28766

As a first approximation, it seems justified to regard the variation in the quantity $\kappa_j(\delta_j - \delta_j^*)$ appearing in Eq. (4.4) as of secondary importance compared to the variation in δ. Actually, $\kappa_j \approx 0.720$ and $[1 - (\delta^*/\delta)]_j \approx 0.45$ for a low-speed turbulent jet, so that the quantity $\kappa_j(\delta_j - \delta_j^*)$ is never greater than about $(1/3)\delta_j$, while $\delta \geqq \delta_j$. Suppose that $\kappa_j(\delta_j - \delta_j^*)$ is regarded as a constant, which corresponds to taking a constant mean value of δ_j—for instance, the value δ_R at the junction point with Region (2), where the effect of variations in δ_j is most important. Then we may define

$$\bar{\delta} = [\delta - \kappa_j(\delta_j - \delta_j^*)]/\delta_R$$

Eq. (4.4) is rewritten in the form

$$\frac{1}{\bar{\delta}}\frac{d\bar{\delta}}{d\theta} = \frac{(\theta/k) + 1}{\sqrt{M^2 - 1}}\frac{1}{1 - \kappa_j} \tag{4.5}$$

The solution of Eq. (4.5) is simply

$$\bar{\delta}/\bar{\delta}_R = e^{[1/(1-\kappa_j)]I(\theta,\,\theta_R)} \tag{4.6a}$$

where

$$I(\theta, \theta_R) = \int_{\theta_R}^{\theta} \frac{(\theta/k) + 1}{\sqrt{M^2 - 1}}\,d\theta \tag{4.6b}$$

and

$$\bar{\delta}_R = 1 - \kappa_j[1 - (\delta^*/\delta)]_j$$

By utilizing the characteristic relation $\theta = \bar{\nu} - \nu$, where

$$\nu(M) = \sqrt{\frac{\gamma+1}{\gamma-1}}\tan^{-1}\left[\sqrt{\frac{\gamma-1}{\gamma+1}}\sqrt{M^2-1}\right] - \tan^{-1}\sqrt{M^2-1}$$

and $\bar{\nu} = \nu(\bar{M})$, the function $I(\theta, \theta_R)$ is evaluated as follows:

$$I(\theta, \theta_R) = \frac{1}{k}[J(M) - J(M_R)] - \left(\frac{\bar{\nu}}{k} + 1\right)\ln\frac{w_c}{w_{c_R}} \tag{4.7}$$

where

$$J(M) = \int_1^M \frac{\nu\,dM}{M\{1 + [(\gamma-1)/2]M^2\}}$$

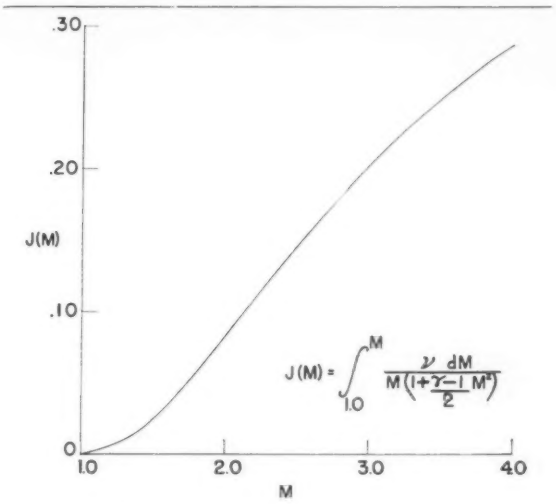

FIGURE 10. THE FUNCTION J(M)

The function $J(M)$ is tabulated in Table 2 and plotted against Mach Number in Fig. 10.

By utilizing Eqs. (4.5), (4.6a), (4.6b), and (2.24), the variation of θ, or $p/\bar{p}$ with axial distance x, is readily calculated. One finds that

$$d\theta/d\bar{x} = [(1 - \kappa_j)k\sqrt{M^2 - 1}]/\bar{\delta} \tag{4.8}$$

or

$$\frac{\bar{x} - \bar{x}_R}{\bar{\delta}_R} = \frac{1}{1 - \kappa_j}\int_{\theta_R}^{\theta}\frac{1}{k}\left(\frac{\bar{\delta}}{\bar{\delta}_R}\right)\frac{d\theta}{\sqrt{M^2 - 1}} \tag{4.9}$$

where $\bar{x} = x/\delta_R$.

When transition occurs in the wake, the mixing rate parameter k is approximated by a step function, as shown in Sketch B (θ_{tr} denotes the value of θ at which abrupt laminar-turbulent transition is assumed to occur). For the range $|\theta_R| \leqq |\theta| \leqq |\theta_{tr}|$, the function $I(\theta, \theta_R)$ in Eqs. (4.6b) and (4.7) is evaluated exactly as before, with $k = k_{\text{turb.}}$. In the laminar region, $|\theta_{tr}| \leqq |\theta| \leqq |\theta_{b'}|$, the integral in Eq. (4.6b) is split into two parts, and

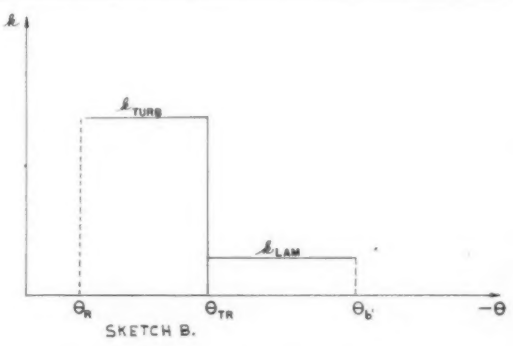

SKETCH B.

$$I(\theta, \theta_R) = \frac{1}{k_{\text{lam.}}}[J(M) - J(M_{tr})] + \frac{1}{k_{\text{turb.}}}[J(M_{tr}) - J(M_R)] - \bar{\nu}\left[\frac{1}{k_{\text{turb.}}}\ln\frac{w_{e_{tr}}}{w_{e_R}} + \frac{1}{k_{\text{lam.}}}\ln\frac{w_e}{w_{e_{tr}}}\right] - \ln\frac{w_e}{w_{e_R}} \quad (4.10)$$

The integral appearing in the relation between θ and x [Eq. (4.9)] is also evaluated in two parts. Details of the calculation are discussed later in connection with the application of the "simplified" theory to the base pressure problem [Section (5)].

Region (2).—In Section (2.5) it was pointed out that a critical point of Eq. (2.30) does not exist when κ = constant, as in Region (1). The condition determining the integral curve must therefore be associated with Region (2). In this region, $\kappa_j \leqq \kappa \leqq 1$ and $f = 1$, or

$$\varphi_1 = \left(1 - \frac{\gamma - 1}{2} w_1^2\right) \Big/ \gamma w_1$$

and the equation corresponding to Eq. (2.30) is

$$\frac{dw_e}{dw_1} = \frac{\varphi_e}{\varphi_1} \frac{\left[\varphi_e\sqrt{\gamma}\left(\frac{\theta}{k} + 1\right) + w_e\sqrt{\gamma} - \frac{2}{w_1\sqrt{\gamma}} + \left(\frac{1 - \frac{\gamma - 1}{2} w_1^2}{w_1^2\sqrt{\gamma}}\right) w_e\right]}{\left[\varphi_e\sqrt{\gamma}\left(\frac{\theta}{k} + 1\right) + w_e\sqrt{\gamma} - \frac{1 + \frac{\gamma + 1}{2} w_1^2}{w_1\sqrt{\gamma}}\right]} \quad (4.11)$$

The critical point of Eq. (4.11) occurs when $w_1 = \sqrt{2/(\gamma + 1)}$, or $M_1 = 1.0$, and, by analogy with the exact solution [Section (3)], the integral curve in Region 2 is made to pass through this point, although it lies outside the region of real flows. The two regions are then joined by requiring that κ_2 equal κ_j at the junction point. Also the dead-water region is assumed to vanish at this point, and therefore δ coincides with δ_j.

Eq. (4.11) is integrated by two different methods:

(1) When $\bar{M} < 2.0$ (approximately), dw_e/dw_1 is so small that the equation can be integrated by an iteration scheme in which $dw_e/dw_1 = 0$ in first approximation. By solving the equation obtained by setting the numerator of the term on the right-hand side of Eq. (4.11) equal to zero, one finds w_e and therefore dw_e/dw_1 as functions of w_1. The value of dw_e/dw_1 so derived is then introduced on the left-hand side of Eq. (4.11), and the resulting equation is again solved for $w_e = f(w_1)$, etc.

(2) When $\bar{M} > 2.0$ (approximately), the first scheme did not converge sufficiently fast. The integral curve is then obtained by passing a parabola with the correct slope and curvature through the critical point at $w_1 = \sqrt{2/(\gamma + 1)}$ and utilizing numerical integration thereafter. This method is similar to the scheme utilized for the "exact" equation [Eq. (2.30)].

The result of a typical integration for the flow in Regions (1) and (2) is shown in the w_e-w_1 plane in Fig. 11 for $\bar{M} = 3.0$ and a turbulent wake ($k = 0.03$). The dashed curve represents the more exact solution obtained by the methods described in Section (3). (Clearly, for the curve passing through the point $w_1 = \sqrt{2/(\gamma + 1)}$, only the segment on which $\kappa_j \leqq \kappa \leqq 1.0$ has any reality.)

Values obtained for θ_R at $\kappa_2 = \kappa_j = 0.720$ are tabulated as follows:

M	θ_R (Deg.)
1.5	−0.38
2.0	−0.54
3.0	−1.24
4.0	−3.38

The value of w_e at the junction point does not differ appreciably from $\bar{w}_e$, so that the character of the solution in Region (1) is not very sensitive to small errors in the value of w_e as determined by this approximate method.

(4.2) *Characteristics of Separated and Reattaching Flows and Recompression in Wakes ("Simplified" Theory)*

Reattaching Flows.—Once it is known that θ_R and the recompression in Region (2) are small, the main characteristics of the recompression in wakes, or of reattaching flows in general, can be predicted from the form of the momentum equation and the flow solution in Region (1) [Eqs. (2.9) or (4.2), and Eqs. (4.6) and (4.8)]. By referring to the momentum equation [Eq. (2.9)] in a jetlike flow ($\tau_w = 0$, $\kappa = \kappa_j$), one sees that the value of the pressure rise Δp times a mean δ is equal to the momentum transported to the dissipative flow, $\int u_e\, d\bar{m}$, which is of the order of magnitude of $\bar{u}_e\, \Delta\bar{m}$, *minus* the net change in momentum of the dissipative flow, which is of the order of magnitude $\kappa_j\bar{u}_e\, \Delta\bar{m} + \bar{m}\kappa_j\Delta u_e$. Now $\Delta u_e \approx \Delta p/\bar{\rho}_e\bar{u}_e$, and $\Delta\bar{m}$ is not much larger in order of magnitude than $\bar{m}$ itself, or

$$\Delta m \approx \bar{\rho}_e\bar{u}_e\delta_j[1 - (\delta^*/\delta)]_j$$

By making use of these approximate relations one finds that (roughly)

$$\Delta p / \bar{\rho}_e \bar{u}_e^2 \approx \delta_j / \delta$$

When $\delta \gg \delta_j$, as in the more familiar case of a "half-jet," then the pressure is practically constant at the ambient value. But when two gas streams converge or when a gas stream is directed toward a surface, then $\delta \to \delta_j$, and large increases in static pressure are made possible by the transport of mass (and momentum) to the internal dissipative flow. This mechanism is not confined to supersonic flows; it is undoubtedly the main factor in the rapid pressure rise observed on an airfoil in low-speed flow when the separated laminar flow reattaches itself as a turbulent region downstream of the "separation bubble" (see, for example, reference 21). Incidentally, for a given mixing rate one would expect a much larger increase in pressure ratio at high velocities, because

$$\frac{\Delta p}{p_1} = \left(\frac{\Delta p}{\rho_e u_e^2}\right) \frac{\rho_e u_e^2}{p_1} \approx M_e^2$$

This conjecture is borne out by the numerical calculations to be discussed later and by experimental evidence.

Qualitatively the form of the pressure distribution in reattaching flows or wake flows can be predicted from the relations (4.6)–(4.8). It is clear that $d\theta/dx$, and therefore $(1/p)(dp/dx)$, is small when $\delta \gg \delta_j$ and reaches its maximum value rapidly when $\delta \to \delta_R$ because of the exponential character of the δ-θ relation. The variation of $\bar{\delta}/\bar{\delta}_R$ with θ for Mach Numbers of 1.5, 2.0, and 3.0 is illustrated for a turbulent wake ($k = 0.03$) in Fig. 12a, while Fig. 12b shows the corresponding axial static pressure distribution for these cases. A typical case with transition in the wake is shown in Fig. 13a, and the corresponding pressure distribution is plotted in Fig. 13b. Here $\bar{M} = 3.0$, $k_{\text{turb.}} = 0.03$, and $Re_c = 2 \times 10^6$. For simplicity $k_{\text{lam.}}$ has been taken constant [see discussion in Section (2.3)] and equal to the flat plate value 0.00124 at $Re_c = 2 \times 10^6$. (These numerical examples are taken from the base pressure calculations to be discussed later.)

From Eqs. (4.6a) and (4.6b) and Figs. 12 and 13, it is clear that $\bar{\delta}/\bar{\delta}_R$ increases rapidly with $|\theta|$. As predicted from the qualitative discussion of reattaching flows, most of the compression occurs near reattachment, in the range $1 \leqq \bar{\delta}/\bar{\delta}_R \leq 5$, say. In fact, by Eqs. (4.6a) and (4.6b),

$$\bar{\delta}/\bar{\delta}_R \approx e^{\theta^*/\lambda} \tag{4.6c}$$

roughly, where

$$\lambda = 2k\sqrt{M^2 - 1}\,(1 - \kappa_j)$$

and M is some average Mach Number. In the base pressure problem, for example, when k is constant, the base pressure ratio drops as h/δ_b or $\bar{\delta}/\bar{\delta}_R$ increases but at a decreasing rate (high Reynolds Number régime).

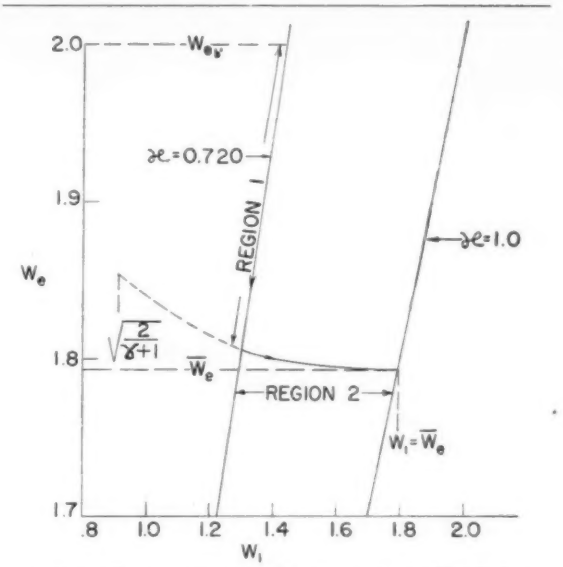

FIGURE 11. RECOMPRESSION IN TURBULENT WAKE. M=3.0, k=.03

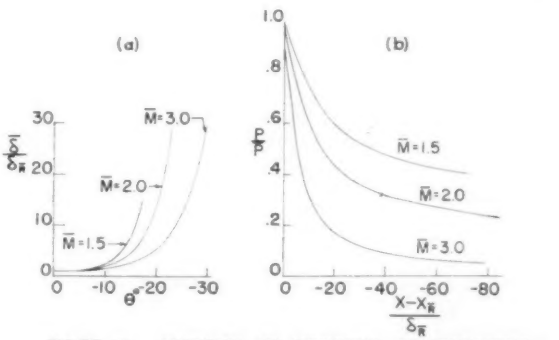

FIGURE 12. VARIATION OF THICKNESS OF DISSIPATIVE FLOW REGION AND THE STATIC PRESSURE ALONG THE AXIS IN TURBULENT WAKE. k=.03 SIMPLIFIED THEORY.

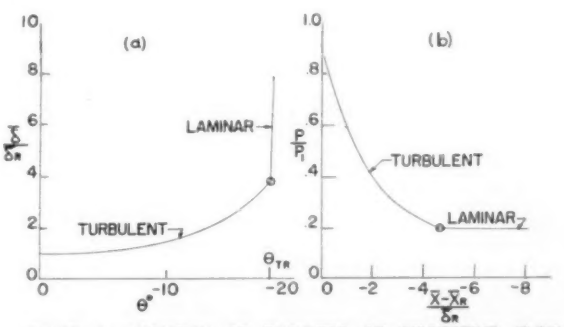

FIGURE 13. VARIATION OF THICKNESS OF DISSIPATIVE FLOW REGION AND STATIC PRESSURE ALONG AXIS. TRANSITION IN WAKE

M=3.0, k_{TURB}=.03, Re_c=2 X 10^6, k_{LAM}=.00124,

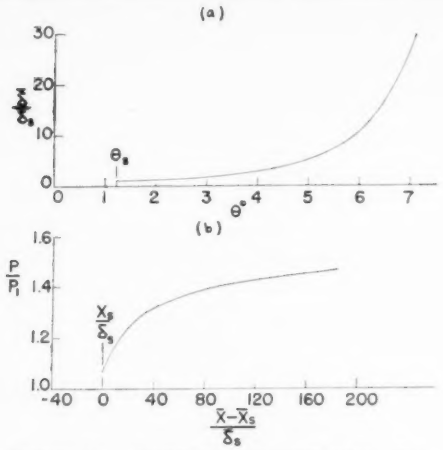

FIGURE 14. VARIATION OF THICKNESS OF SEPARATED LAMINAR FLOW REGION AND STATIC PRESSURE ALONG SURFACE. $M_1 = 2.0$, $Re_{x_s} = 110{,}000$, $k_{LAM} = .0055$, $\theta_s = 1.23°$

Several important conclusions can be drawn from the approximate relation above [Eq. (4.6c)].

(1) For a specified value of $\bar{\delta}/\bar{\delta}_R$ one finds that $\theta \sim \sqrt{k}$, or the compression, as measured by the isentropic flow deflection, increases with increase in mixing rate. Since the pressure ratio is a rather sensitive function of θ, the marked difference between laminar and turbulent reattaching flows is now placed on a quantitative basis. Figs. 13a and 13b bear out the conclusion that the laminar portion of a flow with transition generally contributes little to the recompression.

(2) Since $\theta \sim (M^2 - 1)^{1/4}$, the pressure ratio $\bar{p}/p$ in a reattaching flow increases rapidly with Mach Number [Fig. 12b; see also Section (5.2)].

(3) θ is sensitive to the value of κ_j assumed in the "jet." The factor $(1 - \kappa_j)$ is a measure of the rate at which the internal dissipative flow "destroys" momentum received from the external flow. Experimental data are required to determine this parameter, which in this paper is taken to be 0.720—i.e., the value for a "free" jet at constant pressure.

Separated Flows.—The approximations introduced in Region (1) of the wake behind a supersonic airfoil with a blunt trailing edge [Section (4.1)] are also applicable to separated flows with a supersonic external stream, where the influence of the viscous stress at the surface is negligibly small. An important example of such a flow occurs in the laminar boundary-layer-shock-wave interaction, where the laminar layer separates upstream of the incident shock.

In the separated flow region,

$$\bar{\delta}/\bar{\delta}_s = e^{[1/(1-\kappa_j)]I(\theta,\theta_s)}$$

where

$$\bar{\delta} = [\delta - \kappa_j(\delta_j - \delta_j^*)]/\delta_s \qquad (4.12)$$

and where δ_s is the thickness of the dissipative flow and θ_s is the flow inclination "at separation." [Of course, the value of θ_s cannot be predicted by the simplified mixing theory; it must be obtained by an extension of the usual boundary-layer theory[4] or by integration of Eqs. (2.28) and (2.29) with $\sigma \neq 0$, k variable, and suitable boundary conditions. This problem will be discussed in a later paper.] By referring to the expression for $d\theta/dx$ [Eq. (4.8)], one sees that $(1/p)(dp/dx)$ has its maximum value in this case at the separation point and drops off rapidly downstream because of the exponential character of the δ-θ relation [Equation (4.12)]. An example of such a laminar separated flow is illustrated in Figs. 14a and 14b.

Here, $Re_{x_s} = 1.10 \times 10^5$, $\theta_s = 1.23°$,† $\bar{M} = 2.0$, $k_{\text{lam.}} = 0.0055$.† A pressure distribution of this form is typical of laminar separated or "detached" flows and also of turbulent separated flows, although, in the latter case, because of the much larger mixing rate, the pressure increase is correspondingly larger. A pressure distribution similar to that shown in Fig. 14b is found downstream of flow detachment in an overexpanded supersonic rocket nozzle.[7, 8]

In the case of the laminar boundary-layer-shock-wave interaction, the region upstream of the incident shock is a separated flow, while the flow downstream of the reflected expansion fan is a reattaching flow. Thus the S-shaped pressure distribution on the surface observed experimentally is understandable. Provided that friction is neglected, which is strictly correct only if the plate is cut off at the beginning of Region 2, the reattaching flow can be treated exactly as in the base pressure problem. Therefore, the laminar boundary-layer-shock-wave interaction problem can be solved, at least approximately, by means of the simplified mixing theory, provided a suitable reflection condition for the incident shock wave is introduced. If the incident shock wave is reflected from the "jet" as from a free boundary, then the pressure drop across the reflected expansion fan exactly cancels the pressure rise across the incident wave. In that case $\theta_2 = \theta_3 - 2\theta_w$, where θ_3 is the flow inclination angle in the separated region just upstream of the incident shock, θ_2 is the flow inclination angle in the reattaching flow just downstream of the reflected expansion fan, and θ_w is the flow deflection across the incident shock. The other boundary condition at the junction of the separated and reattaching flow regions is, of course, $\delta_3 = \delta_2$. [θ_R for the reattaching flow is determined from $M_{+\infty}$, see Section (4.1).] In Fig. 15 the calculated static pressure distribution on the wall is shown for $\bar{M} = M_{-\infty} = 2.0$, $\theta_w = 4°$, $Re_{x_s} = 2.5 \times 10^5$, $k_{\text{lam.}} = 0.0037$. For this case the pressure increase on both sides of the shock is about equal, and the flow pattern is nearly symmetrical. The

† The flow conditions at separation were computed by the approximate method of reference 4. The value of $k_{\text{lam.}}$ is taken to be constant at the flat-plate value for a Reynolds Number equal to Re_{x_s}.

asymmetric flow pattern and pressure distribution found at higher Reynolds Numbers, or for stronger incident shocks, appears to be associated with transition in the reattaching flow, which greatly increases the mixing rate and pressure rise in this region. This flow régime can be treated by methods similar to those employed in the base pressure problem for the case when transition occurs in the wake [Section (5)]. A detailed treatment is reserved for a later paper.

For the turbulent boundary layer the situation is more complicated. In this case, the deep penetration of the shock makes it necessary to modify some of the basic assumptions of the present paper at least locally, particularly the assumption of constant pressure across the internal dissipative flow [see Section (6)].

(5) Application of Simplified Mixing Theory to the Base Pressure Problem in Plane Supersonic Flow

(5.1) *Method and Assumptions*

This problem has already been formulated in Section (3) as an application of the more exact theory. When the wake is fully turbulent, the procedure for the simplified theory is similar to that previously described in Section (3), but when transition occurs in the wake, the scheme is somewhat modified.

(*a*) *Turbulent Wake—Transition in Airfoil Boundary Layer.*—When the wake is fully turbulent, it is again assumed that k = constant, and $\bar{\delta}/\bar{\delta}_R$ is then completely determined as a function of θ for every Mach Number $\bar{M}$ by Eqs. (4.6) and (4.7). At the airfoil trailing edge, the boundary condition $\delta = (h/2) + \delta_{b'}$ must be satisfied, or

$$\frac{\bar{\delta}}{\bar{\delta}_R} = \frac{\dfrac{h}{2} + \delta_{b'}}{\delta_R\left[1 - \kappa_j\left(1 - \dfrac{\delta^*}{\delta}\right)_j\right]} - \frac{\kappa_j\left(1 - \dfrac{\delta^*}{\delta}\right)_j}{1 - \kappa_j\left(1 - \dfrac{\delta^*}{\delta}\right)_j} \tag{5.1}$$

(Approximately, $\kappa_j = 0.720$ and $[1 - (\delta^*/\delta)]_j = 0.45$ for a turbulent low-speed isothermal jet.) To every value of

$$\frac{[(h/2) + \delta_{b'}]}{\delta_R} = \frac{\delta_{b'}}{\delta_R}\left[1 + \frac{h}{2\delta_b}\frac{\delta_b}{\delta_{b'}}\right]$$

there corresponds a value of $\bar{\delta}/\bar{\delta}_R$ and therefore a value of $\theta_{b'}$ by Eq. (5.1) and, finally, a value of base pressure ratio $p_{b'}/\bar{p} = f(\theta_{b'}, \bar{M})$. In order to relate this value of the base pressure ratio to δ_b/h, it is necessary to calculate $\delta_{b'}/\delta_R$ and $\delta_{b'}/\delta_b$. The ratio $\delta_R/\delta_{b'}$ is obtained as follows:

By definition,

$$\bar{m}_R = (p_R/\varphi_{eR})\delta_R[1 - (\delta^*/\delta)]_R$$
$$\bar{m}_{b'} = (p_{b'}/\varphi_{eb'})\delta_{b'}[1 - (\delta^*/\delta)]_{b'}$$

so that

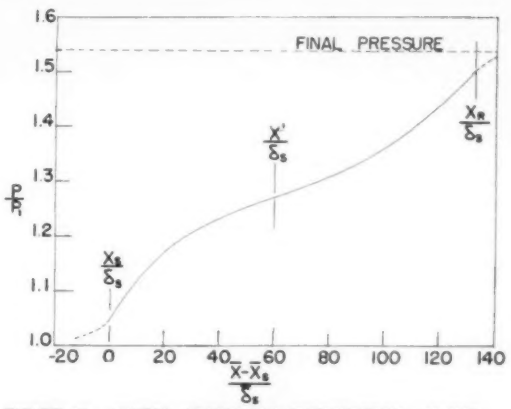

FIGURE 15. STATIC PRESSURE DISTRIBUTION ALONG SURFACE FOR LAMINAR BOUNDARY LAYER — SHOCK WAVE INTERACTION.
$M_{-\infty} = M_1 = 2.0$, $\theta_w = 4°$, $Re_{x_s} = 250{,}000$
$k_{LAM} = .0037$
SIMPLIFIED THEORY

$$\frac{m_R}{m_{b'}} = \frac{(p_R/\varphi_{eR})\,\delta_R}{(p_{b'}/\varphi_{eb'})\,\delta_{b'}} \tag{5.2}$$

where it is assumed, as in Section (3), that

$$1 - \left(\frac{\delta^*}{\delta}\right)_{b'} = \left(1 - \frac{\delta^*}{\delta}\right)_R = \left(1 - \frac{\delta^*}{\delta}\right)_j = \text{const.}$$

By integrating Eq. (2.25) for the mixing rate and dividing through by $m_{b'}$, one obtains

$$\frac{m_R}{m_{b'}} = 1 + \frac{k}{m_{b'}}\int_{x_{b'}}^{x_R}\frac{p}{\varphi_e}\,dx = 1 + \frac{k}{m_{b'}}\int_{\theta_{b'}}^{\theta_R}\frac{p}{\varphi_e}\frac{(d\delta/d\theta)}{(d\delta/dx)}\,d\theta$$

or

$$\frac{m_R}{m_{b'}} = 1 + \frac{p_R/\varphi_{eR}}{p_{b'}/\varphi_{eb'}}\frac{\delta_R}{\delta_{b'}}\left\{\frac{1}{[1 - (\delta^*/\delta)]_j} - \kappa_j\right\}\frac{1}{1 - \kappa_j}D \tag{5.3}$$

where

$$D = \int_{\theta_{b'}}^{\theta_R}\left(\frac{\delta}{\bar{\delta}_R}\right)\frac{(p/\varphi_e)}{(p_R/\varphi_{eR})}\frac{d\theta}{\sqrt{\bar{M}^2 - 1}}$$

Finally, by Eqs. (5.2) and (5.3),

$$\frac{\delta_R}{\delta_{b'}}\left(1 - \left\{\frac{1}{[1 - (\delta^*/\delta)]_j} - \kappa_j\right\}\frac{D}{1 - \kappa_j}\right) = \frac{(p_{b'}/\varphi_{eb'})}{(p_R/\varphi_{eR})} \tag{5.4}$$

For the completely turbulent wake, the integral D is a unique function of $\theta_{b'}$ for every Mach Number $\bar{M}$, according to Eqs. (4.6) and (4.7).

As explained in Section (3), the ratio $\delta_b/\delta_{b'}$ as given by Eq. (3.2b) is obtained by applying the condition of conservation of mass across the expansion around the "corner" at the airfoil trailing edge.

By utilizing Eqs. (5.1), (5.4), and (3.2b), the base pressure ratio is related to $\delta_b/h = (\delta_b/c)(c/h)$. The

variation of base pressure with Reynolds Number at a given Mach Number is obtained by introducing the same postulated variation of δ_b/c with Reynolds Number and Mach Number which is described in Section (3) and illustrated in Fig. 8 for $M = 3.0$.

(*b*) *Transition in Wake—Airfoil Boundary Layer Laminar.*—When transition in the airfoil boundary layer is described in terms of curve (I) of Fig. 8, for example, then for $Re_c < 4 \times 10^6$ the boundary layer is completely laminar, and the transition "point" moves off the body and into the wake. Since the mixing coefficient k in the laminar portion of the wake is a function of Reynolds Number, the relation between $\bar{\delta}/\bar{\delta}_R$ and θ is no longer independent of Reynolds Number, and the procedure outlined in (2a) above must be modified.

In the first place, a statement must be made regarding the transition Reynolds Number in the wake, about which little is known at present. Transition in the wake must depend to a large extent on the previous history of the laminar oscillations in the airfoil boundary layer, as well as on the growth of disturbances along the laminar portion of the wake itself. Based on the meager data available, it is assumed that a "free" high-velocity laminar half-jet, undisturbed by oscillations fed into the jet from an upstream boundary layer, would have a transition Reynolds Number of 4×10^5. Therefore, when $Re_c \ll 4 \times 10^6$, the transition Reynolds Number in the wake must approach a value of 4×10^5, while $Re_{tr_{wake}} = 0$ when $Re_c = 4 \times 10^6$ and transition just reaches the airfoil trailing edge. Taking a linear variation of $Re_{tr_{wake}}$ with Re_c between these two conditions, *roughly*,

$$Re_{tr_{wake}} = 4 \times 10^5 - Re_c/10 \qquad (5.5)$$

at high velocities. [For transition curve (II), $Re_{tr_{wake}} = 3 \times 10^5 - (Re_c/10)$.] A smooth movement of transition from airfoil to wake is presumed. All that can be claimed for this approximation is that it gives the correct *form* of the dependence of transition on Re_c and provides for an accelerated forward movement of transition in the wake with increasing Reynolds Number.

On the basis of this assumption regarding transition in the wake, the variation of base pressure with Reynolds Number at a given Mach Number in this flow régime is calculated by an iteration method. Suppose that c/h is given. For some value of $Re_c < 4 \times 10^6$ a series of trial values of θ_{tr} or the flow deflection angle at the transition point, is selected. The corresponding locations of the transition "point" and values of $Re_{tr_{wake}}$ are calculated by an iteration scheme, in which the value of $\theta_{b'}$ and the base pressure are also calculated. Now the *correct* value of $Re_{tr_{wake}}$ at the prescribed value of Re_c is given by Eq. (5.5), so the proper value of θ_{tr} can be determined from a plot of $Re_{tr_{wake}}$ vs. θ_{tr}, and the corresponding base pressure can be calculated by interpolation.

The details of the method are as follows: Once a trial value of θ_{tr} is selected, the relation between $\bar{\delta}/\bar{\delta}_R$ and θ required in the statement of the boundary condition [Eq. (5.1)] is obtained from Eqs. (4.6) and (4.10). However, the value of the mixing coefficient in the laminar portion of the wake must be known or chosen. For our present purposes, it is sufficient to take $k_{lam.}$ equal to the mixing coefficient in the laminar boundary layer just at the airfoil trailing edge—i.e.,†

$$k_{lam.} = \frac{c_{f_0}/2}{1 - \kappa_0} = \frac{g(M)}{\sqrt{Re_c}} \frac{0.332}{1 - \kappa_0}$$

The Mach Number factor $g(M)$ is obtained from Fig. 19 of Van Driest's paper[18] and is tabulated below:

M	$g(M)$
1.55	0.98
2.0	0.95
3.0	0.91
4.0	0.87
5.0	0.81

The value of κ_0 utilized in calculating $k_{lam.}$ is 0.827, corresponding to $u(\delta)/u_e = 0.9975$, and the corresponding value of κ_j employed is 0.720.‡ A typical plot of $\bar{\delta}/\bar{\delta}_R$ vs. θ with transition in the wake is illustrated in Fig. 13a.

The right-hand side of Eq. (5.1) is also determined as a function of θ by utilizing Eqs. (5.4) and (3.2b), where the value of $[1 - (\delta^*/\delta)]_b$ for the laminar boundary layer with zero heat transfer at the airfoil surface is given by‡

$$3.87/[5.60 + 1.20(\gamma - 1)M_b^2]$$

The value of $[1 - (\delta^*/\delta)]_{b'}$ is taken to be 0.45, exactly as in the case of the fully turbulent jet. The value of $\delta_b/h = (\delta_b/c)(c/h)$ is already known once c/h and Re_c are prescribed, since δ_b/c is given by Eq. (3.5). The correct value of $\theta_{b'}$ for the particular trial value of θ_{tr} is then found from the intersection of the curves of $\bar{\delta}/\delta\bar{\delta}$ and the right-hand side of Eq. (5.1) plotted as functions of θ. The location of the transition point in the wake aft of the trailing edge is then calculated from the relation

$$\frac{l}{\bar{\delta}_R} = \frac{\bar{x}_{b'} - \bar{x}_{tr}}{\bar{\delta}_R} = \int_{(\bar{\delta}/\delta\bar{R})_{tr}}^{\delta_{b'}/\delta_R} \frac{1}{\theta + k_{lam.}} d\left(\frac{\bar{\delta}}{\bar{\delta}_R}\right) \qquad (5.6)$$

and the corresponding value of $Re_{tr_{wake}}$ is given by the relation

$$Re_{tr_{wake}} = \frac{l}{c} Re_c \left(\frac{p_{tr}}{\bar{p}}\right)^n \frac{M_{tr}}{\bar{M}} \qquad (5.7)$$

where

$$n = \frac{\gamma - 1}{\gamma}\left[\frac{1}{2}\frac{\gamma + 1}{\gamma - 1} - m\right]$$

if $\mu \sim T^m$, and

† If $\mu \sim T$, $g(M) = 1.0$.

‡ See footnotes on page 663.

$$\frac{l}{c} = \frac{\bar{l}}{\delta_R}\left[1 - \kappa_j\left(1 - \frac{\delta^*}{\delta}\right)_j\right]\frac{\delta_R}{\delta_b}\frac{\delta_b}{\delta_b}\frac{\delta_b}{c}$$

For air, $\gamma = 1.40$ and $m = 0.76$, so $n = 0.64$.

Since the value of $Re_{tr_{wake}}$ obtained from Eq. (5.7) does not, in general, coincide with the assumed value given by Eq. (5.5), the whole procedure must be repeated for three or four trial values of θ_{tr} in order to determine the correct $Re_{tr_{wake}}$ and base pressure by interpolation with sufficient accuracy. The scheme is repeated for several representative values of Reynolds Number, Re_c. Fortunately, after some experience only a few trials are necessary.

Evidently, for sufficiently low Reynolds Numbers, $\theta_{tr} \to \theta_R$ and the flow in Region (1) becomes completely laminar. For Reynolds Numbers below the value at which θ_{tr} is calculated to be approximately equal to θ_R, the conditions are determined by analogy with the more exact theory. In this theory, conditions upstream of the critical point are unaffected by conditions downstream of this point and are therefore independent of the movement of transition once transition passes the critical point. By analogy, it is assumed now that, once transition passes into Region (2), conditions in Region (1) remain independent of Region (2). The value of θ_R at a given Mach Number $\bar{M}$ is regarded as a constant and the character of the flow solution in Region (1) is determined completely by the variation of laminar mixing rate with Reynolds Number [see Section (5.2)]. At extremely low Reynolds Numbers, the present mixing theory must be modified because δ_b/h is no longer small.

(5.2) *Effect of Reynolds Number on Base Pressure: The Various Flow Régimes*

A sufficient number of numerical examples have been calculated for all flow régimes to indicate the important trends in the variation of base pressure with Reynolds number, Mach Number, c/h, and type of transition in the airfoil boundary layer. Fig. 16 shows the variation at $\bar{M} = 3.0$ of $p_b/\bar{p}$ with Reynolds Number for $c/h = 10.0$, with the two types of assumed boundary-layer transition. [In all the other figures only the calculated base pressure for curve (I) is shown.] In Fig. 9 the curve computed from the simplified theory for $\bar{M} = 3.0$ and $c/h = 3.0$ is shown in comparison with the curve obtained by the "exact" theory [Section (3)]. These curves show a similar qualitative behavior. In view of the assumptions made in the simplified theory and the probable sensitivity of the results of the "exact" theory to the assumed F-κ curve [Sections (2) and (3)], the differences in the numerical values of base pressure should not be taken too seriously at present. The *numerical* results are properly regarded as preliminary.

The effect of Reynolds Number and c/h on base pressure at $\bar{M} = 2.0$ is illustrated in Fig. 17 for values of c/h of 3.0 and 10.0. The low Reynolds Number region at $\bar{M} = 2.0$ is emphasized in Fig. 18 for $c/h =$

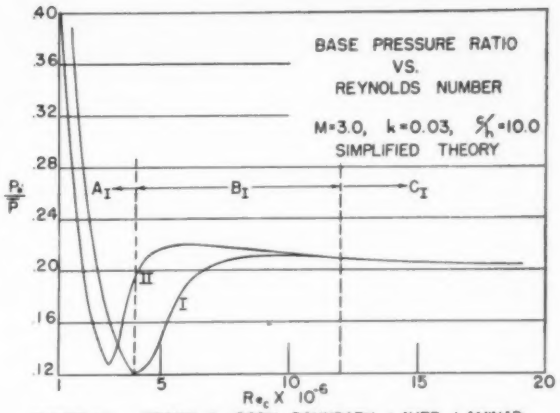

FIGURE 16. REGION A_I - BODY BOUNDARY LAYER LAMINAR, TRANSITION IN WAKE
REGION B_I - TURBULENT WAKE, TRANSITION ON BODY
REGION C_I - FULLY TURBULENT

I & II REFER TO THE TWO DIFFERENT ASSUMED TRANSITION CURVES

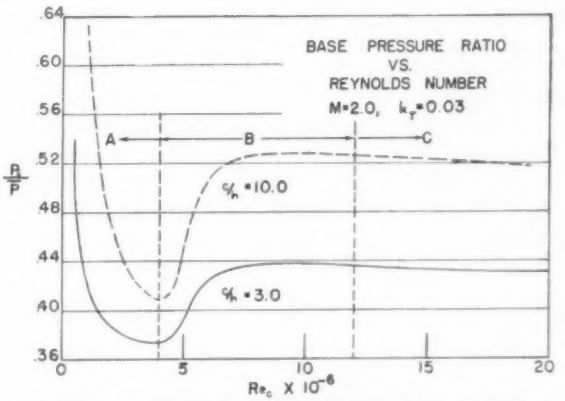

FIGURE 17. REGION A - BODY BOUNDARY LAYER LAMINAR, TRANSITION IN WAKE
REGION B - TURBULENT WAKE, TRANSITION ON BODY
REGION C - FULLY TURBULENT
SIMPLIFIED THEORY - TRANSITION CURVE I

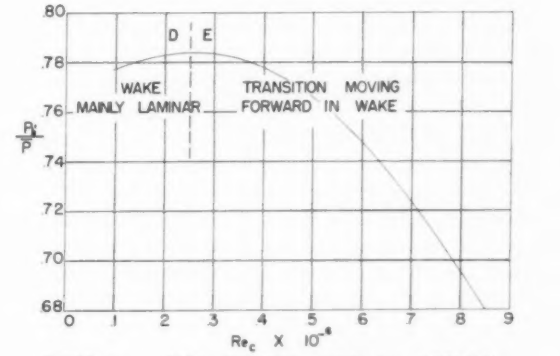

FIGURE 18. BASE PRESSURE RATIO VS REYNOLDS NUMBER IN LOW REYNOLDS NUMBER REGION. M=2.0, k_T=0.03, c/h=10.0

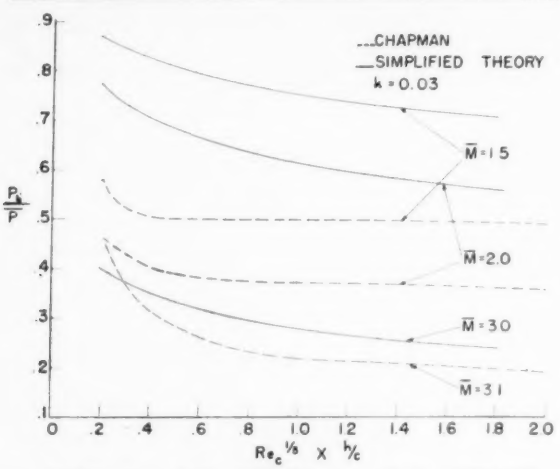

FIGURE 19. BASE PRESSURE IN FULLY TURBULENT REGION.

10.0, and in Fig. 20 the base pressure with airfoil boundary layer laminar to the trailing edge is plotted against the parameter $Re_c^{1/4}h/c$ employed by Chapman.[17] Data for two of the airfoils with blunt trailing edges tested by Chapman in this flow régime are also shown for comparison.

In the "fully turbulent" régimes at high Reynolds Numbers, the base pressure ratio is plotted against the parameter $Re_c^{1/5}h/c$ for $\bar{M} = 1.5$, 2.0, and 3.0 in Fig. 19. Again Chapman's data in this flow régime are shown for comparison; the curves are reproduced from Fig. 28 of reference 17, in which the "mean" curves for the entire "thickness group" of airfoils are presented. The thickness ratios for the group are 0.05, 0.075, and 0.10, and the ratio of airfoil trailing-edge thickness to maximum thickness has the discrete values 0.25, 0.50, 0.75, and 1.0, so that c/h ranges from 10.0 to 80.0 in these tests.

It is remarkable that, in spite of the approximate character of the present mixing theory, it appears to give the correct fluid-mechanical explanation of the observed phenomena and flow régimes in the base pressure problem. Unfortunately, Chapman's data for the blunt trailing edge airfoils do not include the important intermediate régime, in which transition moves upstream in the airfoil boundary layer, but base pressure data on bodies of revolution,[6, 20] which should be at least qualitatively similar to the two-dimensional case, illustrate perfectly the régimes determined by our calculations. Four such flow régimes can be distinguished, in which the contrasting effects of mixing rate variations and variations of δ_b determine the quite different dependence of the base pressure on Reynolds Number in the different flow régimes. In preceding discussions, it has been shown that an increase in k increases the pressure ratio across a compression and therefore decreases the base pressure [Section (4.2)], while an increase in δ_b increases the base pressure [Sections (3) and (4.2)]. These qualitative considerations are borne out by the results of the computations.

In order of increasing Reynolds Number, the four flow régimes are as follows:

(1) At sufficiently low Reynolds Numbers, not only the body boundary layer is laminar but also that region of the wake in which the major portion of the recompression occurs [Region (1)]. Within this régime, as Re_c increases, the laminar mixing rate decreases and the base pressure increases slowly with Reynolds Number (Fig. 18). The decrease in $k_{lam.}$ with increasing Re_c is apparently more than enough to offset the decrease in thickness of the boundary layer at the airfoil trailing edge or the decrease in thickness of the mixing region in the wake. Because of the low laminar mixing rate, the base pressure ratio is relatively high.

(2) As the Reynolds Number is increased, eventually transition begins to move upstream in the wake, and the accompanying large increase in local mixing rate ($k_{turb.} \approx 5$–$10\ k_{lam.}$) counteracts the effects discussed in (1) above. After reaching a local maximum (Fig. 18), the base pressure drops precipitously with increase in Re_c (Figs. 8, 16, 17, and 20). The large increase in local mixing rate is a much more important factor than the accompanying increase in the thickness of the mixing region, which, by itself, would have just the opposite effect on base pressure.

After transition in the wake has moved close to the airfoil trailing edge, the base pressure ratio continues to drop with increasing Reynolds Number, so long as the airfoil boundary layer remains laminar, because of the decrease in boundary-layer thickness at the trailing edge with increasing Reynolds Number. This decrease is expected to be much less rapid than the first steep drop that occurs when transition moves forward in the wake. If the boundary-layer transition Reyn-

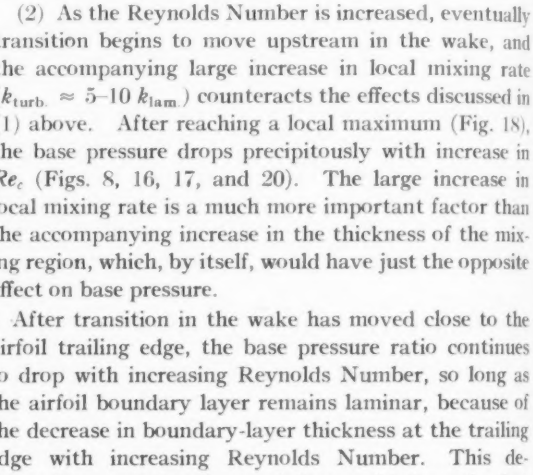

FIGURE 20. TRANSITION IN WAKE, AIRFOIL BOUNDARY LAYER LAMINAR, SHOWING DEPENDENCE OF BASE PRESSURE ON c/h. M=2.0

olds Number is sufficiently high and if the ratio of chord to airfoil trailing edge thickness is low, *but not otherwise*, the base pressure ratio depends only on the ratio δ_b/h or on the parameter $Re_c^{1/2}h/c$ over an appreciable Reynolds Number range in this flow régime [see later discussion, Section (5.2)(*ii*)].

(3) At a sufficiently high Reynolds Number, transition will occur in the airfoil boundary layer just at the trailing edge. When the Reynolds Number is increased still further, presumably the mixing rate in the wake is little affected, but transition moves forward on the airfoil, and the boundary layer at the trailing edge thickens accordingly. Thus, the base pressure ratio at first *increases* with increasing Reynolds Number in this flow régime. However, when transition has moved upstream sufficiently far from the trailing edge, the normal decrease in local turbulent boundary-layer thickness with increasing Reynolds Number begins to offset the thickening effect of the forward movement of transition. The base pressure curve reaches a local maximum and then decreases again with increasing Reynolds Number (Figs. 8, 16, and 17).

(4) Finally, a high Reynolds Number régime is reached in which transition in the airfoil boundary layer is essentially "fixed" and the base pressure ratio drops slowly but noticeably, with increasing Reynolds Number, because of the decrease in turbulent boundary-layer thickness at the trailing edge. In this régime, the base pressure ratio is a function solely of the parameter $Re_c^{1/2}h/c$ (Fig. 19) or of some similar parameter involving the product of h/c and a logarithmic function of Reynolds Number.

Briefly, the effects of Mach Number, c/h-ratio and transition in the airfoil boundary layer on base pressure are as follows:

(*i*) *Transition and Mach Number.*—Whatever affects transition in the airfoil boundary layer also determines the location, shape, and depth of the "valley" in the curve of base pressure ratio versus Reynolds Number at a given Mach Number. Thus, the base pressure is affected by the heat-transfer rate at the airfoil surface, surface pressure gradient, surface roughness, surface irregularities such as sharp corners, free-stream turbulence, etc. Since transition in the airfoil boundary layer is expected also to depend on Mach Number, the Reynolds Number range defining the "valley" in the base pressure curve is a function of Mach Number. The effect of each of these factors on base pressure can now be predicted, at least qualitatively, when its effect on the thickness and character of the boundary layer at the airfoil trailing edge is known.

On the basis of the discussion in Section (4.2), it was expected that, for a given mixing rate, the pressure ratio supported by the wake flow increases rapidly with Mach Number—i.e., the base pressure ratio decreases rapidly with increasing Mach Number (see Fig. 19). This result is probably also significant for other flow phenomena in which mixing is important, such as boundary-layer separation. Of course, the actual numerical values of base pressure depend critically upon the mixing coefficient k. By selecting k as a suitable function of Mach Number, coincidence between the theoretical computations and experimental data could be obtained. By referring to Fig. 19 one may conclude tentatively that the mixing rate at low supersonic Mach Numbers is probably of the order of 0.05 (somewhat larger than the constant value of 0.03 assumed in this paper) and that k apparently decreases with increasing Mach Number. Some support for this tentative conclusion comes from recent experimental work on the rate of spreading of a supersonic turbulent stream into quiescent air.

(*ii*) *Chord to Trailing-Edge Thickness Ratio (Transition in Wake).*—In general, the higher the ratio of chord to trailing-edge thickness, the larger is δ_b/h and the higher the base pressure ratio at a given Reynolds Number and a fixed Mach Number.† The effect of c/h ratio is particularly interesting in the intermediate *wake* transition region, because the rate of upstream movement of transition in the wake with increasing Reynolds Number is governed largely by the parameter c/h. The transition Reynolds Number $Re_{tr_{wake}}$ is determined by Re_c [Eq. (5.5)], and therefore so is the ratio $l/c = Re_{tr_{wake}}/Re_c$, where l is the distance from airfoil trailing edge to wake transition "point." But the important parameter governing the character of the wake flow is the ratio l/h. When the transition "point" just enters the significant recompression region,

$$\frac{l}{h} = \frac{l}{c}\frac{c}{h} \approx \frac{2}{\theta_{b'}} \tag{5.8}$$

roughly. Two important conclusions can now be drawn:

(a) At a given Reynolds Number Re_c, the laminar flow region occupies a larger portion of the wake the larger the c/h ratio. In other words, the forward movement of transition into the major recompression region and the accompanying drop in base pressure begins at higher Reynolds Numbers the higher the c/h ratio. For very large c/h the base pressure ratio is nearly unity, and $\theta_{b'}$ is small and varies nearly linearly with h/c. Therefore, by Eq. (5.8), l/c approaches a limit, and the Reynolds Number marking the transition between the two flow régimes also approaches an upper limit as c/h increases. These conclusions seem to be borne out by the data presented in Figs. 14 and 15 of reference 17.

(b) For large c/h, a significant variation in l/h occurs with only a small variation in l/c and, therefore, in Re_c. Once the transition point does begin to move forward into the major recompression region, the base pressure drops steeply in a narrow Reynolds Number range. On

† Thus the effect of increasing body length to obtain higher Reynolds Numbers in a series of experiments is certainly much different from the effect obtained when c/h is fixed and ambient density is increased. This fact was pointed out by Bogdonoff.[38]

the other hand, for small c/h, the upstream movement of transition in the wake extends over a wider Reynolds Number range, and the curve of base pressure vs. Re_c is much "flatter" in this flow régime (Figs. 17 and 20). Since this effect of c/h ratio is greatly accentuated at extremely large values of c/h, it may be responsible for the almost discontinuous change in base pressure observed by Chapman[17] under certain conditions for airfoils with extremely thin trailing edges ($c/h = 80$).

In the flow régime characterized by the forward movement of transition in the wake with increasing Reynolds Number, the base pressure evidently depends not only upon δ_b/h but also upon the location of transition. In general, therefore, one would not expect the base pressure to be correlated solely against the parameter δ_b/h, or $Re_c^{1/2}h/c$ in this régime, but to depend also on c/h. Such a correlation exists only when transition in the wake is located close to the airfoil trailing edge over a significant range of Reynolds Numbers below the airfoil boundary-layer transition Reynolds Number. By referring to Eq. (5.8), one sees that this condition is fulfilled only when: (1) the boundary-layer transition Reynolds Number is high and the value of $Re_{tr_{wake}}$ varies only slowly with Re_c (l/c varies slowly with Re_c); (2) c/h is small. In Fig. 20, neither the theoretically calculated base pressure nor Chapman's data are correlated by the parameter $Re_c^{1/2}h/c$, largely because Re_{tr} in the airfoil boundary layer is certainly not greater than 4×10^6 (probably $Re_{tr} \approx 2 \times 10^6$ in these experiments) and the values of c/h are already too large. At low Reynolds Numbers, the curves of base pressure ratio vs. $Re_c^{1/2}h/c$ for various c/h values tend to converge and cross as shown in Fig. 20 and in Figs. 14 and 15 of reference 17, because the base pressure is approaching a local maximum of the type illustrated in Fig. 18. However, at high Reynolds Numbers these curves diverge considerably. For example, any attempt to construct a "universal" curve of base pressure ratio vs. $Re_c^{1/2}h/c$ by utilizing data obtained at one Reynolds Number over a range of c/h values could lead to appreciable errors.

In the case of blunt-based bodies of revolution,[6] transition in the body boundary layer apparently occurs at high Reynolds Numbers ($Re_{tr} > 6 \times 10^6$), and the base pressure ratio may be correlated against the parameter $Re_L^{1/3}D/L$ over a definite range of L/D values (L is body length and D is base diameter).

The ability of the present theory to predict even such details of the base pressure phenomena is another confirmation of the correctness of the basic mechanism assumed.

(6) Future Investigations

The success of the mixing theory in furnishing a qualitative fluid-mechanical explanation of the phenomena occurring in the base pressure problem encourages us to attempt to apply this theory to other problems involving the interaction between a dissipative flow region and an adjacent nearly isentropic stream. However, in certain cases, either some of the basic assumptions of the present paper must be modified or the outer boundary of the dissipative flow region must be carefully redefined. In some cases, perhaps the most serious assumption is that the static pressure is constant across the dissipative flow and equal to the local value p_e in the external stream at $y = \delta$. In a turbulent boundary-layer-shock-wave interaction, for example, the incident oblique shock is reflected and refracted as it enters the layer, but apparently penetrates to the sonic velocity line close to the surface. The main reflected shock wave appears to emerge from this same region.[16, 22] In the important interaction region, the static pressure is certainly not uniform across a plane transverse to the flow in the supersonic portion of the boundary layer, but the pressure is probably nearly constant across the subsonic and transonic zones close to the wall. Presumably, it is also this region that is most strongly affected by an increasing static pressure along the surface. It might be correct physically to define this region as the new dissipative flow and to treat the supersonic portion of the boundary layer as an "external" inviscid rotational flow. Experimental and theoretical studies are required to settle this point.

The mixing theory including friction [Eq. (2.30)] is expected to furnish information about the turbulent boundary layer in an adverse pressure gradient away from shock waves. It is important to determine whether the maximum pressure increase that can be supported by a turbulent layer without separation increases rapidly with Mach Number, as we have found for the recompression in the wake flow.

In many respects, laminar boundary-layer-shock-wave interaction appears to be simpler than the turbulent case, because upstream separation occurs even for weak incident shocks and the incident shock wave is reflected from the separated flow very nearly as if this flow were a free boundary. The static pressure is probably nearly constant across the low-velocity region between the jetlike outer boundary and the surface. The approximate solution indicated in the present paper [Section (4.2)] must be regarded as a first step; in a later paper, the important influence of surface friction on the reattaching flow and the surface pressure distribution downstream of the reflected expansion "fan" will be discussed.

Another important basic assumption of the present mixing theory is that the stagnation enthalpy is constant across the flow. For separated flows and wakes, there is some question whether the mixing process may not create regions of low stagnation enthalpy near a surface or just aft of a body. This question is best settled by experiment. For flows attached to a surface, the present theory can probably be extended to cases where the surface heat transfer rate is not zero.

The present theory is capable not only of giving a qualitative explanation of all these interaction phenomena but should furnish realistic quantitative predictions once the F-κ curve is known and the dependence of mixing coefficient k on the parameters m, w_e, and κ is determined. This information is required particularly in the turbulent case. By specifying the quantities that must be known, the theory also serves as a useful guide to experimental investigations.

(7) Conclusions

(1) An important property of supersonic wake flows or of reattaching supersonic flows directed toward a solid surface is the existence of a singularity in the basic differential equation, or "critical point" in the flow which acts much like the throat of a nozzle in determining the base pressure, for example. One important reason for the marked difference between laminar and turbulent interactions is the fact that the turbulent mixing rate is five to ten times larger than the laminar mixing rate.

(2) According to the present mixing theory, separated flows, as well as reattaching flows, are capable of supporting considerable pressure increases at high velocities. The maximum compression, as measured by the isentropic flow deflection, is roughly proportional to the square root of the mixing rate parameter and also to $(M^2 - 1)^{1/4}$, where M is some average Mach Number. Thus, the pressure ratio increases rapidly with Mach Number, or the base pressure ratio, for example, decreases rapidly with Mach Number. In separated flows, the pressure gradient along the surface is a maximum at separation and drops off steeply downstream; in reattaching flows or wake flows, the pressure gradient is negligible some distance upstream of the "reattachment point" and increases rapidly toward a maximum as this point is approached. The inflected surface pressure distribution observed in laminar boundary-layer-shock-wave interactions is now understandable, and the distribution itself can be calculated approximately.

(3) When the present mixing theory is applied to the problem of determining the base pressure for a supersonic airfoil with a blunt trailing edge, it gives the correct fluid-mechanical explanation of the observed phenomena. Four different flow régimes can be distinguished. In order of increasing Reynolds Number they are as follows:

(*i*) A low Reynolds Number region in which not only the airfoil boundary layer is laminar but also the region of the wake in which the major portion of the recompression occurs. In this régime the base pressure ratio $p_{b'}/\bar{p}$ *increases* slowly with Reynolds Number Re_c because of the decreasing laminar mixing rate.

(*ii*) A régime in which transition to turbulent flow moves upstream in the wake and the base pressure curve reaches a local maximum and then drops precipitously with increasing Reynolds Number because of the large increase in mixing rate. If the ratio of chord to airfoil trailing-edge thickness (c/h) is low or if the boundary-layer transition Reynolds Number is high (*but not otherwise*), an appreciable range of Reynolds Numbers exists for which transition in the wake is located quite near the base, but the airfoil boundary layer remains laminar. In this range, $p_{b'}/\bar{p}$ continues to decrease with increasing Reynolds Number because of the decreasing boundary-layer thickness at the airfoil trailing edge, and the governing parameter is $Re_c^{1/2}h/c$.

(*iii*) A régime in which transition, having "jumped" from the wake to the airfoil boundary layer, moves forward on the airfoil with increasing Reynolds Number. In this régime, $p_{b'}/\bar{p}$ at first *increases* with increasing Reynolds Number because of the increase in boundary-layer thickness at the airfoil trailing edge as the transition point moves forward. Eventually, the normal decrease in local turbulent boundary-layer thickness with increasing Reynolds Number begins to offset the thickening effect of the forward movement of transition, and the base pressure curve reaches a local maximum and then begins to drop with increasing Reynolds Number.

(*iv*) A high Reynolds Number régime in which transition on the airfoil is practically "fixed" far from the trailing edge and the base pressure drops slowly with increasing Reynolds Number because of the decreasing turbulent boundary-layer thickness at the airfoil trailing edge. The governing parameter here is $Re_c^{1/5}h/c$.

Clearly, anything that affects transition in the airfoil boundary layer or in the wake will affect the "valley" in the curve of base pressure versus Reynolds Number. The effect of a given parameter can be predicted, at least qualitatively, once its influence on the character and thickness of the airfoil boundary layer at the trailing edge is known.

Qualitative agreement is found between these theoretical predictions and calculations and the base pressure data of Bogdonoff and Chapman on blunt-based bodies of revolution and Chapman's data on supersonic airfoils with blunt trailing edges.

(4) Considerable theoretical and experimental work remains to be done in extending this mixing theory to axially symmetric flows and to boundary-layer-shock-wave interactions and other flows, and in carefully determining the dependence of the mixing rate and the mean temperature-mean velocity relation on the flow parameters.

References

[1] Tsien, H. S., and Finston, M., *Interaction Between Parallel Streams of Subsonic and Supersonic Velocities*, Journal of the Aeronautical Sciences, Vol. 16, No. 9, pp 515–528, September, 1949.

[2] Lighthill, M. G., *Reflection at a Laminar Boundary Layer of a Weak, Steady Disturbance to a Supersonic Stream, Neglecting Viscosity and Heat Conduction*, Quart. Journ. Mech. & Applied Math., Vol. III, pp. 303–325, 1950.

(*Concluded on following page*)

[3] Schubauer, G. B., and Klebanoff, P. S., *Investigation of Separation of the Turbulent Boundary Layer*, N.A.C.A. T.N. No. 2133, August, 1950.

[4] Lees, L., *Interaction Between the Laminar Boundary Layer over a Plane Surface and an Incident Oblique Shock Wave*, Princeton University Aeronautical Engineering Laboratory, Report No. 143, January 24, 1949.

[5] Ritter, A., *On Reflection of a Weak Shock Wave from a Laminar Boundary Layer*, Paper presented at meeting of Fluid Dynamics Div., Amer. Phys. Soc., Cornell Univ., Ithaca, N.Y., September 11–12, 1951.

[6] Chapman, D. R., *An Analysis of Base Pressure at Supersonic Velocities and Comparison with Experiment*, N.A.C.A. T.N. No. 2137, July, 1950.

[7] Summerfield, M., Foster, C. R., and Swan, W. C., *Flow Separation in Overexpanded Supersonic Nozzles*, Presented at a meeting of Institute of Heat Transfer and Fluid Mechanics, Los Angeles, June, 1948.

[8] Summerfield, M., *Fundamental Problems in Rocket Research*, Journal of the American Rocket Society, pp. 78–98, June, 1950. (See especially pp. 94–95.)

[9] Stewartson, K., *Correlated Incompressible and Compressible Boundary Layers*, Proc. Roy. Soc. (A), Vol. 200, No. 1060, pp. 84–100, December 22, 1949.

[10] Falkner, V. M., and Skan, S. W., *Some Approximate Solutions of the Boundary Layer Equations*, British A.R.C., R. & M. No. 1314, 1930.

[11] Hartree, D. R., *On an Equation Occurring in Falkner and Skan's Approximate Treatment of the Equations of the Boundary Layer*, Proc. Cambridge Phil. Soc., Vol. 33, p. 237, 1937.

[12] Howarth, L., *On the Solution of the Laminar Boundary Layer Equations*, Proc. Roy. Soc. (A), Vol. 164A, pp. 547–579, 1938.

[13] Chapman, D. R., *Laminar Mixing in a Compressible Fluid*, N.A.C.A. T.R. No. 958, 1950.

[14] Thwaites, B., *Approximate Calculation of the Laminar Boundary Layer*, Aeronautical Quarterly, Vol. 1, Part 3, pp. 245–280, November, 1949.

[15] von Doenhoff, A. E., and Tetervin, N., *Determination of General Relations for the Behavior of Turbulent Boundary Layers*, N.A.C.A. T.R. No. 772, 1943.

[16] Bogdonoff, S. M., and Solarski, A., *A Preliminary Study of a Turbulent Boundary Layer-Shock Wave Interaction*, Princeton University Aeronautical Engineering Laboratory Report No. 184, November 30, 1951.

[17] Chapman, D. R., Wimbrow, W. R., and Kester, R. H., *Experimental Investigation of Base Pressure on Blunt-Trailing-Edge Wings at Supersonic Velocities*, N.A.C.A. T.N. No. 2611, January, 1952.

[18] Van Driest, E. R., *Turbulent Boundary Layer in Compressible Fluids*. Journal of the Aeronautical Sciences, Vol. 18, No. 3, pp. 145–160, 216, March, 1951.

[19] Wilson, R. E., *Turbulent Boundary Layer Characteristics at Supersonic Speeds—Theory and Experiment*, Journal of the Aeronautical Sciences, Vol. 17, No. 9, pp. 585–593, September, 1950.

[20] Bogdonoff, S. M., *A Preliminary Study of Reynolds Number Effects on Base Pressure at $M = 2.95$*, Journal of the Aeronautical Sciences, Vol. 19, No. 3, p. 201, March, 1952.

[21] Bursnall, W. J., and Loftin L. K., *Experimental Investigation of Localized Regions of Laminar-Boundary Layer Separation*, N.A.C.A. T.N. No. 2338, April, 1951.

[22] Bardsley, O., and Mair, W. A., *The Interaction between an Oblique Shock-Wave and a Turbulent Boundary Layer*, Phil. Mag., Ser. 7, vol. 42, pp. 29–36, January, 1951.

Proceedings

Third Anglo-American Aeronautical Conference

Now Available

Proceedings of the Joint Conference between the Royal Aeronautical Society and the Institute, held in Brighton last September, are now ready for distribution in England. These volumes contain all of the full-length papers and discussions presented at the Conference. Only a limited supply is available for distribution.

Order Direct from

The Royal Aeronautical Society

4 Hamilton Place — London, W. 1, England

Send remittance with order:
£5.5.0 ($14.70), postage prepaid.

(10% U.S. Customs Duty
Payable upon Receipt.)

A Method for Reducing the Analysis of Complex Redundant Structures to a Routine Procedure

L. B. WEHLE, JR.,* AND WARNER LANSING*

Grumman Aircraft Engineering Corporation

(I) SUMMARY

A general method based on minimum strain energy is given for the analysis of statically indeterminate structures. Matrix methods are used throughout.

The procedure divides the work into three phases: (1) the writing of the equilibrium equations that determine the load distribution in the structure after it has been made statically determinate; (2) the tabulation of the flexibilities of the individual members comprising the structure; and (3) the self-checking matrix operations, which can be performed in a routine manner. In connection with phase (2), formulas and curves are provided for some of the elements used most frequently in idealizing aircraft structures.

The method has been applied at the design stage to various components of several modern aircraft. For purposes of demonstration, a simplified example is worked out in this paper. The structure representing the root portion of a sweptback wing, having taper in plan form and thickness and nonparallel tapered bulkheads, is idealized, and its load distribution and deformation characteristics are obtained.

(II) INTRODUCTION

CHANGING MISSIONS OF high- and low-speed aircraft are constantly giving rise to new structural arrangements that must be designed to minimum weight. Some of these structures are highly indeterminate and of such an unfamiliar form that neither the commonly used short-cut methods nor previous test experience provides sufficiently accurate information for structural design. The method presented here was developed for this type of structure and reduces the analysis to a routine procedure.

The basis for the procedure is the commonly used method of least work, which Levy[1] and Lang and Bisplinghoff[2] have recently demonstrated in connection with certain swept and unswept wings and which other authors[3–5] have applied to similar problems. As usually employed, this method is cumbersome and somewhat disorganized; however, if airplanes are to be completed on schedule, a procedure that is routine and yet can be applied to any irregular structure should be available to designers. The procedure given here is an attempt to fill that need, and it has been successfully applied to the design of the unique structures found in several sweptback wings, as well as to other problems such as those involving rigid frames and thick plates.

Simplicity is obtained in this method by separating the various operations required by any indeterminate analysis. This permits the intermediate results to be visualized while the calculations are in process and allows most of the operations to be distributed to computers for maximum efficiency.

In this paper the theoretical development used to justify the recommended procedure is first given. There follows a summary of those formulas that are actually required in the computation, together with a discussion of the procedure to be followed. Thereafter, a collection is included of the elastic properties of a number of the structural elements which may be encountered in an aircraft problem. In order to demonstrate the application to an actual structure, an example is given of the analysis of a simplified swept two-cell box.

(III) SYMBOLS

P_m, P_n, P_u = applied loads

q_i, q_j = member loads, any load acting directly upon an individual member; this includes any applied load or reaction acting directly upon a member and all redundant loads

q_r, q_s, q_t = redundant loads

γ_{im}, γ_{jn} = unit load distribution due to applied loads when all redundant loads are set equal to zero; ith (jth) member load due to a unit mth (nth) applied load

γ_{ir}, γ_{js} = unit load distribution due to redundant loads when all applied loads are set equal to zero; ith (jth) member load due to a unit rth (sth) redundant load

Γ_{rm}, Γ_{sn} = rth (sth) redundant load due to a unit mth (nth) applied load

Γ_{im} = unit load distribution in redundant structure; ith member load due to a unit mth applied load

U_a = strain energy of ath structural member

U = strain energy of entire structure

α_{aij} = flexibility influence coefficient for the ath member; displacement at load q_i due to a unit member load q_j, where q_i and q_j include all loads acting on the member except those at assumed support points

α_{ij} = sum of α_{aij} terms for all members

Presented at the Structures Session, Twentieth Annual Meeting, I.A.S., New York, January 28–February 1, 1952.

* Structural Methods Engineer.

α_{mn}, α_{ms}, α_{rn}, α_{rs} = flexibility influence coefficients for the statically determinate structure; displacement at load P_m or q_r due to a unit load P_n or q_s

A_{mn} = flexibility influence coefficient for the redundant structure; displacement at load P_m due to a unit load P_n

δ_{ai} = displacement of ath member at load q_i with respect to assumed support points

δ_m = displacement of redundant structure at load P_m

$[\ ]$ = a matrix

$\{\ \}$ = a column matrix

$[\ ]'$ = the tranpose of a matrix

$[\ ]^{-1}$ = the inverse of a matrix

(IV) Theory

The purpose of this section is to justify the procedure, discussed in Section (V) for solving structural problems.

(1) Statically Determinate Load Distribution

The structure to be analyzed is idealized as consisting of a number of structural elements such as axially loaded bars, shear panels, beams, or any other convenient elements whose deformation characteristics are either known or can be easily obtained. The structure as a whole is acted upon by certain externally applied loads that are designated by P's, each P having assigned to it a separate numerical subscript. For the purpose of the derivation, these subscripts are described only by the letters m, n, or u. The loads acting on the members are designated by q's, each q having a different numerical subscript which is symbolized by i or j. The q's may represent forces, shear flows, moments, etc., and as such may be considered as generalized forces. The extent to which the internal loads are broken down into separate q's will depend upon both equilibrium and energy considerations. This point is discussed more completely in the next section.

With certain of the member loads considered as redundant and therefore as having arbitrary magnitudes along with the applied loads, a balanced load distribution may be obtained by first writing the proper equations of equilibrium. These equations will be of the form

$$c_{11}q_1 + \ldots + c_{1i}q_i + \ldots + c_{1m}P_m + \ldots = 0 \quad (1)$$

Designating the numerical subscripts of the redundant member loads by r, s, or t, these equations may be solved to yield expressions for the member loads in terms of the applied loads and redundants

$$\left.\begin{aligned} q_1 &= \ldots + \gamma_{1m}P_m + \ldots + \gamma_{1r}q_r + \ldots \\ &\vdots \\ q_i &= \ldots + \gamma_{im}P_m + \ldots + \gamma_{ir}q_r + \ldots \end{aligned}\right\} \quad (2a)$$

in which a trivial relation $q_i = q_r$ or $q_i = P_m$ is introduced wherever a member load is also a redundant load or an applied load—that is, where the subscripts i and r or i and m are identical. This result may be written in matrix form as

$$\{q_i\} = [\gamma_{im}]\{P_m\} + [\gamma_{ir}]\{q_r\} \quad (2b)$$

In this equation the γ's may be regarded as load distributions in the statically determinate structure due to unit applied loads or redundants. The numerical calculations will be more compact if the terms on the right-hand side of Eq. (2b) are combined. It may be rewritten as

$$\{q_i\} = [\gamma_{im}\vdots\gamma_{ir}]\{P_m\vdots q_r\} \quad (2c)$$

in which a dashed line indicates partitioning of a matrix.

(2) Strain Energy

The strain energy to be minimized is collected from the individual members. Each member deforms under the loads q applied to it by adjoining members. For any member a, certain of these loads may be regarded as reactions; the rest, as causing deflection of the structure relative to these reactions. The relative deflection δ_{ai} at the load q_i depends on the loads applied at that point and at other points.

$$\delta_{ai} = \alpha_{ai1}q_1 + \alpha_{ai2}q_2 + \ldots + \alpha_{aij}q_j + \ldots \quad (3a)$$

In matrix notation the set of equations is given by

$$\{\delta_{ai}\} = [\alpha_{aij}]\{q_j\} \quad (3b)$$

It is seen that the α_a's describe the flexibility of member a. Thus, α_{aij} is the member displacement at q_i relative to the chosen reactions and brought about by applying a unit value of the jth load. The energy in each member is

$$U_a = (1/2)(q_1\delta_{a1} + q_2\delta_{a2} + \ldots + q_i\delta_{ai} + \ldots) \quad (4a)$$

or

$$U_a = (1/2)[q_i]\{\delta_{ai}\} \quad (4b)$$

Substituting Eq. (3b) into Eq. (4b), the energy in any one member is

$$U_a = (1/2)[q_i][\alpha_{aij}]\{q_j\} \quad (4c)$$

Since few of the members will be acted upon by more than one or two loads that do not have to be regarded as reactions, each α_{aij} matrix is made up largely of zero elements. The strain energy for the entire structure, in terms of the member loads, is the sum of expressions of the form of Eq. (4c) for all members.

$$U = U_1 + U_2 + \ldots + U_a + \ldots \quad (5a)$$

$$= (1/2)[q_i][\alpha_{ij}]\{q_j\} \quad (5b)$$

where

$$[\alpha_{ij}] = [\alpha_{1ij}] + [\alpha_{2ij}] + \ldots + [\alpha_{aij}] + \ldots \quad (5c)$$

The next requirement is to determine the strain energy for the structure as a function of the applied loads P_m and the redundants q_r. This can be obtained by substituting Eq. (2c) in Eq. (5b).

$$U = 1/2[P_m|q_r][\gamma_{im}|\gamma_{ir}]'[\alpha_{ij}][\gamma_{jn}|\gamma_{js}]\{P_n|q_s\} \tag{6a}$$

where the primed symbol [ ]′ is used to denote a matrix in which the rows and columns are interchanged.

Letting

$$[\gamma_{im}|\gamma_{ir}]'[\alpha_{ij}][\gamma_{jn}|\gamma_{js}] = \left[\begin{array}{c|c}\alpha_{mn} & \alpha_{ms} \\ \hline \alpha_{rn} & \alpha_{rs}\end{array}\right] \tag{6b}$$

the energy becomes

$$U = \frac{1}{2}[P_m|q_r]\left[\begin{array}{c|c}\alpha_{mn} & \alpha_{ms} \\ \hline \alpha_{rn} & \alpha_{rs}\end{array}\right]\{P_n|q_s\} \tag{6c}$$

(3) Solution of Member Loads

If Eq. (6c) is differentiated[6] with respect to one of the redundants q_t, the result is

$$\frac{\partial U}{\partial q_t} = \frac{1}{2}[P_m|q_r]\{\alpha_{mt}|\alpha_{rt}\} + \frac{1}{2}[\alpha_{ts}|\alpha_{ts}]\{P_n|q_s\} \tag{7a}$$

Since r and s are interchangeable, m and n are interchangeable, and the square array of α's in Eq. (6c) is symmetrical about its diagonal, the two terms of Eq. (7a) are equivalent and the equation may be rewritten

$$\partial U/\partial q_t = [\alpha_{tn}|\alpha_{ts}]\{P_n|q_s\} \tag{7b}$$

Applying the principle of minimum strain energy, Eq. (7b) must be equated to zero, and as many equations of this form as there are redundants may be written by letting t assume, successively, all the values of r. The resulting set of equations,

$$[\alpha_{rn}|\alpha_{rs}]\{P_n|q_s\} = 0 \tag{7c}$$

may be solved for the redundant member loads to give

$$\{q_s\} = -[\alpha_{rs}]^{-1}[\alpha_{rn}]\{P_n\} \tag{8a}$$

By letting

$$[\Gamma_{rm}] = [\Gamma_{sn}] = -[\alpha_{rs}]^{-1}[\alpha_{rn}] \tag{8b}$$

this same result may be rewritten

$$\{q_r\} = [\Gamma_{rm}]\{P_m\} \tag{8c}$$

Eq. (8c) can now be substituted back into Eq. (2b) to obtain the values of all the member loads in terms of the applied loads only.

$$\{q_t\} = [\gamma_{tm}]\{P_m\} + [\gamma_{tr}][\Gamma_{rm}]\{P_m\} \tag{9a}$$

The same result may be written more compactly as

$$\{q_t\} = [\gamma_{tm}|\gamma_{tr}]\left[\begin{array}{c}I \\ \hline \Gamma_{rm}\end{array}\right]\{P_m\} \tag{9b}$$

in which $[I]$ = unit diagonal matrix.

If

$$[\Gamma_{tm}] = [\gamma_{tm}|\gamma_{tr}]\left[\begin{array}{c}I \\ \hline \Gamma_{rm}\end{array}\right] \tag{9c}$$

then

$$\{q_t\} = [\Gamma_{tm}]\{P_m\} \tag{9d}$$

and $[\Gamma_{tm}]$ is the unit load distribution matrix for the indeterminate structure. Each term Γ_{tm} is the value of the tth member load when the structure is subjected to a unit value of the mth applied load.

(4) Deflections of Redundant Structure

If in Eq. (7b) the differentiation is performed with respect to an applied load P_u instead of a redundant load q_t, Eq. (7b) becomes

$$\partial U/\partial P_u = [\alpha_{un}|\alpha_{us}]\{P_n|q_s\} \tag{10a}$$

By Castigliano's theorem, this is equal to the deflection δ_u at the uth applied load. Letting u assume, successively, all the values for m, the deflections δ_m corresponding to the applied loads are

$$\{\delta_m\} = [\alpha_{mn}|\alpha_{ms}]\{P_n|q_s\} \tag{10b}$$

Substituting Eq. (8c) in Eq. (10b),

$$\{\delta_m\} = [\alpha_{mn}|\alpha_{ms}]\left[\begin{array}{c}I \\ \hline \Gamma_{sn}\end{array}\right]\{P_n\} \tag{11a}$$

Letting

$$[A_{mn}] = [\alpha_{mn}|\alpha_{ms}]\left[\begin{array}{c}I \\ \hline \Gamma_{sn}\end{array}\right] \tag{11b}$$

$$\{\delta_m\} = [A_{mn}]\{P_n\} \tag{11c}$$

An element of the A_{mn} matrix represents the displacement at the mth applied load due to a unit nth applied load.

(V) Procedure

Since all of the steps in Section (IV) are not required in solving a problem a summary is given of those items which are needed in obtaining the unit load distributions and deflections. In addition certain necessary details are discussed.

(1) Summary of Formulas

Eq. (2c), $[\gamma_{im}|\gamma_{ir}]$ (load distribution from the equations of statics).

Eq. (4c), $[\alpha_{aij}]$ (flexibilities of individual members to be obtained from formulas and curves).

Eq. (5c), $[\alpha_{ij}]$ (sums of member flexibilities).

Eq. (6b),

$$\left[\begin{array}{c|c} \alpha_{mn} & \alpha_{ms} \\ \hline \alpha_{rn} & \alpha_{rs} \end{array}\right] = [\gamma_{im}|\gamma_{ir}]'[\alpha_{ij}][\gamma_{jn}|\gamma_{js}]$$

(flexibility of determinate structure).

Eq. (8b), $[\Gamma_{rm}][\Gamma_{sn}] = -[\alpha_{rs}]^{-1}[\alpha_{rn}]$ (solution for redundant loads in terms of unit applied loads).

Eq. (9c),

$$[\Gamma_{im}] = [\gamma_{im}|\gamma_{ir}]\left[\begin{array}{c} I \\ \hline \Gamma_{rm} \end{array}\right]$$

(unit load distributions for indeterminate structure).

Eq. (11b),

$$[A_{mn}] = [\alpha_{mn}|\alpha_{ms}]\left[\begin{array}{c} I \\ \hline \Gamma_{sn} \end{array}\right]$$

(flexibility influence coefficients of indeterminate structure).

(2) Setting Up the Problem

For the structure as a whole, certain of the external loads are reactions; the rest are applied loads and are designated by P_m. If a reaction is also a redundant, it is designated by a q_r symbol and treated accordingly. Any load that acts directly on a member may be designated by q_i and may be included in the analysis; this includes applied loads, external reactions, and redundant loads. However, it is of advantage to include only (1) those loads that will be of importance in interpreting the analysis, (2) those loads that are used to express the individual member flexibilities (*i.e.*, at least one load per member), and (3) all redundants.

In connection with the foregoing item (2), a distinguishing feature of this analysis procedure is the breakdown of the load distribution into individual member loads for each element. Although this may entail the inclusion of a large number of loads in the calculations, it greatly simplifies the determination of member influence coefficients, which may then be copied directly from the standard texts or from the collection of elementary cases in Section (VI).

When the equilibrium equations are set up, they must be independent, and the total number of equations must be equal to the number of member loads q_i considered, less the number of redundants q_r. Engineering judgment is still necessary in selecting the redundant member loads, although certain rules are available for determining both the degree of redundancy and the particular redundant loads.

(3) Determining Member Influence Coefficients

A collection of influence coefficients for structural elements has been included in Section (VI). Some are also available in standard references. Section (VI) includes most of the structural elements that occur in indeterminate problems, but it is by no means complete, and the flexibilities of other elements may be desired in some problems. Although the flexibilities of special elements may be calculated, it is well to remember that it is this aspect of a structure which is most unpredictable because of thickness tolerances, connection deflections, buckling, shear lag, etc.; consequently, the engineering approximation involved in using flexibilities for standard members and loadings may often be justified.

Since one or more of the loads on any member may be considered as reactions and since the choice of reactions is arbitrary, the energy of a member may usually be expressed in terms of one of a number of sets of influence coefficients. Care in selecting these reactions may allow the omission of certain of the q_i's from the problem. For this reason, certain alternative sets of influence coefficients are given in Section (VI).

In some cases it may be an advantage to solve the problem by parts, obtaining the flexibilities of parts of the structure by the foregoing method and then combining the parts in a simpler final operation.

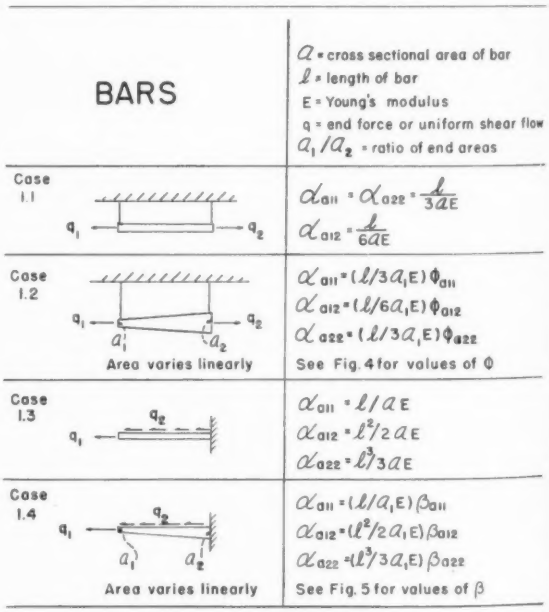
BARS
a = cross sectional area of bar
l = length of bar
E = Young's modulus
q = end force or uniform shear flow
a1/a2 = ratio of end areas
Case 1.1
Case 1.2
Area varies linearly
See Fig. 4 for values of Φ
Case 1.3
Case 1.4
Area varies linearly
See Fig. 5 for values of β

Fig. 1. Flexibilities of bars.

(4) Matrix Operations

One of the large labor items is the solving of the equations of equilibrium [Eq. (1)] to obtain the statically determinate load distribution [Eq. (2c)]. The authors have usually used the Gauss elimination method for this step, although other good methods are available.

It is well to emphasize that all matrix operations should carry check rows or check columns in order that mechanical errors may be detected as soon after they are made as possible. This check should be made even if the calculations are performed by means of IBM equipment.

Eq. (8b) of the summary of formulas calls for the inversion of $[\alpha_{rs}]$ and its post multiplication by $-[\alpha_{rn}]$. Although this indicates the end result desired, the authors have usually found it more convenient to solve Eq. (7c) for $[\Gamma_{rm}]$ directly by the Gauss elimination method.

In a design problem, the applied loads P_m may occur in a number of different combinations corresponding to different analysis conditions. In this case the P's may better be arranged in a rectangular matrix, where the typical element P_{mc} is the value of the mth applied load in the cth condition. Eq. (9d) is then written

$$[q_{ic}] = [\Gamma_{im}][P_{mc}] \tag{9e}$$

(VI) Formulas and Curves for Flexibilities of Certain Structural Elements

The separation of a complex structure into its components results in a number of elements whose flexibilities may be obtained from simple formulas. This section presents the formulas for the simplest commonly used elements such as rectangular shear panels and constant section bars and beams. However, since these idealizations are not usually met with in practice, the more generalized cases such as bars and beams of varying section and shear panels of parallelogram, trapezoidal, and quadrilateral shape are also included (see Figs. 1, 2, 3, 4, and 5).

(VII) An Example

An example that demonstrates the method has the idealized structure shown in Figs. 6 and 7. As can be seen, it is a two-cell cantilever sweptback box, which is symmetrical about its chord plane, is tapered in three directions, and has a single elastic tip bulkhead. The idealization concentrates the direct load-carrying material into bars at the front, main, and rear beams, plus a capstrip for the bulkhead, leaving the covers and webs loaded by edge shears only. This particular structure is selected only for convenience in demonstrating the method; in an actual wing the idealization would have to be more detailed.

The loads have been broken down into four applied loads and 17 member loads, of which three are redundant. The applied loads $P_{18 \ldots 21}$ consist of a

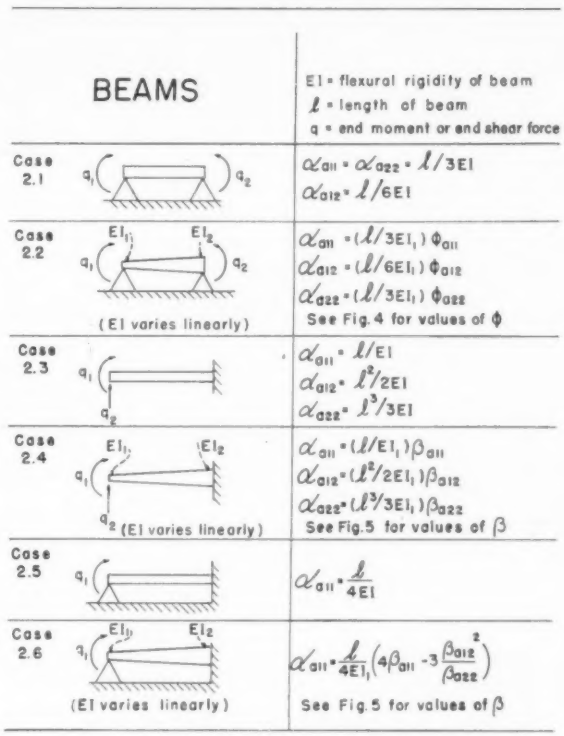

FIG. 2. Flexibilities of beams.

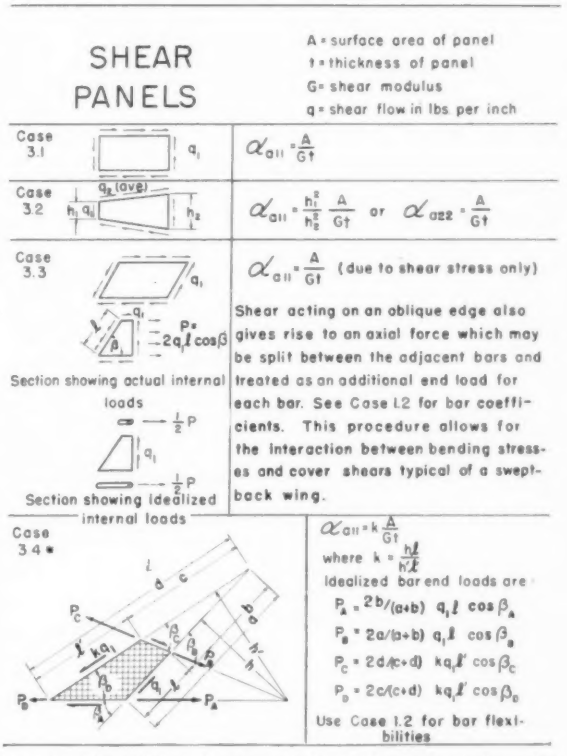
SHEAR PANELS
A = surface area of panel
t = thickness of panel
G = shear modulus
q = shear flow in lbs per inch
Case 3.1
$\alpha_{a11} = \frac{A}{Gt}$
Case 3.2
$\alpha_{a11} = \frac{h_1^2}{h_2^2}\frac{A}{Gt}$ or $\alpha_{a22} = \frac{A}{Gt}$
Case 3.3
$\alpha_{a11} = \frac{A}{Gt}$ (due to shear stress only)
$P = 2q_1 l \cos\beta$
Shear acting on an oblique edge also gives rise to an axial force which may be split between the adjacent bars and treated as an additional end load for each bar. See Case 1.2 for bar coefficients. This procedure allows for the interaction between bending stresses and cover shears typical of a sweptback wing.
Section showing actual internal loads
Section showing idealized internal loads
Case 3.4*
$\alpha_{a11} = k\frac{A}{Gt}$
where $k = \frac{hl}{h'l'}$
Idealized bar end loads are
$P_A = 2b/(a+b)\ q_1 l \cos\beta_A$
$P_B = 2a/(a+b)\ q_1 l \cos\beta_B$
$P_C = 2d/(c+d)\ kq_1 l' \cos\beta_C$
$P_D = 2c/(c+d)\ kq_1 l' \cos\beta_D$
Use Case 1.2 for bar flexibilities

FIG. 3. Flexibilities of shear panels. * Approximate formulas in Case 3.4 were derived from reference 7.

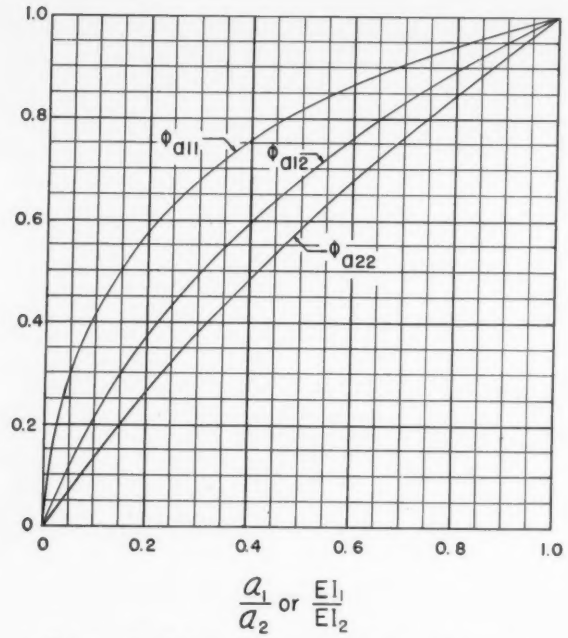

FIG. 4. Coefficients ϕ for tapered bars and beams.

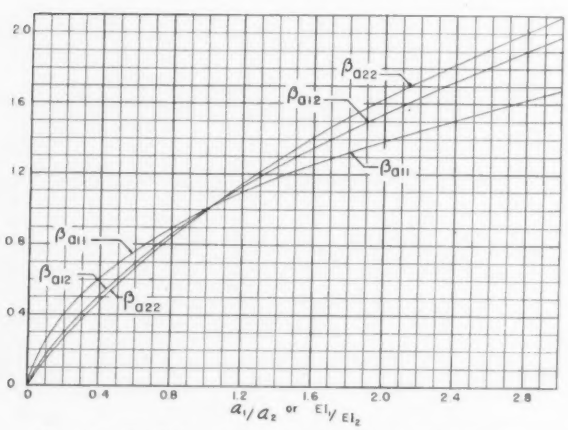

FIG. 5. Coefficients β for tapered bars and beams.

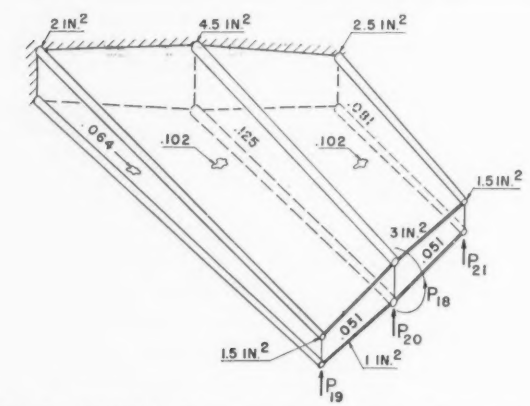

FIG. 6. Applied loads and structural element dimensions for example structure.

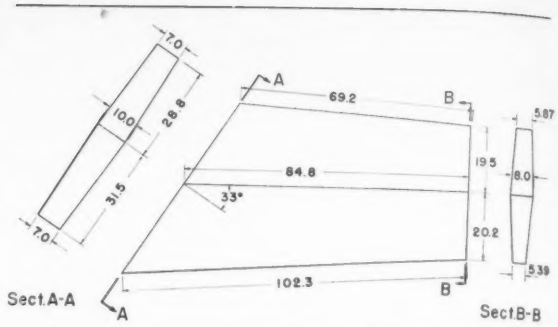

FIG. 7. Plan view and sections of example structure.

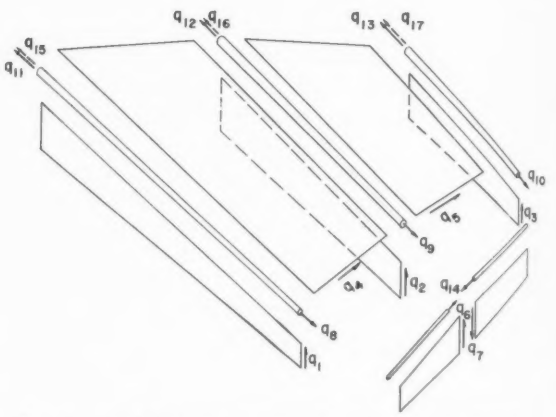

FIG. 8. Load designation diagram for example structure.

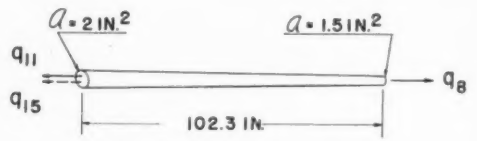

FIG. 9. Front beam capstrip.

due to unit load P_m or q_r

Load q_i	m,r / 18	19	20	21	1	11	13
1					1.000000		
2	-.006539	.202672	.124780	.049784	-2.303231	-.015334	.005062
3	-.000012	-.080191		.077412	1.181478	.009490	-.009398
4	.004157				1.167160	.014793	
5	-.004632	.070578		-.068132	-1.039844	-.008352	-.006904
6	.000613	-.084132			.453648		
7	-.000452	.043146		.050008	-.635681	-.005106	.005056
8	-.281000						
9	-.835000						
10	-.306000						
11						1.000000	
12	-1.000000	-.980989	-.847254	-.719504		-.670644	-.730310
13							1.000000
14	.102346	-.252394			32.186060	.298693	
15	.065015				18.254382	.231363	
16	-.002905	.067845		-.030837	3.128466	.012689	-.004458
17	-.073186	.115132		-.076486	16.429535	-.131962	-.109083

FIG. 10. $[\gamma_{im} : \gamma_{ir}]$, load distribution in determinate structure.

bending moment and shears at the front, main, and rear beams, respectively, all acting at the outboard end. The bending moment P_{18} is assumed to enter the structure distributed according to engineering beam theory and is in units of 10 in.lbs. The shear forces $P_{19} \ldots _{21}$ are in units of 1 lb.

The breakdown into structural elements, together with member load designations $q_1 \ldots _{17}$ is illustrated in Fig. 8. Because of symmetry, only the member loads above the chord plane need be considered. In the case of each shear panel, the average shear flow on only one of the edges is represented by a q because the average shear flow on each of the other three edges may be given by this q times the proper numerical constant, as determined by statics. This permits the omission of three nonessential internal loads for each panel.

The member loads q_{15}, q_{16}, and q_{17} shown at the inboard ends of the three bars represent the axial stress components of the shear in the swept covers. Since the idealization of the structure places all axially effective material in the bars, this component must be included with the bar loads in the energy calculations even though it is not physically applied to the bar ends. Hence, the loads are shown dashed. Values may be obtained for these loads by use of shear panel Case 3.4.

The three member loads selected as redundant in this analysis are the shear flow in the front beam web q_1 and the forces at the inboard ends of the front and rear bars q_{11} and q_{13}. The 14 equilibrium equations, used to find the determinate load distribution, may be described as follows:

Eqs. (1), (2), and (3), loads at outboard ends of bars due to tip bending moment P_{15}.

Eqs. (4), (5), and (6), spanwise equilibrium of bars.

Eq. (7), bending equilibrium at root section.

Eq. (8), moment equilibrium for tip bulkhead in its own plane.

Eq. (9), vertical equilibrium at attachment of rear beam to tip bulkhead.

Eq. (10), chordwise equilibrium of forward cap of tip bulkhead.

Eq. (11), chordwise equilibrium of rear cap of tip bulkhead.

Eqs. (12), (13), and (14), determination of axial component of skin shear load.

The dimensions entering these equations are scaled from a $^1/_8$-size plan view and therefore represent lengths projected onto the chordal plane. The fourth equation is typical; it places the front beam capstrip in equilibrium.

$$q_{11} + 102.3(0.771q_1 - 0.661q_4) - q_8 = 0$$

Here, and also at the stage where the member influence coefficients are written down, mere slide rule accuracy is necessary. The machine calculations representing the subsequent steps require greater precision in order that the final results may be as accurate as the initial data.

	1	2	3	4	5	6	7	8	9	10	11	12	13	14	15	16	17
1	15330	10200	10070	07000	04200	05210	02335										
2								42.2	16.88	26.7	17.56	7.58	11.62		17.56	7.58	11.62
3								19.56	7.58		36.6	13.76			36.6	13.76	
4										11.62			20.7	26.5			20.7
5								19.56	7.58	11.62	36.6	13.76	20.7		36.6	13.76	20.7
6																	
7																	

FIG. 11. $[\alpha_{ij}]$, sum of member flexibilities.

due to unit load P_m

load q_i \ m	18	19	20	21
1	-.002233	.067753	.022315	-.005433
2	-.002535	.063612	.076486	.056828
3	.000920	.008035	.043735	.094429
4	.000416	.048117	.008016	-.016694
5	.001489	.038204	.008232	-.034542
6	-.000400	-.053396	.010123	-.002465
7	-.000953	-.004321	-.023529	.040854
8	-.281000	0	0	0
9	-.835000	0	0	0
10	-.306000	0	0	0
11	-.076721	-2.092985	-1.218725	-.699830
12	-.614498	-6.226511	-5.406657	-4.389111
13	-.457408	-2.983541	-3.078920	-3.200362
14	-.003606	-.629638	.165782	-.411066
15	.006503	.752550	.125379	-.261091
16	.029243	1.355606	.254093	-.792394
17	.023521	.603630	.130058	-.545768

FIG. 12. $[\Gamma_{im}]$, load distribution in redundant structure.

The next step is to obtain the flexibility influence coefficients for the individual members of the structure. These are written using the formulas and curves of Section (VI). Case 1.2 is used for the bars even though the edge shears in the tapered panels are actually variable rather than constant. The difference should be negligible here, although in extreme cases it would be necessary to take this factor into account

A typical flexibility calculation is that for the front beam capstrip. This bar is shown in Figs. 8 and 9. Applying Case 1.2 of Section (VI),

$$\alpha_{a11,11} = \alpha_{a11,15} = \alpha_{a15,15} = \frac{102.3 \times 0.804}{3 \times 1.5} = 18.30$$

$$\alpha_{a11,8} = \alpha_{a15,8} = \frac{102.3 \times 0.860}{6 \times 1.5} = 9.78$$

$$\alpha_{a8,8} = (102.3 \times 0.928)/(3 \times 1.5) = 21.1$$

For convenience, the modulus of elasticity is taken as $E = 1$ and Poisson's ratio is 0.3. The influence coefficients for the other members are calculated in a like manner, and all are assembled in the α_{ij} matrix, Fig. 11.

displacement at P_m due to unit load P_n

m \ n	18	19	20	21
18	38.0	111.7	118.6	125.1
19	111.6	910.1	648.8	499.1
20	118.6	648.8	698.0	676.4
21	125.1	499.1	676.4	926.2

FIG. 13. $[A_{mn}]$, flexibility of redundant structure.

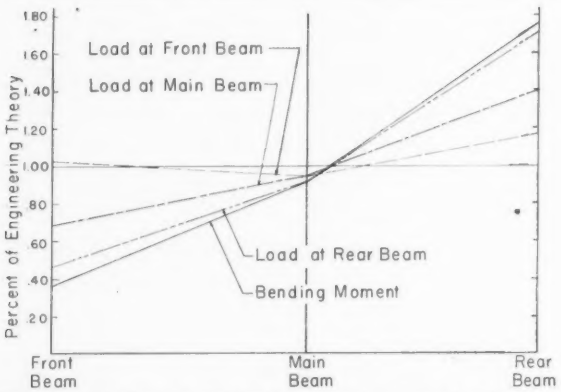

FIG. 14. Axial stress distribution at root compared with engineering beam theory.

The remaining work is entirely mechanical. The solution of the equilibrium equations yields the $[\gamma_{im}; \gamma_{ir}]$ matrix of Eq. (2c), and this result is shown in Fig. 10. Note that one's are inserted where a member load is also a redundant—that is, for q_1, q_{11}, and q_{13}. Following this, the matrix multiplications listed in the summary of formulas, Section (VI), may be carried out. The final result in the form of the unit load distribution $[\Gamma_{im}]$ and the flexibility influence coefficients $[A_{mn}]$ for the redundant structure are given in Figs. 12 and 13.

It is interesting to see that even this simplified structure exhibits the characteristic behavior of a sweptback wing with built-in root. Perhaps the most significant feature is the concentration of axial loading in the rear beam at the inboard end. The variation from engineering beam theory distribution in this region is shown in Fig. 14.

(VIII) References

[1] Levy, S., *Computation of Influence Coefficients for Aircraft Structures with Discontinuities*, Journal of the Aeronautical Sciences, Vol. 14, No. 10, p. 547, October, 1947.

[2] Lang, A. L., and Bisplinghoff, R. L., *Some Results of Sweptback Wing Structural Studies*, Journal of the Aeronautical Sciences, Vol. 18, No. 11, p. 705, November, 1951.

[3] Hemp, W. S., *On the Analysis of Statically Indeterminate Structures*, Aeronautical Research Council Reports and Memoranda No. 2396, 1950.

[4] Goran, L. A., *A Minimum Energy Solution and an Electrical Analogy for the Stress Distribution in Stiffened Shells*, Journal of the Aeronautical Sciences, Vol. 18, no. 6, p. 407, June, 1951.

[5] Heldenfels, R. R., Zender, G. W., and Libove, C., *Stress and Distortion Analysis of a Swept Box Beam Having Bulkheads Perpendicular to the Spars*, N.A.C.A. T.N. No. 2232, November, 1950.

[6] Frazer, R. A., Duncan, W. J., and Collar, A. R., *Elementary Matrices*, 1st Ed., p. 43; University Press, Cambridge, 1938.

[7] Garvey, S. J., *The Quadrilateral Shear Panel*, Aircraft Engineering, Vol. 23, No. 267, p. 134, May, 1951.

[8] Lansing, W., and Wehle, L. B., Jr., *Theory and Procedure for Applying the Method of Least Work to the Elastic Analysis of Complex Aircraft Structures*, Grumman Report No. E-91, July 1, 1950.

Changes of Address

Since the Post Office Department does not as a rule forward magazines to forwarding addresses, it is important that the Institute be notified of changes in address 30 days in advance of publishing date to ensure receipt of every issue of the JOURNAL and REVIEW.

Notices should be printed legibly and sent directly to:

Institute of the Aeronautical Sciences, Inc.

2 East 64th Street, New York 21, New York

A Second-Order Solution for an Oscillating Two-Dimensional Supersonic Airfoil*

ALEXANDER WYLLY†
The RAND Corporation

SUMMARY

This paper presents a second-order solution for the forces and moments produced by an oscillating two-dimensional airfoil of arbitrary cross section. This solution, valid to the second order in angle of attack and thickness, is obtained by means of an iteration procedure.

One part of this paper is concerned with the development of a linearized (or first-order) velocity potential, which is of suitable form for use in the iteration procedure. This velocity potential is developed as a power series approximation, in frequency, to the exact linearized solution. The first six terms of this series are shown to be within a few per cent of the complete linearized solution when the reduced frequency ($\bar{\omega} = \omega\bar{C}/\beta^2 v_0$) is less than 1.3.

The second part of this paper is devoted to the development of the second-order solution in angle of attack. This latter is developed with the use of the above-mentioned series approximation to the linearized solution, and, since the linearized solution valid to the second order in frequency was utilized in the iteration procedure, the final solution is valid to the second order in angle of attack and frequency.

The second-order terms were found to have a relatively strong influence on the final solution, particularly for the pitching moment. It will be seen that in many cases the second-order terms are larger in magnitude than the corresponding first-order terms and, thus, reverse the tendencies indicated by first-order theory. In particular, it was shown that the theoretical instability predicted by linearized theory for an airfoil of zero thickness is completely eliminated for an airfoil having a thickness ratio as small as $4^1/_2$ per cent.

The damping moment for a $7^1/_2$ per cent thick airfoil was compared with that given by British experimental tests. The second-order solution is shown to be in much better agreement with the experimental data than the linearized theory; however, the magnitudes of the damping moments predicted by second-order theory are appreciably lower than those indicated by experiment.

SYMBOLS

c = speed of sound
$\bar{C}$ = chord of airfoil
C_L = lift coefficient
C_M = pitching moment coefficient
C_P = pressure coefficient; subscripts u and l refer to upper and lower surfaces
f = an arbitrary function of $(x - y\beta)$, which is defined as $f(\zeta) = f'(\zeta) = 0$ for $\zeta \leq 0$; $f'(\zeta) = \partial f(\zeta)/\partial\zeta$, and f and f' are continuous
g = an arbitrary function of $(x - y\beta)$, which is defined as $g(\zeta) = g'(\zeta) = 0$ for $\zeta \leq \bar{C}$, and g and g' are continuous
H = a function of the first-order (in α) velocity potential, which forms the nonhomogeneous portion of the wave equation to be satisfied by the second-order velocity potential
p = pressure
q = perturbation velocity = $\sqrt{u^2 + v^2}$
t = time
T = thickness of airfoil
u, v = perturbation velocities in the x, y directions
V_0 = free-stream velocity
x, y = coordinates, fixed in the leading edge of the airfoil with the positive x axis in the direction of the free stream
x_0 = nondimensional position of the point of rotation
α = angle of attack = $\alpha_M \cos \omega t$
α_M = maximum angle of attack, $\alpha_M << 1$
β = $\sqrt{M_0^2 - 1}$
ρ = density
$\bar{\Phi}$ = complete velocity potential
Φ = complete perturbation velocity potential
Φ_n^m = perturbation velocity potential correct to mth order in angle of attack α and nth order in frequency ω
φ_n^m = one term in series expansion of Φ_n^m, it includes the mth term in α and the nth term in frequency
φ = the portion of φ_n^2 which satisfies the nonhomogeneous wave equation; the "particular solution"
σ = the portion of φ_n^2 which satisfies the boundary conditions on the surface; the "correction potential"
ψ, θ = terms used in place of φ and σ for the discussion of more complex airfoils
ω = angular frequency in rad. per sec.
$\bar{\omega}$ = the reduced frequency = $\omega\bar{C}/\beta^2 V_0$
$(\ )_0$ = (subscript zero) free-stream condition

(I) INTRODUCTION

THE LINEARIZED THEORY for the supersonic, irrotational, nonviscous flow of a perfect gas past an oscillating wing is at present in a reasonably complete state of development. Progressing from the first investigations of nonstationary flow, by Possio[2] and von Borbély,[3] many authors have considered the two-dimensional oscillating airfoil problem. More recently, a number of linearized solutions[4–9] have been determined for nonstationary three-dimensional wings. Thus it seems probable that within a few years the first-order solution for almost any plan form will be available. The purpose of this paper is to extend the linearized solution for an oscillating two-dimensional airfoil to include the higher-order terms in angle of attack and thickness so that the relative importance of, and the tendencies indicated by, the second-order terms may be evaluated.

Received July 30, 1951.

* Based on Doctoral Thesis,[1] California Institute of Technology, 1951.

† Research Engineer, Missiles Division.

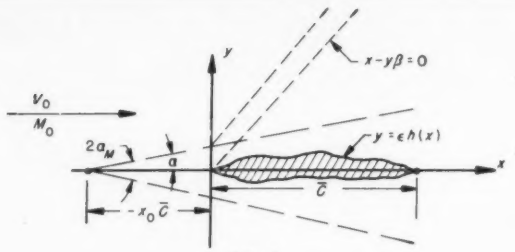

FIG. 1.

This paper is divided into three principal parts. The first part gives a general discussion of the problem. In this section the iteration procedure is applied to the complete nonlinear potential equation, and the partial differential equations that must be satisfied by the first- and second-order velocity potentials are determined. The first- and second-order boundary conditions are also discussed in this first part. The differential equations and the boundary conditions then completely specify the problem.

In the second part, a first-order solution, whose form and properties are satisfactory for use in the iteration procedure, is developed. In the iteration process each step of the iteration is dependent on the previous solution. Hence, to determine the second-order velocity potential, a first-order potential that is defined throughout the entire x, y plane and which is of a comparatively simple closed form must be available. A linearized velocity potential that satisfied these requirements was determined by Guderley[10] in 1946. In this paper Guderley produced the first two terms of the series expansion (in frequency†) of the linearized velocity potential. In the present paper, the expressions for both the first two terms and for the first six terms are presented. These solutions are valid throughout the whole x, y plane and are in a simple closed form.

In the third section of this paper, the second-order solution in angle of attack is developed for the case of a flat plate, a wedge airfoil, a double-wedge airfoil, and an airfoil of general cross-sectional shape. The lift and pitching moment coefficients for several modified double-wedge airfoils with different thickness ratios are compared with the coefficients as calculated by linearized theory. Finally, the damping moments predicted by first- and second-order theory are compared with those given by British experimental data.

† There is a tendency for the expression "order" to become confusing in this paper, since order can refer to the maximum angle of attack α_M, the thickness parameter ϵ, and the frequency ω. The maximum angle of attack and the thickness determine the order of the solution in the usual sense of the word—i.e., the first order (in α_M or ϵ) is the linearized solution. The maximum angle of attack and the thickness parameter are taken to be of similar magnitude, α_M is of $0(\epsilon)$, and for brevity are referred to as order in angle of attack. Any order solution in angle of attack may then be expanded into a series solution in powers of the frequency. Terms of this expansion are referred to as order in frequency.

(II) General Discussion of Problem

(A) *The Iteration Procedure*

The problem to be considered is the study of the surface pressures produced by the uniform flow of a perfect gas past an oscillating airfoil of general shape (see Fig. 1). The airfoil is required to be slender and the maximum angle of attack α_M is required to be small. The airfoil rotates about a point ($x = x_0\bar{C}$) located a nondimensional distance x_0 downstream from the leading edge. The angle of attack is defined by the symbol $\alpha = \alpha_M \cos \omega t$, where ω is the angular velocity of the oscillation. The angular velocity is limited by requiring that the reduced frequency be small. The flow is uniform upstream from the leading edge and is irrotational, isentropic, and nonviscous. The assumption that the flow is irrotational and isentropic is valid in this problem, since the effects of rotationality and changes in entropy are of third and higher order in angle of attack.

Under these assumptions we can derive the nonstationary Bernoulli equation [Eq. (1)] and the two-dimensional nonstationary potential equation [Eq. (2)] from Euler's equation, the equation of continuity, the condition of irrotationality, and the isentropic expression for the speed of sound.

$$\bar{\Phi}_t + \frac{1}{2} q^2 + \frac{c^2}{\gamma - 1} = \frac{c_0^2}{\gamma - 1} \tag{1}$$

$$\bar{\Phi}_{xx}(c^2 - \bar{\Phi}_x^2) + \bar{\Phi}_{yy}(c^2 - \bar{\Phi}_y^2) - \bar{\Phi}_{tt} - 2\bar{\Phi}_x\bar{\Phi}_y\bar{\Phi}_{xy} - 2\bar{\Phi}_x\bar{\Phi}_{xt} - 2\bar{\Phi}_y\bar{\Phi}_{yt} = 0 \tag{2}$$

The complete potential equation, Eq. (2), is nonlinear and cannot be solved directly. The approach to be used is that first suggested by Prandtl. It is assumed that the velocity potential $\bar{\Phi}$ may be approximated by the expression,

$$\bar{\Phi} = V_0 x + \alpha\varphi^1 + \alpha^2\varphi^2 + \alpha^3\varphi^3 + \ldots + \alpha^n\varphi^n \tag{3}$$

The term V_0x has been included in Eq. (3); hence, the φ's represent the perturbation potential, φ^n representing the nth-order potential. Since in this study only the second-order potential is desired, the terms φ^n for $n > 2$ may be neglected. Putting the series expansion for $\bar{\Phi}$ [Eq. (3)] into Eq. (2) and replacing the speed of sound c in Eq. (2) by its corresponding function of $\bar{\Phi}$ from Eq. (1), the potential equation becomes: *terms containing* α,

$$\Box\varphi^1 = \beta^2\varphi_{xx}{}^1 - \varphi_{yy}{}^1 + \frac{2M_0^2}{V_0}\varphi_{xt}{}^1 + \frac{M_0^2}{V_0^2}\varphi_{tt}{}^1 = 0 \tag{4}$$

here V_0/c_0 has been replaced by the Mach Number M_0 and $\beta = \sqrt{M_0^2 - 1}$; *terms containing* α^2,

$$\Box\varphi^2 = H(\varphi^1) = -\frac{M_0^2}{V_0^2}\left[(\gamma - 1)\,(\varphi_{xx}{}^1 + \varphi_{yy}{}^1) \times \left(\varphi_x{}^1 + \frac{1}{V_0}\,\varphi_t{}^1\right) + 2\varphi_x{}^1\left(\varphi_{xx}{}^1 + \frac{1}{V_0}\,\varphi_{xt}{}^1\right) + 2\varphi_y{}^1\left(\varphi_{xy}{}^1 + \frac{1}{V_0}\,\varphi_{yt}{}^1\right)\right] \quad (5)$$

These are the differential equations that must be satisfied by the first- and second-order potentials φ^1 and φ^2. Both of these equations are linear and may be solved by the usual methods applicable to linear differential equations. The method of solution is now apparent. First, one obtains the first-order solution φ^1 that satisfies Eq. (4), the homogeneous wave equation, and the proper first-order boundary conditions. Then, the function $H(\varphi^1)$ is calculated. Next, a second-order potential φ^2, which satisfies Eq. (5) (the nonhomogeneous wave equation) and the proper second-order boundary conditions, is determined.

The expression for the speed of sound c will be needed for the determination of the pressure coefficient. From Eqs. (1) and (3),

$$c^2 = c_0^2 - (\gamma - 1)\,\{V_0\Phi_x{}^2 + \Phi_t{}^2 + (1/2)\,[V_0{}^2 + (\Phi_x{}^1)^2 + (\Phi_y{}^1)^2]\} \quad (6)$$

The pressure coefficient C_p is determined by substituting the ratio $(c/c_0)^2$ from Eq. (6) into the isentropic relationship between the pressure and the speed of sound. The expression for the pressure coefficient is found to be

$$C_p = -2\left\{\frac{1}{V_0}\,\Phi_x{}^2 + \frac{1}{V_0{}^2}\,\Phi_t{}^2 - \frac{1}{2V_0{}^2}\left[\beta^2(\Phi_x{}^1)^2 - (\Phi_y{}^1)^2 + \frac{2M_0{}^2}{V_0}\,\Phi_x{}^1\Phi_t{}^1 + \frac{M_0{}^2}{V_0{}^2}\,(\Phi_t{}^1)^2\right]\right\} \quad (7)$$

The third- and higher-order terms have, of course, been neglected.

(B) *Boundary Conditions*

The flow is required to satisfy two boundary conditions:

(1) The resultant velocity must be tangent to the surface of the body.

(2) All perturbation velocities must vanish upstream from the plane $x = 0$.

From the theory of hyperbolic differential equations it is known that these two requirements are sufficient to determine the solution.

First, consider the tangency condition. If the surface of the plate is given as $y = h(x, t)$, the tangency condition at the surface of the body is

$$\{[\Phi_y{}^2 - (\partial h/\partial t)]/(V_0 + \Phi_x{}^2)\}_{y=h} = \partial h/\partial x \quad (8)$$

Here, the numerator on the left represents the difference in vertical velocity between the flow and the plate, while the term $(V_0 + \Phi_x{}^2)$ is the resultant velocity in the direction of flow. If Φ^2 is replaced by $\alpha\varphi^1 + \alpha^2\varphi^2$, where $\alpha\varphi^1$, $\partial h/\partial x$, and $\partial h/\partial t$ are of the order α while $\alpha^2\varphi^2$ is of order α^2, the boundary condition at the surface to first-order in α is

$$(\varphi_y{}^1)_{y=0} = V_0\,(\partial h/\partial x) + (\partial h/\partial t) \quad (9)$$

The second-order tangency condition may be determined by setting $\Phi^2 = \alpha\varphi^1 + \alpha^2\varphi^2$ and subtracting out the first-order equation [Eq. (9)]. The second-order tangency condition is found to be

$$(\varphi_y{}^2)_{y=0} = (\partial h/\partial x)\,(\varphi_x{}^1)_{y=0} + [(\varphi_y{}^1)_{y=0} - (\varphi_y{}^1)_{y=h}] \quad (10)$$

Now consider the condition that the perturbation potential vanish for $x \leq 0$. This requirement may be stated and satisfied in two physically different, and yet mathematically similar, ways. Since both definitions are used later, both will be presented.

The first approach requires that two conditions be imposed on the so-called timelike surface $x = 0$ and one condition along the spacelike surface of the body. The previously mentioned tangency condition is spacelike; hence, we have to impose two conditions on the plane $x = 0$. These are

$$\left.\begin{aligned}\Phi(0, y, t) &= 0\\ \Phi_x(0, y, t) &= 0\end{aligned}\right\} \quad (11)$$

These conditions, along with the differential equation and the tangency condition, completely specify the problem.

The second approach specifies the potential upstream by requiring that the potential be zero on the Mach line from the leading edge of the airfoil.

$$\varphi^1(x, x/\beta, t) = 0 \quad (12)$$

As expressed by Eq. (12), the potential goes to zero on the Mach wave through the origin and not on the oscillating Mach line from the leading edge. However, since the movement of the airfoil is considered to be small, the movement of the Mach wave only produces effects of a second order in angle of attack. Therefore, since this criterion will only be used in the determination of the first-order solution, the second-order effects may be neglected.

(III) First-Order Solution in Angle of Attack

In 1946, Guderley[10] wrote a paper entitled "The Pressure Distribution on a Flat Plate Oscillating with a Small Frequency." In this unpublished paper he produced, without any development, the first two terms of the series expansion in frequency (of the linearized velocity potential) for the flow over an oscillating flat plate. A similar solution will now be developed. The method of attack is interesting because it allows an algebraic determination of any desired number of the terms of the series expansion. The method is not restricted

to oscillatory motions but actually appears to be useful in the solution of any two-dimensional nonstationary supersonic airfoil problem.

The location of the surface of the airfoil (see Fig. 1) is given by the relation $y = \alpha(x - x_0\bar{C})$ (for $0 \leq x \leq \bar{C}$), where $\alpha = \alpha_M \cos \omega t$. The tangency condition, Eq. (9), is, thus,

$$(\varphi_y{}^1)_{y=0} = V_0\alpha + \dot{\alpha}(x - x_0\bar{C}) \tag{13}$$

Now consider the series expansion of φ^1 in powers of a nondimensionalized frequency $\bar{\omega}$. The so-called reduced frequency $\bar{\omega}$ ($\bar{\omega} = \omega\bar{C}/\beta^2 V_0$) is initially required to be small ($\bar{\omega} \ll 1$) in order that the higher order terms in frequency may be neglected. Later it will be seen that the sixth-order solution gives a good approximation to the exact solution for $\bar{\omega} < 1.4$. The series approximation to φ^1 is

$$\varphi^1 = \varphi_1{}^1 + \bar{\omega}\varphi_2{}^1 + \bar{\omega}^2\varphi_3{}^1 + \ldots + \bar{\omega}^n\varphi_{n+1}{}^1 = \Phi_{n+1}{}^1 \tag{14}$$

where $\varphi_n{}^1$ is the nth-order term in the series. It should be noted that, while the so-called first-order term in frequency does not contain $\bar{\omega}$, this term does contain the parameter $\alpha = \alpha_M \cos \omega t$. Thus, this term is due to the instantaneous position of the airfoil and is the first-order term in the frequency expansion.

From Eq. (13) it was seen that $\varphi_y{}^1$ at $y = 0$ was of the form

$$(\varphi_y{}^1)_{y=0} = V_0\alpha + \dot{\alpha}(x - x_0\bar{C})$$

Hence, $\Phi_2{}^1$ must be

$$\Phi_2{}^1 = \int_0^y (\varphi_y{}^1)_{y=0}\, dy + \alpha\{Ax + Dy^2 + Hxy + Fx^2 + Jx^3 + \ldots\} + \dot{\alpha}\{Bx + Ey^2 + Gx^2 + Ixy + Kx^3 + \ldots\} \tag{15}$$

where $A, B, \ldots, K$ are functions of x_0, $\bar{C}$, M_0, and velocity. The higher terms in frequency (i.e., $\ddot{\alpha}$, $\dddot{\alpha}$, etc.) are not included, since only a second-order solution in frequency is desired. $\Phi_2{}^1$ may now be determined algebraically by substituting Eq. (15) into Eqs. (4) and (12). When this is done, it will be seen that a set of n algebraic equations is derived which is exactly sufficient to determine the n unknown coefficients $A, B, \ldots, n$. To simplify the algebra, the unknown coefficients $J, \ldots, n$ will be taken to be zero immediately, although the same result would be obtained if they were allowed to remain through the derivation.

By integrating Eq. (15), it is found that $\Phi_2{}^1$ is of the form

$$\Phi_2{}^1 = yV_0\alpha + yx\dot{\alpha} - y\dot{\alpha}x_0C + \alpha\{Ax + Dy^2 + Fx^2 + Hxy\} + \dot{\alpha}\{Bx + Ey^2 + Gx^2 + Ixy\} \tag{16}$$

Now, substituting Eq. (16) into Eqs. (4) and (12), it follows that

$$\Box\Phi_2{}^1 = 0 = \beta^2(2F\alpha + 2G\dot{\alpha}) - (2D\alpha + 2E\dot{\alpha}) + (2M_0^2/V_0)(A\dot{\alpha} + 2xF\dot{\alpha} + 2Hy\dot{\alpha}) + 0(\ddot{\alpha})$$

$$\Phi_2{}^1\left(x, \frac{x}{\beta}, t\right) = 0 = \frac{V_0\,\alpha x}{\beta} + \frac{x^2\dot{\alpha}}{\beta} + \frac{xx_0C\dot{\alpha}}{\beta} + A\alpha x + B\dot{\alpha}x + \frac{D\alpha x^2}{\beta^2} + \frac{E\dot{\alpha}x^2}{\beta} + F\alpha x^2 + G\dot{\alpha}x^2 + \frac{H\alpha x^2}{\beta} + \frac{I\dot{\alpha}x^2}{\theta}$$

Rearranging these two equations according to the variables α, $\dot{\alpha}$, x, and y, a set of eight simultaneous algebraic equations with eight unknowns is determined. Again note that, if twenty unknown coefficients had been used, there would have been twenty simultaneous equations and the last twelve coefficients would be given as zero. Solving these eight simultaneous equations, the unknown coefficients are found to be

$$A = -\frac{V_0}{\beta}; \quad E = \frac{1 - 2M_0^2}{2\beta}; \quad G = \frac{1}{2}\beta^2$$

$$B = x_0\bar{C}/\beta; \quad D = F = H = I = 0$$

Hence, to the second order in frequency the linearized velocity potential is given as

$$\Phi_2{}^1 = y^2(\dot{\alpha}/2\beta)(1 - 2M_0^2) + y[\dot{\alpha}(x - x_0\bar{C}) + \alpha V_0] + (x^2\dot{\alpha}/2\beta^3) + (x/\beta)(x_0\bar{C}\dot{\alpha} - \dot{\alpha}V_0) \tag{17}$$

Eq. (17) is the solution given by Guderley for the potential of a flat plate oscillating such that $\bar{\omega} \ll 1$. As will be seen later, this solution approximates the exact linearized solution within a few per cent for $\bar{\omega} \leq 0.3$ (this would include such motion as control movements, stability, etc.).

The previously determined second-order solution will now be extended to include the linearized solution valid to the sixth order in frequency. Since the method is exactly the same as that given previously for the second-order solution in frequency, only the final equations will be presented. The determination of the solution is further simplified by the two following rules:

(*a*) No term Ax^ny may appear, since $\Phi_y \neq 0$ and the tangency y conditions would be changed.

(*b*) The symmetry shown in the first two terms of the series expansion is continued throughout the higher terms, and thus $\varphi_n{}^1 = F(x^my^p)$, where $[m + p = n, 0 \leq (m \text{ and } p) \leq n]$.

The final sixth-order solution in frequency which satisfies the requirements of Eqs. (4), 9, and 12 to 0 ($\bar{\omega}^6$) is presented below.

$$\Phi_0^1 = V_0\alpha\left(y - \frac{x}{\beta}\right) + \dot{\alpha}\left[y^2\left(\frac{1-2M_0^2}{2\beta}\right) + xy + x^2\left(\frac{1}{2\beta^3}\right) - x_0\bar{C}\left(y - \frac{x}{\beta}\right)\right] - \frac{\ddot{\alpha}M_0^2}{V_0}\left[x^2\left(\frac{1}{4\beta_6}\right) - y^3\left(\frac{1}{2}\right) + xy^2\left(\frac{2\beta^2-1}{4\beta^3}\right) - \frac{x_0\bar{C}}{2\beta}\left(\frac{x^2}{\beta^2} - y^2\right)\right] + \frac{\ddot{\alpha}M_0^2}{V_0^2}\left\{x^4\left(\frac{1+4M_0^2}{48\beta^7}\right) - y^4\left(\frac{2-12M_0^2+8M_0^4}{48\beta^3}\right) + \frac{xy^3}{6} - \frac{x^2y^2}{8\beta^5} - x_0\bar{C}\left[-\frac{x^3}{12\beta^5}(2M_0^2+1) + \frac{xy^2}{4\beta^3} + \frac{y^3}{6}\right]\right\} - \frac{\overset{\text{IV}}{\alpha}M_0^4}{192\,V_0^3}\left\{x^5\left(\frac{3+4M_0^2}{\beta^9}\right) - 8y^5 - \frac{10x^3y^2}{\beta^7} + \frac{xy^4}{\beta^5}(8M_0^4 - 20M_0^2 + 15) - 4x_0\bar{C}\left[\frac{x^4}{\beta^7}(2M_0^2+3) - \frac{6x^2y^2}{\beta^5} + \frac{y^4}{\beta^3}(3-2M_0^2)\right]\right\} + \frac{\overset{\text{V}}{\alpha}M_0^4}{1920\,V_0^4}\left[x^6\left(\frac{8M_0^4+9M_0^2+1}{\beta^{11}}\right) - \frac{5x^4y^2}{\beta^9}(15M_0^2+1) + \frac{4x^5x_0\bar{C}}{7\beta^9}(28M_0^4+109M_0^2+8) + \frac{40x_0\bar{C}x^3y^2}{7\beta^7}(11M_0^2-6) + \frac{15x^2y^4}{\beta^7}(1-3M_0^2) + 16xy^5 - 16x_0\bar{C}y^5 + \frac{y^6}{3}(15 - 99M_0^2 + 121M_0^4 - 48M_0^6) + \frac{20x_0\bar{C}xy^4}{7\beta^5}(25M_0^2+8)\right] \quad (18)$$

In the calculation of the linearized pressure on the oscillating plate, only the potential on the plane $y = 0$ is required. This potential is presented in Eq. (19).

$$(\Phi_0^1)_{y=0} = -\frac{V_0\alpha x}{\beta} + \dot{\alpha}\left(\frac{x^2}{2\beta^3} + \frac{x_0\bar{C}x}{\beta}\right) - \frac{\ddot{\alpha}M_0^2}{V_0}\left(\frac{x^3}{4\beta^5} - \frac{x_0\bar{C}x^2}{2\beta^3}\right) + \frac{\ddot{\alpha}M_0^2}{V_0^2}\left[x^4\left(\frac{1-4M_0^2}{48\beta^7}\right) + \frac{x_0\bar{C}x^3}{12\beta^5}(2M_0^2+1)\right] - \frac{\alpha M_0^4}{192\,V_0^3}\left[x^5\left(\frac{3+4M_0^2}{\beta^9}\right) - \frac{4x_0\bar{C}x^4}{\beta^7}(2M_0^2+3)\right] + \frac{\overset{\text{V}}{\alpha}M_0^4}{1{,}920\,V_0^4}\left[x^6\left(\frac{8M_0^4+9M_0^2+1}{\beta^{11}}\right) + \frac{4x_0\bar{C}x^5}{7\beta^9}(28M_0^4+109M_0^2+8)\right] \quad (19)$$

The fourth-order solution included in Eq. (19) has previously been obtained by Watkins,[11] who expanded the first-order solution in powers of $\bar{\omega}$ and then integrated to obtain the fourth-order solution in frequency.

The linearized pressure coefficient (C_p) may be determined by substituting the potential Φ_0^1 [Eq. (18)] for Φ in Eq. (6) after the higher-order terms in α have been dropped from Eq. (6). Then, the section lift coefficient is given by the expression

$$C_L = \frac{4\alpha_M}{\beta}\left(\cos\omega t\left\{1 - \frac{\bar{\omega}^2}{12}(M_0^2+2+6x_0\beta^2) + \frac{\bar{\omega}^4}{960}[4M_0^6+27M_0^4+4M_0^2+20x_0\beta^2(4M_0^4+M_0^2)]\right\} - \frac{\bar{\omega}}{2}\sin\omega t\left\{(M_0^2-2-2x_0\beta^2) + \frac{\bar{\omega}^2}{24}(M_0^4+4M_0^2+12x_0\beta^2M_0^2) - \frac{\bar{\omega}^4}{20{,}160}\left[7(2M_0^8+16M_0^6+9M_0^4) + 30x_0\beta^2(19M_0^6+10M_0^4)\right]\right\}\right) \quad (20)$$

The pitching moment coefficient as calculated about the point of rotation x_0 is

$$C_M = -\frac{4\alpha_M}{\beta}\left(\cos\omega t\left\{\left(\frac{1}{2}-x_0\right) - \frac{\bar{\omega}^2}{16}[M_0^2+2+x_0(4M_0^2-8) - 8x_0^2\beta^2] + \frac{\bar{\omega}^4}{5{,}670}\left[(20M_0^2+135M_0^4+20M_0^2) + x_0(360M_0^6-396M_0^4-120M_0^2) - 120x_0^2\beta^2(4M_0^4+M_0^2)\right]\right\} - \frac{\bar{\omega}}{6}\sin\omega t\left\{[2M_0^2 - 4 - 3x_0(2\beta^2-1) + 6x_0^2\beta^2] + \frac{\bar{\omega}^2M_0^2}{40}[(4M_0^2+16) + x_0(40M_0^2-65) - 60x_0^2\beta^2] - \frac{\bar{\omega}^4M_0^4}{6{,}720}[24M_0^4+192M_0^2+108 + x_0(936M_0^4-552M_0^2-563) - 30x_0^2\beta^2(19M_0^2+10)]\right\}\right) \quad (21)$$

The solution for the lift, Eq. (20), will now be compared with the lift as determined by the exact linearized solution. The exact solution was computed from the tabular data presented by von Borbély.[3] The comparisons will be made at three Mach Numbers (M_0 = 10/9, 10/7, and 10/5) and plotted versus $\beta^2\bar{\omega}$. The reason for plotting versus $\beta^2\bar{\omega}$ is that it tends to separate the results that otherwise lie close to each other. As may be seen from Eq. (20), the lift is given in the form

$$C_L = (4\alpha_M/\beta)(P\cos\omega t + Q\sin\omega t)$$

where P and Q are functions of ($\bar{\omega}$, M_0, and x_0). Fig. 2 shows the function P as calculated from the second-order, fourth-order, sixth-order, and exact solutions. Fig. 3 shows the function Q under the same conditions.

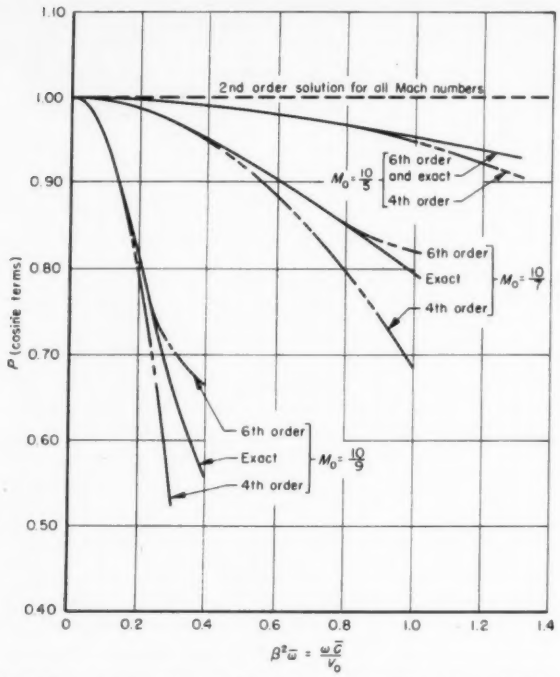

FIG. 2. Comparison of the even terms in the series solution and the exact solution for the linearized lift of an oscillating airfoil.

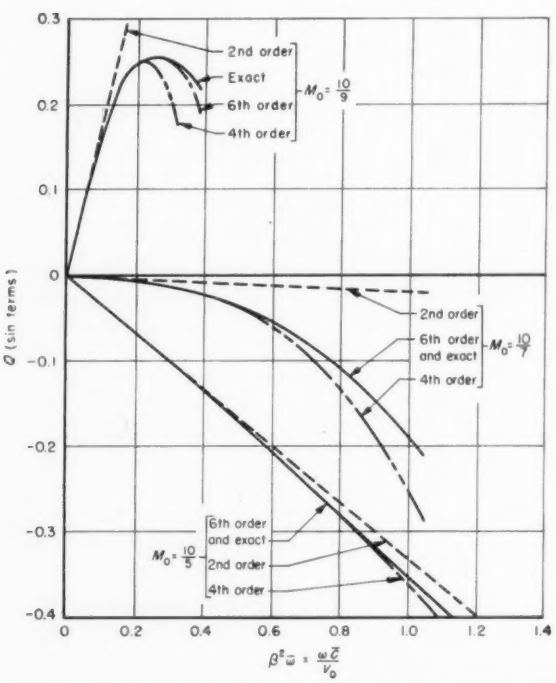

FIG. 3. Comparison of the odd terms in the series solution and the exact solution for the linearized lift of an oscillating airfoil.

Both Figs. 2 and 3 are presented for the condition $x_0 = 0$—that is, the case when the airfoil is rotating about its leading edge. It will be noted that for relatively low-speed motions such as are found in stability calculations or control deflections the second-order solution in frequency is within a few per cent of the exact solution. For high-speed motions such as flutter, the sixth-order solution may give a sufficiently accurate result.

(IV) THE SECOND-ORDER SOLUTION IN ANGLE OF ATTACK

(A) *The Flat-Plate Solution*

When the first-order potential [Eq. (17)] is substituted into the right-hand side $[H(\varphi^1)]$ of the nonhomogeneous wave equations [Eq. (5)], another difficulty becomes apparent. Consider the first term $(\varphi_1{}^1)$ of Eq. (17). The first derivative with respect to y gives $V_0\alpha$; the second derivative is thus zero. The second derivative is then zero ahead of the line $x = y\beta$, since $\varphi_1{}^1$ is defined as zero ahead of the Mach line from the leading edge and is also seen to be zero downstream from this Mach line. However, since $(\varphi_1{}^1)_y$ is a discontinuous function, $(\varphi_1{}^1)_{yy}$ is infinite along the Mach line from the leading edge. The second derivative is then given as zero everywhere except at the Mach line from the leading edge at which point it is infinite. Since it would be difficult to work with this velocity potential, another method of attack which eliminates the discontinuous derivatives was chosen. The method was that employed by Van Dyke,[12] and is also mentioned on page 365 of Courant and Friedrichs,[13] for the stationary flow problem.

In attacking the steady-flow problem, Van Dyke generalized the airfoil shape so that the ordinate of the airfoil is given as $y = \epsilon f(x)$. The function $f(x)$ is undefined, except that the surface and the slope of the surface are required to be continuous and to go to zero at the leading edge (i.e., $f(x) = f'(x) = 0$ at $x = 0$). Now there is no discontinuity in velocity occurring at the leading edge or, for that matter, anywhere in the flow field. The iteration process was then utilized and an expression for the pressure was determined. This solution showed that the second-order pressure at any point on the airfoil depended only on the slope $\epsilon f'(x)$ of the airfoil at that point. Therefore, suppose that $\epsilon f(x)$ was required to represent a flat airfoil everywhere except in the region $0 \leq x \leq \delta$ where the original restrictions on $f(x)$ are still enforced. The general solution is still valid for this problem. Now the solution remains valid no matter how small δ is allowed to become, and as $\delta \to 0$ the pressure is known everywhere on the airfoil except for an infinitesimal distance aft of the leading edge. In the limit where $\delta = 0$, the pressure is known everywhere except at the point $x = 0$. This is the flat-plate solution. Van Dyke[12] has further shown that, in the limit, the velocity components and the pressure are known everywhere in the flow field except in

the fan-shaped region $y = [(x/\beta) + \nu] \pm \nu$ extending from the leading edge of the airfoil. The expression for ν was shown to be equal to the angle that the shock (as given by second-order theory) lies ahead of the Mach wave, or for an expansion 2ν represents the width of the Prandtl-Meyer expansion fan. The iteration process, as applied to the case of an airfoil of zero thickness by means of the "general solution" attack, was thus shown to be successful except within the previously mentioned fanlike region of order ϵ lying near the Mach line from the leading edge.

A similar procedure will now be applied to the problem of an oscillating flat plate. A first-order† velocity potential $\Phi_2{}^1(f, f')$, such that $\Phi_2{}^1(f, f')$ becomes the previously determined first-order solution $\Phi_2{}^1(x, y)$ when $f = f(x - y\beta) = x - y\beta$, must be determined. A general potential that satisfies these requirements is found to be

$$\Phi_2{}^1 = -\alpha V_0\left(\frac{f}{\beta}\right) + \dot{\alpha}\left[\frac{M_0{}^2 xf}{\beta^3} + \frac{x_0\bar{C}f}{\beta} - \left(\frac{M_0{}^2}{\beta^3} + \frac{1}{\beta}\right)\int_0^{x-y\beta} f(\zeta)\, d\zeta\right] \quad (22)$$

Eq. (22) reduces to Eq. (17) when $f(x - y\beta)$ is set equal to $x - y\beta$ and obviously satisfies the boundary conditions [Eq. (11)] that Φ and Φ_x are equal to zero at $x = 0$. Also, Eq. (22) satisfies the requirement $\Box\, \Phi_2{}^1 = 0 + 0(\tilde{\omega}^2)$, since all of the first-order terms cancel identically. Thus, $\Phi_2{}^1$ [Eq. (22)] satisfies the wave equation [Eq. (4)] and the boundary condition [Eq. (11)], and for the case $f(\zeta) = \zeta$ the boundary condition is that of an oscillating plate [Eq. (13)].

† For the remainder of this report, order will refer to angle of attack unless otherwise stated.

Now, having determined a satisfactory first-order general potential $\Phi_2{}^1$, a general second-order potential φ^2 must be found which will satisfy Eqs. (5), (10), and (11). Substituting Eq. (22) into Eq. (5), it follows that

$$\Box\varphi^2 = -\frac{\alpha^2 V_0(\gamma + 1)M_0{}^4}{\beta^2} f'f'' + \alpha\dot{\alpha}\left[\frac{2M_0{}^6(\gamma + 1)}{\beta^4} xf'f'' + \frac{2M_0{}^4(\gamma + 1)x_0\bar{C}}{\beta^2} f'f'' - \frac{2M_0{}^4(\gamma + 1)}{\beta^2} ff'' + \frac{M_0{}^4(3 - 2M_0{}^2)(\gamma + 1)}{\beta^4}(f')^2\right] \quad (23)$$

Now let $\varphi^2 = \varphi + \sigma$, where φ is a particular solution that satisfies the nonhomogeneous wave equation, Eq. (23), and σ is the correction potential that makes φ^2 satisfy the boundary conditions [Eqs. (10) and (11)]. A function φ that satisfies Eq. (23) is

$$\varphi = \alpha^2 V_0\left[-\frac{M_0{}^4(\gamma + 1)}{4\beta^3} y(f')^2 + \frac{M_0{}^2(\gamma + 1)}{4\beta^4}\int_0^{x-y\beta} (f')^2\, d\zeta + \frac{M_0{}^2(\gamma + 1)x_0\bar{C}}{4\beta^2}(f')^2\right] + \alpha\dot{\alpha}\left[\frac{M_0{}^6(\gamma + 1)}{2\beta^5} xy(f'^2 - \frac{M_0{}^4(\gamma + 1)}{\beta^4} xff'\right] \quad (24)$$

That φ does satisfy Eq. (23) may be verified by direct substitution. It is also apparent that $\varphi = \varphi_x = 0$ at $x = 0$.

Now σ must satisfy the wave equation, the boundary conditions [Eq. (11)], and the tangency condition

$$(\sigma_y)_{y=0} = -(\varphi_y)_{y=0} + (\alpha f'\Phi_{2x}{}^1)_{y=0} + [(\Phi_{2y}{}^1)_{y=0} - (\Phi_{2y}{}^1)_{\text{sur.}}] \quad (25)$$

Let the surface of the general airfoil be given as $y = \alpha f'(x - x_0\bar{C})$. Now consider Eq. (25); the first term may be determined from Eq. (24) and the second term from Eq. (22). To determine $\Phi_{2y}{}^1$ at the surface [see the third term of Eq. (25)], expand f and f' in a Maclaurin series—i.e.,

$$\alpha f(x - y\beta)_{y=\alpha f'(x-x_0\bar{C})} = \alpha f(x) - \alpha^2\beta(x - x_0\bar{C})\,[f'(x)]^2 + 0(\alpha^3) \quad (26)$$

Thus the equation for $(\sigma_y)_{y=0}$ is complete, and it only remains to determine σ. The expression for σ is given below [Eq. (27)]. As given, the equation is seen to be lengthy; however, the starred terms are only included so that the expression for σ will be complete, since these terms go to zero in the case of a flat plate [i.e., when $f(\zeta) = \zeta$ and, hence, $f''(\zeta) = 0$]. For purposes of brevity, the method of determining σ is not shown (for further details, see reference 1).

$$\sigma = \alpha^2 V_0 \left\{ ff' - \int_0^{x-y\beta} f(\zeta)\, d\zeta \left[\frac{(\gamma+1)(M_0^4 + M_0^2) - 4M_0^2\beta^2}{4\beta^4} \right] + x_0\bar{C}f' - x_0\bar{C} \int_0^{x-y\beta} f'f''\, d\zeta \left[\frac{M_0^2(\gamma+1)}{2\beta^2} \right]^* \right\} + \alpha\dot{\alpha} \left\{ yff' \left(\frac{2M_0^2}{\beta} \right) + x \int_0^{x-y\beta} f\, d\zeta \times \left[\frac{(\gamma+1)(M_0^6 + M_0^4) - 4\beta^2 M_0^2}{2\beta^6} \right] - x_0\bar{C}xf' \left(\frac{2M_0^2}{\beta^2} \right) + xx_0\bar{C} \int_0^{x-y\beta} f'f''\, d\zeta \left[\frac{M_0^4(\gamma+1)}{\beta^4} \right]^* + (x - y\beta) \int_0^{x-y\beta} f''\, d\zeta \left(\frac{2M_0^2}{\beta^2} \right)^* - \int_0^{x-y\beta} \int_0^{\zeta} f''(\eta)\, d\eta\, d\zeta \left(\frac{2M_0^2}{\beta^2} \right)^* + \int_0^{x-y\beta} ff'\, d\zeta \left(\frac{2M_0^2}{\beta^2} \right) + \left[\frac{2M_0^4}{\beta^4} - (\gamma+1)\frac{M_0^6 + M_0^4}{2\beta^6} \right] \right\} (x - y\beta) \int_0^{x-y\beta} (f')^2\, d\zeta - \int_0^{x-y\beta} \int_0^{\zeta} [f'(\eta)]^2\, d\eta\, d\zeta \Bigg\} + \left[\frac{M_0^4(\gamma+1)}{\beta^4} \right] \left[\int_0^{x-y\beta} \int_0^{\zeta} f'(\eta) f''(\eta)\, d\eta\, d\zeta^* - (x - y\beta) \int_0^{x-y\beta} f'f''\, d\zeta^* \right] \Bigg\} \quad (27)$$

The complete solution Φ_2^2 valid to the second order in frequency and angle of attack is

$$\Phi_2^2 = \Phi_2^1 + \varphi + \sigma \quad (28)$$

where Φ_2^1, φ and σ are given by Eqs. (22), (24), and (27).

The second-order solution for the forces and moments on a flat plate can be determined from Eq. (28); however, since the second-order terms are zero for an airfoil of zero thickness, the solution is the same as that given in Eqs. (20) and (21).

(*B*) *The Wedge Airfoil*

Consider an oscillating wedge that has a thickness ratio 2ϵ [thickness = (2ϵ) chord]; the ordinate for the upper surface is given as

$$y = \alpha(x - x_0\bar{C}) + \epsilon x \quad (29)$$

The general problem is similar to the zero thickness problem considered in Section (IV). In fact, the problem and the method of solution are so similar that only the major steps and the final results will be given for the case of the wedge.

The first-order potential Φ_2^1 for the wedge is found to be

$$\Phi_2^1 = -V_0(\alpha + \epsilon)\frac{f}{\beta} + \dot{\alpha}\left[\frac{M_0^2 xf}{\beta^3} + \frac{x_0\bar{C}f}{\beta} - \left(\frac{M_0^2}{\beta^3} + \frac{1}{\beta} \right) \int_0^{x-y\beta} f(\zeta)\, d\zeta \right] \quad (30)$$

where the general first-order potential satisfies the homogeneous wave equations [$\Box\Phi = 0 + 0(\bar{\omega}^2)$] and the boundary conditions, Eqs. (9) and (11).

By substituting Φ_2^1 [Eq. (30)] into Eq. (5), the nonhomogeneous wave equation that is to be satisfied by the particular solution can be determined. Now let the second-order solution φ^2 be composed of a particular solution ψ and a correction potential θ. The particular solution that satisfies the nonhomogeneous wave equation is then,

$$\psi = -(\alpha + \epsilon)^2 \frac{V_0 M_0^4(\gamma+1)}{4\beta^3} y(f')^2 + \alpha(\alpha + 2\epsilon)V_0 \left[\frac{M_0^2(\gamma+1)}{4\beta^4} \int_0^{x-y\beta} (f')^2\, d\zeta + \frac{M_0^2(\gamma+1)}{4\beta^2} x_0\bar{C}(f')^2 \right] + \dot{\alpha}(\alpha + \epsilon) \left[\frac{M_0^6(\gamma+1)}{2\beta^5} xy(f')^2 - \frac{M_0^4(\gamma+1)}{\beta^4} xff' \right] \quad (31)$$

As before $\psi = \psi_x = 0$ at $x = 0$; hence, the correction potential θ must satisfy the conditions $\Box\theta = 0$, $\theta = \theta_x = 0$ at $x = 0$, and

$$(\theta_y)_{y=0} = -(\psi_y)_{y=0} + (\alpha + \epsilon)f'[(\Phi_2^1)_x]_{y=0} + [(\Phi_{2_t}^1)_{y=0} - (\Phi_{2y})_{y=-(\alpha+\epsilon)f-x_0\bar{C}f']} \quad (32)$$

By substituting Eqs. (30) and (31) into Eq. (32) and neglecting terms of order α^3, the required correction potential θ is found to be

$$\theta = V_0(\alpha+\epsilon)^2\left\{\int_0^{x-y\beta}(f')^2\,d\zeta\left[1-\frac{4\beta^2-(\gamma+1)(M_0^4+M_0^2)}{4\beta^4}\right]-ff'\right\}+V_0\alpha(\alpha+\epsilon)x_0\bar{C}f'+$$
$$V_0\epsilon^2\int_0^{x-y\beta}(f')^2\left[\frac{M_0^2(\gamma+1)}{4\beta^4}\right]+\dot{\alpha}(\alpha+\epsilon)\left(-2\int_0^{x-y\beta}ff'\,d\zeta-\frac{x_0\bar{C}}{\beta^2}\int_0^{x-y\beta}(f')^2\,d\zeta+\right.$$
$$\left.(x-y\beta)\int_0^{x-y\beta}(f')^2\,d\zeta-\int_0^{x-y\beta}\int_0^{\zeta}[f'(\eta)]^2\,d\eta\,d\zeta\right\}\times\left[(\gamma+1)\left(\frac{2M_0^6-3M_0^4}{2\beta^6}\right)+\frac{M_0^2-2M_0^4}{\beta^4}\right]+$$
$$x_0\bar{C}_0\int_0^{x-y\beta}f'\,d\zeta\left(\frac{M_0^2}{\beta^2}\right)+x\int_0^{x-y\beta}(f')^2\,d\zeta\left[(\gamma+1)\left(\frac{M_0^6+M_0^4}{2\beta^6}\right)-\frac{2M_0^4}{\beta^4}\right]+yff'\left(\frac{2M_0^2}{\beta}\right)-$$
$$x_0\bar{C}(x-y\beta)f'\frac{M_0^2}{\beta^2}\Big)+\alpha\dot{\alpha}\left\{-x_0\bar{C}xf'\frac{2M_0^2}{\beta^2}+\left(\frac{M_0^2}{\beta^2}+1\right)x_0\bar{C}f+\frac{2M_0^2}{\beta^2}\int_0^{x-y\beta}ff'\,d\zeta-f\left(\frac{2M_0^2}{\beta^2}\right)-\right.$$
$$\left.x_0^2\bar{C}^2f'+(x-y\beta)f'\frac{2M_0^2}{\beta^2}\right\}+\dot{\alpha}\epsilon\left\{\left[\int_0^{x-y\beta}\int_0^{\zeta}(f')^2\,d\eta\,d\zeta-(x-y\beta)\int_0^{x-y\beta}(f')^2\,d\zeta\right]\frac{M_0^2}{\beta^2}+\right.$$
$$\left.\frac{M_0^2}{\beta^2}\int_0^{x-y\beta}ff'\,d\zeta-x_0\bar{C}x\frac{M_0^2}{\beta^2}f'+x\frac{M_0^2}{\beta^2}\int_0^{x-y\beta}(f')^2\,d\zeta\right\} \quad (33)$$

Thus, the complete second-order velocity potential is

$$\Phi_2{}^2 = \Phi_2{}^1 + \psi + \theta$$

where $\Phi_2{}^1$, ψ, and θ are given by Eqs. (30), (31), and (33). This completes the general solution. Now consider the solution (in x, y, t) to the oscillating wedge problem.

Setting $f(x-y\beta) = x - y\beta$, the potential $\Phi_2{}^2$ may be determined. Then the pressure coefficient C_p [Eq. (17)] on the surface of the wedge [$y = (\alpha+\epsilon)x - x_0\bar{C}\alpha$] is found to be

$$C_p = \frac{2}{\beta}\left((\alpha+\epsilon)-\frac{\dot{\alpha}}{V_0}\left[x_0\bar{C}+\frac{x}{\beta^2}(2-M_0^2)\right]+(\alpha+\epsilon)^2\left[\frac{(\gamma+1)M_0^4-4\beta^2}{4\beta^3}\right]+\right.$$
$$\left.\frac{\dot{\alpha}}{V_0}(\alpha+\epsilon)\left\{\frac{x}{2\beta^5}[\gamma(M_0^6-4M_0^4)-3M_0^6+10M_0^4-10M_0^2]-\frac{x_0\bar{C}}{2\beta}[M_0^2(\gamma+1)-4]\right\}\right) \quad (34)$$

This is the pressure coefficient for the upper surface of the wedge. The pressure coefficient on the lower surface is equal to, and 180° out of phase with, that of the upper surface. The discussion of the second-order lift and pitching moment will be taken up later.

(C) *The Double-Wedge Airfoil*

The problem now under consideration is the effect of a sharp bend or break in the upper surface of the wedge. As a convenient reference term, this problem has been entitled the double-wedge problem, since the solution will certainly be applicable to such an airfoil shape. Consider the oscillating wedge as shown in Fig. 4. This problem must be solved in two parts, one part representing the solution for

$$x/\beta \le y \le (x/\beta) + (\bar{C}/\beta)$$

and one part representing the solution for

$$(x/\beta) + (\bar{C}/\beta) \le y \le (x/\beta) + (1/\beta)(\bar{C}+\bar{Z})$$

Of course, the previous wedge solution will take care of the solution for the diverging section of the wedge (i.e., $x \le \bar{C}$). In addition, it will be necessary only to consider the effect, on the pressure, of a discontinuity in the slope of an oscillating flat plate; therefore, ϵ will be set equal to zero.

The problem for $x < \bar{C}$ is identical to that solved by the potential for the flow past the oscillating airfoil of zero thickness, Eq. (28).

For $x > \bar{C}$, the complete second-order potential is $\Psi_2{}^2$ ($\Psi_2{}^2 = \psi_2{}^1 + \psi + \theta$). A new function g will now be defined such that $g = g_x = 0$ at $x = \bar{C}$. Later, for the specific problem of the broken plate, $g(\zeta)$ will specifically be defined as $g(\zeta) = g(x - y\beta - \bar{C})$; thus, $\partial g/\partial x = g'$ and $\partial g/\partial y = -\beta g'$. The first-order potential must satisfy the conditions

$$\left.\begin{aligned}&\Box\psi_2{}^1 = 0\\&(\psi_{2y}{}^1)_{y=0} = V_0(\alpha f' + \delta g') + \dot{\alpha}\left[-x_0\bar{C}f' + \left(\frac{M_0^2}{\beta^2}+1\right)f - \frac{M_0^2x}{\beta^2}f'\right]\\&\psi_2{}^1 = \varphi_2{}^1 \text{ and } \psi_{2x}{}^1 = \varphi_{2x}{}^1 \text{ at } x = \bar{C}.\end{aligned}\right\} \text{1st order} \quad (35)$$

The last condition requires that there be no discontinuity in the potential or its x derivative anywhere in the flow. In particular, there can be no discontinuities near the Mach line from the break in the plate. The second-order potential ψ^2 must satisfy the conditions

$$\left.\begin{aligned} \Box\psi_2{}^2 &= H(\psi_2{}^1) \\ \{[\psi_{2y}{}^2 - (\partial y/\partial t]/(V_0 + \psi_{2x}{}^2)\}_{\text{sur.}} &= \partial y/\partial x \\ \psi_2{}^2 &= \varphi_2{}^2 \text{ and } \psi_{2y}{}^2 = \varphi_{2x}{}^2 \text{ at } x = \bar{C} \end{aligned}\right\} \text{2nd order} \tag{36}$$

Again the boundary conditions allow no discontinuities in the flow. Now, note that this problem is similar to the double-wedge problem in α and ϵ. In fact, if δg were replaced by ϵf, the problems would be identical except for the requirements on φ and φ_x. However, it is apparent that this boundary condition would be satisfied in both cases. The determination of the solution for $x > \bar{C}$ is much simplified by this fact. A first-order potential is seen to be

$$\psi_2{}^1 = -\frac{1}{\beta}(\alpha f + \delta g) + \dot{\alpha}\left[+\frac{M_0{}^2 x f}{\beta^3} + \frac{x_0\bar{C}f}{\beta} - \left(\frac{M_0{}^2}{\beta^3} + \frac{1}{\beta}\right)\int_0^{x-y\beta} f(\zeta)\, d\zeta\right] \tag{37}$$

The method of solution which leads to the complete second-order potential is exactly the same as that previously employed for the flat plate or wedge airfoil. Since these equations are lengthy, they will not be presented; however, the equations and the steps involved in their development are presented in reference 1.

The pressure coefficient C_p as determined from the second-order potential is given below.

For $x < \bar{C}$, the pressure coefficient $C\rho$ is given by Eq. (34) when ϵ is set equal to zero.

$$C_{pu} = \frac{2}{\beta}\left\{(\alpha) - \left(\frac{\dot{\alpha}}{V_0}\right)\left[x_0\bar{C} + \frac{x}{\beta^2}(2 - M_0{}^2)\right] + (\alpha^2)\left[\frac{A}{2\beta}\right] - \left(\frac{\dot{\alpha}}{V_0}\alpha\right)\left[\frac{x}{\beta^3}D + \frac{x_0\bar{C}}{2\beta}B\right]\right\} \tag{38}$$

where $A = [(\gamma + 1)M_0{}^4 - 4\beta^2]/2\beta^2$, $B = M_0{}^2(\gamma + 1) - 4$, and

$$D = [\gamma(4M_0{}^4 - M_0{}^6) + 3M_0{}^6 - 10M_0{}^4 + 10M_0{}^2]/2\beta^2$$

For $x > \bar{C}$, the complete potential indicates that the pressure coefficient $C\rho$ is again given by Eq. (35) if ϵ is set equal to $-\delta$.

$$C_{pu} = \frac{2}{\beta}\left\{(\alpha - \delta) - \left(\frac{\dot{\alpha}}{V_0}\right)\left[x_0\bar{C} + \frac{x}{\beta^2}(2 - M_0{}^2)\right] + (\alpha - \delta)^2\left[\frac{A}{2\beta}\right] - \left[\frac{\dot{\alpha}}{V_0}(\alpha - \delta)\right]\left[\frac{x}{\beta^3}D + \frac{x_0\bar{C}}{2\beta}B\right]\right\} \tag{39}$$

Thus the effect of a corner on the pressure has been determined. The third term $[(A/2\beta)(\alpha - \delta)^2]$ of this equation is rather interesting, since it is the square of the instantaneous slope multiplied by exactly the same term first produced by Busemann for the second-order solution for the flow past a stationary surface. Thus, if the angle of attack is not a function of time ($\dot{\alpha} \equiv 0$), this solution reduces to that given by Busemann.

(*D*) *The General Airfoil*

Consider the airfoil shown in Fig. 1. From the results for the oscillating double wedge, it is apparent that by a series of n steps the pressure on the surface of an airfoil with n breaks also is calculated. Then, independent of the shape of the airfoil ahead of the surface in question, the pressure at that point would be the same as that given by the equation for the pressure on the aft portion of double-wedge airfoil. Thus it is apparent that the pressure at any point is independent of the shape of the remainder of the airfoil and depends only on x_0, $M_0\gamma$ and the slope and the rate of change of slope at that point. Hence, the pressure on the general airfoil of Fig. 1 may be expressed in the form: *on the upper surface,*

$$C_{pu} = \frac{2}{\beta}\left\{\left(\alpha + \frac{dy_u}{dx}\right) - \left(\frac{\dot{\alpha}}{V_0}\right)\left[x_0\bar{C} + \frac{x}{\beta^2}(2 - M_0{}^2)\right] + \left(\alpha + \frac{dy_u}{dx}\right)^2\left(\frac{A}{2\beta}\right) - \left(\frac{\dot{\alpha}}{V_0}\right)\left(\alpha + \frac{dy_u}{dx}\right)\left[\frac{x}{\beta^3}D + \frac{x_0\bar{C}}{2\beta}B\right]\right\} \tag{40a}$$

on the lower surface,

$$C_{pl} = \frac{2}{\beta}\left\{\left(-\alpha - \frac{dy_l}{dx}\right) + \left(\frac{\dot{\alpha}}{V_0}\right)\left[x_0\bar{C} + \frac{x}{\beta^2}(2 - M_0{}^2)\right] + \left(\alpha + \frac{dy_l}{dx}\right)^2\left(\frac{A}{2\beta}\right) - \left(\frac{\dot{\alpha}}{V_0}\right)\left(\alpha + \frac{dy_l}{dx}\right)\left[\frac{x}{\beta^3}D + \frac{x_0\bar{C}}{2\beta}B\right]\right\} \tag{40b}$$

(E) *Lift and Pitching Moment Coefficients for a Modified Double-Wedge Airfoil*

Consider the specific problem of the modified double-wedge airfoil as shown in Fig. 5. From Eqs. (40a) and (40b) the pressure difference ($C_{p_T} = C_{p_u} - C_{p_L}$) between the upper and lower surfaces of the modified double wedge is found to be

$$C_{p_T} = \frac{4\alpha_M}{\beta}\left\{\cos\omega t\left(1 + \zeta\frac{A\epsilon}{\beta}\right) + \frac{\tilde{\omega}}{2}\sin\omega t\left[2x_0\beta^2 + 2\frac{x}{\bar{C}}(2 - M_0^2) + \zeta\frac{\epsilon}{\beta}\left(\frac{x}{\bar{C}}D + x_0\beta^2 B\right)\right]\right\} \tag{41}$$

where $\zeta = 1$ for $0 < x < \bar{C}/3$; $\zeta = 0$ for $\bar{C}/3 < x < 2\bar{C}/3$; and $\zeta = -1$ for $2\bar{C}/3 < x < \bar{C}$.

Hence, the lift coefficient C_L is

$$C_L = (4\alpha_M/\beta)\{\cos\omega t + (\tilde{\omega}/2)\sin\omega t[2x_0\beta^2 + (2 - M_0^2) - (4\epsilon/9\beta)D]\} \tag{42}$$

while the pitching moment coefficient C_M may be expressed in the following form:

$$C_M = -\frac{2\alpha_M}{\beta}\cos\omega t\left[1 - 2x_0 - \frac{4\epsilon}{9\beta}A\right] + \frac{\tilde{\omega}}{3}\sin\omega t\left[2\left(2 - M_0^2 - \frac{2\epsilon}{3\beta}D\right) + x_0\left(6\beta^2 - 3 + \frac{2}{3}\frac{\epsilon}{\beta}(2D - B\beta^2)\right) - 6x_0^2\beta^2\right] \tag{43}$$

Now consider the importance of the second-order terms in angle of attack. For the lift coefficient

$$C_L = (4\alpha_M/\beta)\,[P\cos\omega t + (\tilde{\omega}/2)\,Q\sin\omega t]$$

a plot of the function Q vs. Mach Number is presented on Fig. 5 for three thickness ratios ($T/\bar{C} = 0, 0.05, 0.10$). It appears that the second-order effects in angle of attack (see Fig. 5) are most predominant at the low Mach Numbers. However, since the higher order terms in frequency are small for $M_0 < 1.4$, the relative importance of the second-order terms in angle of attack is approximately constant throughout the Mach Number range $1.2 < M_0 < 2.0$.

For the moment coefficient where

$$C_M = -(2\alpha_M/\beta)\,[R\cos\omega t + (\tilde{\omega}/3)S\sin\omega t]$$

the functions R and S are plotted versus Mach Number for three thickness ratios ($T/C = 0, 0.05, 0.10$) on Figs. 6 and 7. As before, the second-order terms have about the same relative importance throughout the Mach Number range $1.2 < M_0 < 2.0$. The second-order terms are especially important for the odd (sin) terms in frequency. In Fig. 7, it is seen that the second-order terms in angle of attack actually are of greater magnitude than the first-order terms for most of the Mach Number range. It is this fact that causes the unstable tendencies, noted by Garrick and Rubinow for the case of airfoils of zero thickness, to be eliminated and the motion to be stable when the effects of thickness are considered. When the Mach Number is less than $\sqrt{2}$ (for this case of $x_0 = 0$), the function S is seen to be positive for the case of a flat plate ($T/C = 0$). This term being positive corresponds to negative damping—i.e., an unstable motion. However, when the effect of thickness is considered (see Fig. 7), the function S is seen to be negative throughout the whole Mach Number range. This is further indicated in Fig. 8. In Fig. 8, the curve labeled $T/\bar{C} = 0$ is the curve

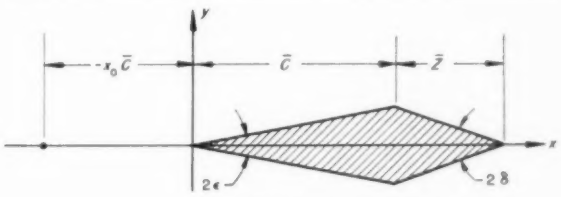

FIG. 4.

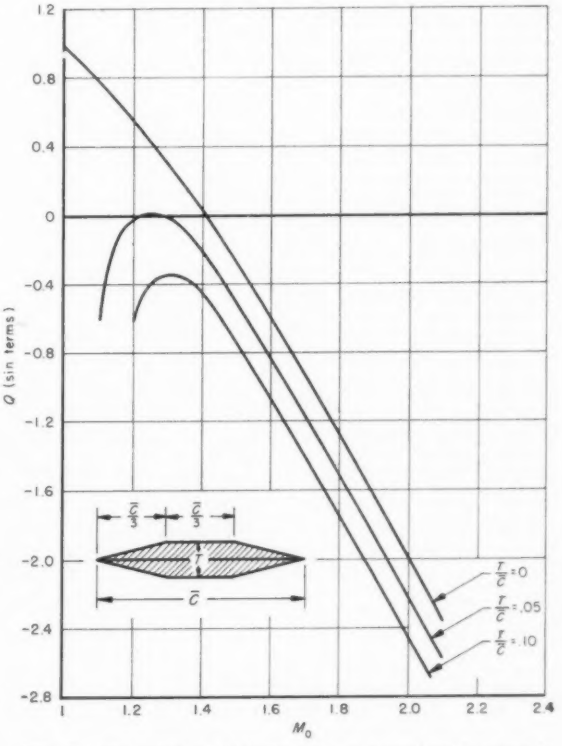

FIG. 5. The effect of thickness on the second-order terms in frequency for a modified double-wedge airfoil rotating about its leading edge.

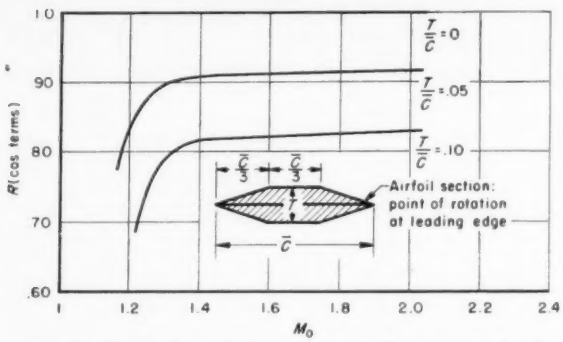

FIG. 6. Comparison of the even terms in the second-order solution for the pitching moment of a modified double-wedge airfoil at three thickness ratios.

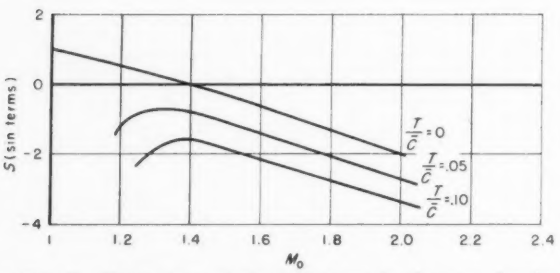

FIG. 7. Comparison of the odd terms in the second-order solution for the pitching moment of a modified double-wedge airfoil at three thickness ratios.

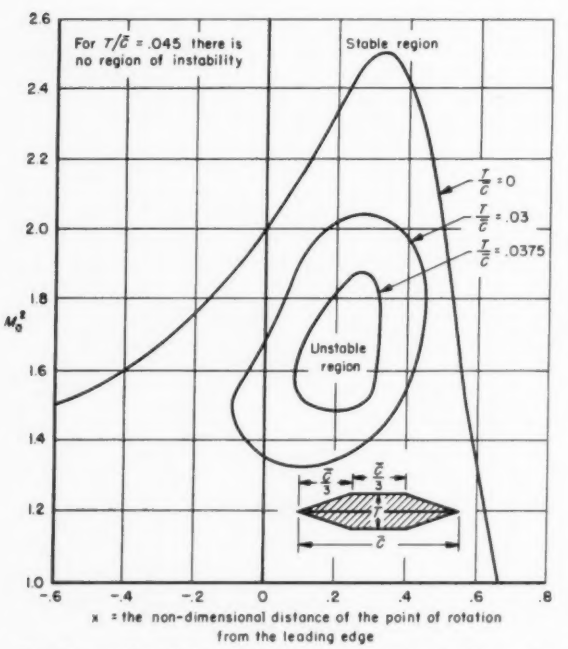
For $T/\bar{C}$ = .045 there is no region of instability
Stable region
$\frac{T}{C}$ = 0
$\frac{T}{C}$ = .03
$\frac{T}{C}$ = .0375
Unstable region
M_0^2
x = the non-dimensional distance of the point of rotation from the leading edge

FIG. 8. Region of instability for an oscillating double wedge airfoil as a function of Mach Number (M_0) and the thickness ratio ($T/\bar{C}$).

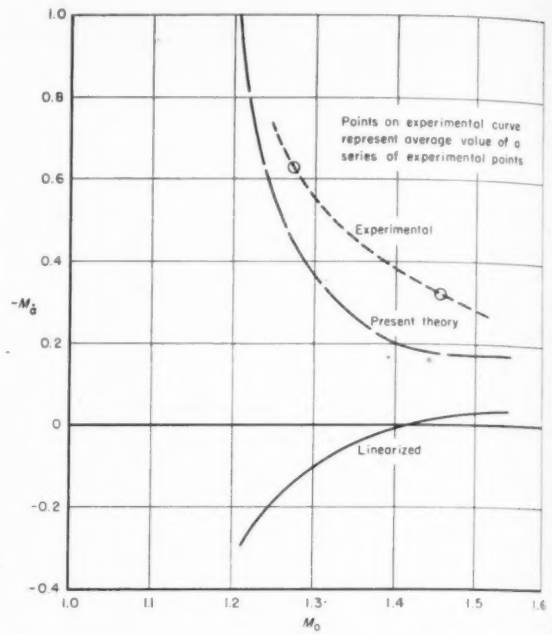

FIG. 9. Comparison of experimental and theoretical damping in pitch for a $7^1/_2$ per cent thick biconvex airfoil.

as presented by Garrick and Rubinow,[14] which indicates that an airfoil of zero thickness will be unstable for all points of rotation less than $x_0 = {}^2/_3$ for some range of Mach Numbers. The curves for a thickness ratio ($T/\bar{C}$) of 0.03 and 0.0375 show that the region of instability rapidly disappears with any finite thickness, and in this case the instability disappears for $T/\bar{C} \geq 0.045$.

(V) Comparison with Experimental Results

In a paper[15] published in *The Journal of the Royal Aeronautical Society*, Beavan and Holder present the damping coefficients determined from supersonic tests of a 12-in. span, $7^1/_2$-per cent thick, biconvex airfoil. By utilizing Eqs. (40a) and (40b) and assuming a parabolic representation for the circular arc airfoil, the pitching moment coefficient for a $7^1/_2$ per cent thick airfoil is found to be

$$C_M = -\frac{2\alpha_M}{\beta}\left\{\cos\omega t\left(1 - 2x_0 - \frac{0.05A}{\beta}\right) + \frac{\bar{\omega}}{3}\sin\omega t\left[4 - 2M_0^2 - \frac{0.15D}{\beta} + x_0\left((6M^2 - 9 + \frac{0.15D}{\beta} - 0.075B\beta\right) - 6x_0^2\beta^2\right]\right\} \quad (44)$$

The results given in reference 15 are given in the form of a nondimensional damping parameter $M_{\dot{\alpha}}$, where

$$M_{\dot{\alpha}} = (V_0/2C)\,(\partial C_M/\partial\dot{\alpha})$$

(*Concluded on page 704*)

Partially Plastic Rotating Discs*

MELVIN ZAID†

Sperry Gyroscope Company‡

ABSTRACT

The solution is obtained for the flat rotating disc in the plastic region. Strains are assumed to be small, and elastic compressibility is considered in order to avoid discontinuities at the elastic-plastic boundary.

The distortion energy theory is used, and results are obtained for both strain and nonstrain hardening materials.

Comparison is made to previous solutions based on the maximum shear theory and also to the numerical solutions obtained by Nadai and Donnell, all of which neglected elastic compressibility.

NOMENCLATURE

D	=	flow function for tension
E	=	modulus of elasticity
H	=	$1 + D$
P_1	=	$\dfrac{[\sigma_t' - (\sigma_r'/2)] - (3/2)[(\sigma_r - \sigma_t)/r]}{\sigma_t - (\sigma_r/2)}$
Q_7	=	$\dfrac{[(1/2) - \nu]Tr}{\sigma_t - (\sigma_r/2)}$
T, T_1, T_2	=	$\left(\dfrac{\gamma}{g}\right)\omega^2, \left(\dfrac{\gamma}{g}\right)\left(\dfrac{\omega^2}{s_0}\right)a^2, \left(\dfrac{\gamma}{g}\right)\left(\dfrac{\omega^2}{s_0}\right)b^2$
a	=	radius to plastic-elastic boundary
b	=	radius to outer rim of disc
e	=	effective strain $(\sqrt{2}/3)\times \sqrt{(e_1 - e_2)^2 + (e_2 - e_3)^2 + (e_3 - e_1)^2}$
e_1, e_2, e_3	=	principal strains (elastic plus plastic)
e_r, e_t, e_z	=	radial, tangential, and axial strains (total)
r	=	radius
r_1, r_2	=	r/a, r/b
s	=	effective stress $(\sqrt{2}/2)\times \sqrt{(s_1 - s_2)^2 + (s_2 - s_3)^2 + (s_3 - s_1)^2}$
s_0	=	yield stress
s_1, s_2, s_3	=	principal stresses
s_1, s_t, s_z	=	radial, tangential, and axial stresses
γ	=	weight of disc per unit volume
ϵ	=	Ee/s_0
$\epsilon_r, \epsilon_t, \epsilon_z$	=	Eer/s_0, Ee_t/s_0, Ee_z/s_0
ν	=	Poisson's ratio
ρ	=	radial displacement
σ	=	s/s_0
σ_r, σ_t	=	s_r/s_0, s_t/s_0
ω	=	angular speed of disc (radions/unit time)

Primes denote differentiation with respect to radius r, r_1, or r_2.

(I) INTRODUCTION

THE PROBLEM OF THE THIN DISC is frequently encountered in the design of rotating parts. The engineer often desires information on the speed necessary to cause complete yielding of the disc. The stresses and strains in the elastic region have long been known, but it was not until 1929 that solutions were presented for the plastic region. In a paper by Nadai and Donnell,[1] solutions were presented which were based on the maximum shear theory and on the distortion energy theory. The results, assuming the latter theory, led to numerical integrations and had to be presented graphically.

In the contents of this paper the distortion energy theory is used, and an exact solution in the form of an infinite series is presented. A further exact but simple solution for "almost constant" yield stress is developed and extended to the arbitrary stress-strain law. The latter of the two solutions is to be recommended because of its simplicity and flexibility. Inasmuch as the stresses are statically determinate, any later assumptions with regard to strain do not affect the agreement between the solutions for stresses obtained from the article by Nadai and Donnell[1] and this paper.

In solving for strains it was assumed, in the above-mentioned paper, that the volume remains constant. In effect, this means that the elastic strains are extremely small as compared to those in the plastic region. It can be shown that in the partially plastic disc this is not the case; moreover, in almost any plastic-elastic problem such an assumption will lead to serious discontinuities at the plastic-elastic boundary. To avoid such an occurrence, the more general stress-strain relations are utilized.

Since the paper of Nadai and Donnell presents the solution of strains based on the maximum shear theory, no comparison is made beyond the fact that the discontinuities exist at the plastic-elastic boundary. However, Fisher[3] has, by numerical means, evaluated the plastic-elastic coefficient and obtained strains based on the assumptions of Nadai and Donnell, using the distortion energy theory. A comparison is made on the basis of these results.

Infinitesimal strains are assumed, and, based upon this, exact solutions for stress and strain at any point in the disc are obtained for a general stress-strain law. Since this often requires considerable labor in the form of the numerical solution of differential equations, it has been found necessary to introduce specified stress-strain laws.

Received March 8, 1952.

* The author wishes to thank Prof. C. W. MacGregor for his helpful discussions concerning this problem while at M.I.T.

† Senior Engineer.

‡ Division of The Sperry Corporation.

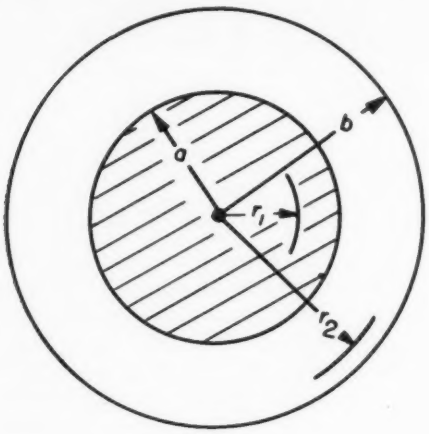

FIG. 1.

(II) THEORY

As the rotational speed of a thin disc is gradually increased, yielding starts at the center. The plastic-elastic boundary then progresses outward with in-increase of speed until complete yielding of the disc occurs, as in Fig. 1.

It is assumed that (*a*) the material is homogeneous and isotropic; (*b*) Hooke's law applies in the elastic region; (*c*) the sum of the total strains is

$$e_1 + e_2 + e_3 = \frac{1 - 2\nu}{E}(s_1 + s_2 + s_3)$$

(*d*) the ratios of the principal strain differences to the corresponding stress differences are equal; and (*e*) there is a unique relationship between effective stress and effective strain. Assumption (*c*) takes into consideration the compressibility of the material even in the plastic region. It is assumed that the total strains in the plastic region are made up of two components. These satisfy the condition that the change of volume equals $(1 - 2\nu)/E$ times the sum of the principal strains. Further, the plastic component satisfies the relation that it has no volume change; hence, the elastic component must produce the entire volume change. This leads to assumption (*c*).

The effective stress at a point is defined as

$$s = (\sqrt{2}/2)\times \sqrt{(s_1 - s_2)^2 + (s_2 - s_3)^2 + (s_3 - s_1)^2} \quad (1)$$

and the effective strain as

$$e = (\sqrt{2}/3)\sqrt{(e_1 - e_2)^2 + (e_2 - e_3)^2 + (e_3 - e_1)^2} \quad (2)$$

where s_1, s_2, s_3 are the principal stresses and e_1, e_2, e_3 are the principal strains.

Assumption (*e*) can be derived from a tension test in the form

$$s = f(e) \quad (3)$$

For the case of the thin disc,

$$s_1 = s_r, \qquad e_1 = e_r$$
$$s_2 = s_t, \qquad e_2 = e_t$$
$$s_3 = s_z = 0, \qquad e_3 = e_z$$

From the assumptions and the above definitions, one can write the equation of effective stress, strain, and the stress-strain laws in dimensionless variables as

$$\sigma = (\sqrt{2}/2)\sqrt{(\sigma_r - \sigma_t)^2 + \sigma_r^2 + \sigma_t^2} \quad (4)$$

$$\epsilon = (\sqrt{2}/3)\sqrt{(\epsilon_r - \epsilon_t)^2 + (\epsilon_t - \epsilon_z)^2 + (\epsilon_z - \epsilon_r)^2} \quad (5)$$

$$\epsilon_r = \sigma_r(1 + D) - \sigma_t[\nu + (D/2)] \quad (6)$$

$$\epsilon_t = \sigma_t(1 + D) - \sigma_r[\nu + (D/2)] \quad (7)$$

$$\epsilon_z = -(\sigma_r + \sigma_t)[\nu + (D/2)] \quad (8)$$

$$\epsilon = (2/3)\sigma[1 + \nu + (3/2)D] \quad (9)$$

$$\frac{\epsilon_r - \epsilon_t}{\sigma_r - \sigma_t} = \frac{\epsilon_t - \epsilon_z}{\sigma_t} = \frac{\epsilon_z - \epsilon_r}{-\sigma_r} = \frac{3}{2}\frac{\epsilon}{\sigma} \quad (10)$$

The equilibrium of the disc is

$$\sigma_t - \sigma_r - r_{1,2}(d\sigma_r/dr_{1,2}) - T_{1,2}r_{1,2}^2 = 0 \quad (11)$$

For compatibility of strains

$$r_{1,2}(d\epsilon_t/dr_{1,2}) = \epsilon_r - \epsilon_t \quad (12)$$

Introducing Eq. (10) and the stress-strain relations (6) (7), and (8), one obtains

$$(dH/dr_{1,2}) + P_1H = Q_2 \quad (13)$$

It should be noted that $r_{1,2}$ depends on whether the radius of the plastic-elastic boundary (*a*), or the radius of the outer rim (*b*) is used. It will be found that the solution is most easily obtained in terms of r_1, but, for a meaning to be attached to the solution, it is always necessary to refer to a/b; here, r_2 will be necessary. In this connection it should be noted that, for the elastic solution, $a = T_1 = 0$, leaving angular speed (ω) as an indefinite value. Since ω is an important variable and is often desired for comparison, it is necessary to introduce r_2 and, hence, T_2, which is never zero unless $\omega = 0$.

(III) SOLUTION FOR STRESSES

Case (1) Elastic

Here $D = D' = 0$, $H = 1$, $H' = 0$. Using Eqs. (11) and (13), the solution is easily obtained as

$$\sigma_r = C_1 - C_2r_2^{-2} - (T_2/8)(3 + \nu)r_2^2 \quad (14)$$

$$\sigma_t = C_1 + C_2r_2^{-2} - (T_2/8)(3\nu + 1)r_2^2 \quad (15)$$

Eqs. (14) and (15) will be used to determine the stresses in the elastic region. We can prescribe σ_r, σ_t at $r_2 = a/b$ and σ_r at $r_2 = 1$, and there are three unknowns, C_1, C_2, and a/b. The usual case will be take $\sigma_r]_{r_2=1} = 0$, and

$$\sigma_{re}]_{r_2=a/b} = \sigma_{rp}]_{r_2=a/b}$$

$$\sigma_{te}]_{r_2=a/b} = \sigma_{tp}]_{r_2=a/b}$$

although the zero radial stress condition is by no means mandatory.

Case (2) Elastic-Plastic (Nonstrain-Hardening Material)

Plastic Region.—Here, the plastic region is assumed to be in the region $0 \leq r_1 \leq 1$. The case of $r_1 = r_2 = 1$ represents complete yielding, whereas $r_1 = 0$ indicates an elastic disc. Eqs. (4) and (11) completely specify the stresses; these are

$$\sigma_r^2 + \sigma_t^2 - \sigma_r\sigma_t = 1 \tag{16}$$

$$\sigma_t - \sigma_r - r_1(d\sigma_r/dr_1) - T_1r_1^2 = 0 \tag{17}$$

From Eq. (17) it is easy to see that, for $r_1 = 0$, $\sigma_r = \sigma_t$, since stresses are finite at this point. The solution of Eqs. (16) and (17) can be obtained numerically and have been utilized to check the accuracy of the following analysis. However, a far more powerful method will be formulated.

From the Cauchy-Kowalewski[4] existence proposition, it is known that, having the values at a point, the Eqs. (16) and (17) can be expanded in a Taylor Series which will converge in a sufficiently small region. The extent of this region is not easily determined, but a series of examples show that in all cases two or three expansions will cover the entire disc. Before proceeding, it is best to list the required derivatives of Eqs. (16) and (17).

$$\sigma_r' = (1/r_1)\,(\sigma_t - \sigma_r - T_1r_1^2) \tag{18a}$$

$$\sigma_r'' = (1/r_1)\,(\sigma_t' - 2\sigma_r' - 2T_1r_1) \tag{18b}$$

$$\sigma_r''' = (1/r_1)\,(\sigma_t'' - 3\sigma_r'' - 2T_1) \tag{18c}$$

$$\sigma_r'''' = (1/r_1)\,(\sigma_t''' - 4\sigma_r''') \tag{18d}$$

. . . . . .

$$\sigma_r^n = (1/r_1)\,(\sigma_t^{n-1} - n\sigma_r^{n-1}) \tag{18e}$$

$$1 = \sigma_r^2 + \sigma_t^2 - \sigma_r\sigma_t \tag{19a}$$

$$0 = 2\sigma_r\sigma_r' + 2\sigma_t\sigma_t' - \sigma_r\sigma_t' - \sigma_t\sigma_r' \tag{19b}$$

$$0 = 2\sigma_r\sigma_r'' + 2\sigma_r'^2 + 2\sigma_t\sigma_t'' + 2\sigma_t'^2 - \sigma_r\sigma_t'' - 2\sigma_r'\sigma_t' - \sigma_t\sigma_r'' \tag{19c}$$

$$0 = 2\sigma_r\sigma_r''' + 6\sigma_r'\sigma_r'' + 2\sigma_t\sigma_t''' + 6\sigma_t'\sigma_t'' - \sigma_r\sigma_t''' - 3\sigma_r'\sigma_t'' - 3\sigma_t'\sigma_r'' - \sigma_t\sigma_r''' \tag{19d}$$

. . . . . .

Eqs. (18) and (19) are best solved for σ_t^n, σ_r^n numerically. There are now two likely starting places for a series expansion. These are at $r_1 = 0$ or 1, the former being discarded because of the resulting indeterminate expressions. Hence, the procedure is as follows:

Let $r_1 = 1$ and assume a value of T_1, σ_r. Use this in Eq. (19a) to evaluate σ_t; then proceed to Eq. (18a) for σ_r'. Using the known values of σ_r, σ_t, σ_r', and T_1 in Eq. (19b), it is easy to evaluate σ_t'. In this manner one proceeds back and forth between Eqs. (18) and (19) to evaluate σ_r^n, σ_t^n, at $r_1 = 1$.

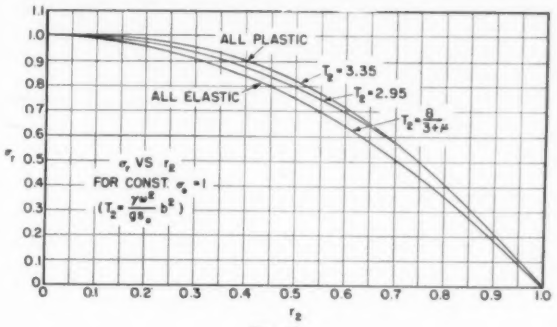

FIG. 2.

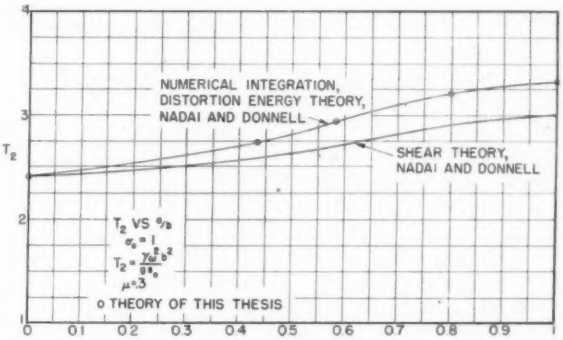

FIG. 3.

The solution is then presented in a Taylor expansion about this point:

$$\sigma_r = \sigma_r(1) - \frac{1 - r_1}{1!}\sigma_r'(1) + \frac{(1 - r_1)^2}{2!}\sigma_r''(1) - \ldots \tag{20}$$

There still remains one boundary condition $\sigma_r = 1$ at $r_1 = 0$. In this connection it will be noted that we had assumed both T_1, $\sigma_r(1)$, but these are not independent. Instead, they are related through the boundary condition at $r_1 = 0$, which will only be satisfied when the correct values of this combination are chosen.

The values of σ_t, σ_r at $r_1 = 1$ are then used as boundary conditions for the elastic region, where this solution is carried out as described in Case (1).

Fig. 2 presents some results and serves as a guide for estimations of T_1, $\sigma_r(1)$ for other solutions. From this figure it is seen that $T_2 = 2.43$, start of yield, and $T_2 = 3.35$, complete penetration of yield. Therefore, the increase of speed for complete penetration is $\omega_p = 1.175\omega_e$, or $17\frac{1}{2}$ per cent. This value should be compared with the 11 per cent based on the theory of maximum shear and the 17 per cent based on distortion energy obtained by Nadai and Donnell.

Fig. 3 presents a graph of T_2 vs. a/b, so that a definite radius of penetration may be assigned to each speed.

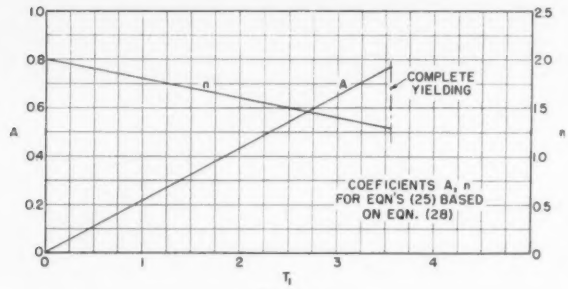

FIG. 4.

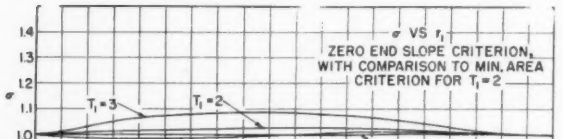

FIG. 5.

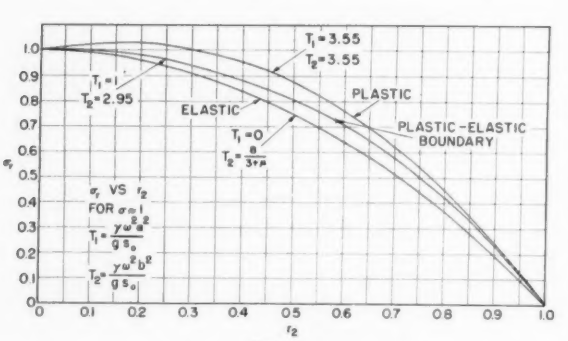

FIG. 6.

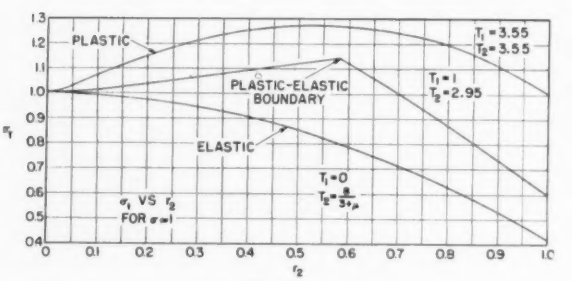

FIG. 7.

Case (3) Elastic Plastic ("Almost" Constant σ)

By allowing the stress-strain curve to vary very little from that of a nonstrain-hardening material, a simple solution can be obtained. This method is capable of extension to more general types of materials.

Let us assume that the stresses can be written as

$$\sigma_r = \sum_1^k A_n r_1^n - (1/2)T_1 r_1^2 + C \tag{21}$$

$$\sigma_t = \sum_1^k G_n r_1^n - (1/2)T_1 r_1^2 + C \tag{22}$$

or, as a special case,

$$\sigma_r = A r_1^n - (1/2)T_1 r_1^2 + C \tag{23}$$

$$\sigma_t = G r_1^n - (1/2)T_1 r_1^2 + C \tag{24}$$

Eqs. (21) and (22) will lead to a "perfect material" if enough terms are taken, but the work becomes too great. Eqs. (23) and (24) lead to variations of approximately 2 to 3 per cent from the ideal; the latter is used in this paper.

Using Eqs. (23) and (24) in the equilibrium Eq. (17), there results

$$G - A(n+1) = 0 \tag{25}$$

Let us further specify $\sigma = 1$, at $r_1 = 0$, 1 and $d\sigma/dr_1 = 0$ at $r_1 = 1$, and we will automatically find $d\sigma/dr_1 = 0$ at $r_1 = 0$ if we stipulate that $n > 1$. The three conditions, when applied to Eq. (16), lead to

$$C = 1 \tag{26}$$

$$2(n^2 + n + 1)A^2 + (n+2)(2 - T_1)A + T_1[(1/2)T_1 - 2] = 0 \tag{27}$$

$$4n(n^2 + n + 1)A^2 + 2n(n+2)A - T_1(n^2 + 4n + 4)A - 4T_1 - 2T_1^2 = 0 \tag{28}$$

Fig. 4 presents n, A vs. T_1. Eq. (25) leads to G once these values are known. Thus, by assuming an arbitrary T_1, one can compute σ_r, σ_t in conjunction with Fig. 4 and Eqs. (23), (24), (25), and (26). Eq. (16) is then checked, and σ vs. r_1 is plotted to see the degree of "perfect" material obtained. Typical results are shown in Fig. 5. By changing n slightly but still satisfying $\sigma = 1$ at $r_1 = 1$, 0, a slight improvement can be obtained. This is also shown in Fig. 5. The elastic region is solved as in Case (2). Typical results for stress vs. r_1 are shown in Figs. 6 and 7. A comparison with those obtained by methods of Case (2) shows almost zero deviation.

Case (4) Variable σ (an Inverse Method)

Let us take the solution in the form

$$\sigma_r = A_1 r_1^n - (1/2)T_1 r_1^2 + F r_1 + C \tag{29}$$

$$\sigma_t = G_1 r_1^n - (1/2)T_1 r_1^2 + E_1 r_1 + C \tag{30}$$

also, we will assume that $r_1 = r_2$ or that the disc is completely plastic. This is not a necessary restriction but leads to some simplification. The boundary conditions are

$$\left.\begin{matrix}\sigma_r = 0\\ \sigma_t = \sigma\end{matrix}\right\} r_1 = 1 \qquad \left.\begin{matrix}\sigma_r = C\\ \sigma_t = C\end{matrix}\right\} r_1 = 0 \tag{31}$$

Using these and the solution given above in Eqs. (4) and (17) leads to

$$\left.\begin{aligned} C &= \sigma_{(r=0)} \\ F &= 2/3\sigma_{(r=0)}' \\ E_1 &= 2F \\ A_1 &= (\sigma_{(r=0)}/n) - (F/n) \\ T_1 &= 2(A_1 + C + F) \\ G_1 &= A_1(n+1) \end{aligned}\right\} \tag{32}$$

Eqs. (32) can be solved in two ways:

(a) Specify $\sigma_{(r=0)}$, $\sigma_{(r=1)}$, $\sigma'_{(r=0)}$ and solve for various parameters of n.

(b) Specify T_1 and only two values of the effective stress or its derivatives such as $\sigma_{(r=0)}'$, $\sigma_{(r=0)}$ or $\sigma_{(r=1)}$, and then solve for n.

Both methods are useful. Method (a) will indicate the relation between speed and the stress strain curves, while Method (b) will give a family of curves (σ-ϵ), which gives complete yielding at a specified speed.

In all cases after the values of the coefficients are determined from Eqs. (32), they will be used in conjunction with Eqs. (4), (29), and (30) to determine the curve σ vs. r_1. Figs. 8 and 9 show such results for the case of $\sigma_{(r=0)}' = 0, -0.2$, respectively. In both cases the value $\sigma_{(r=0)}/\sigma_{(r=1)} = 2$ was used. It is quite feasible and not too difficult to obtain a complete set of such curves, so that any arbitrary stress-strain curve can be almost exactly represented and results obtained by interpolation.

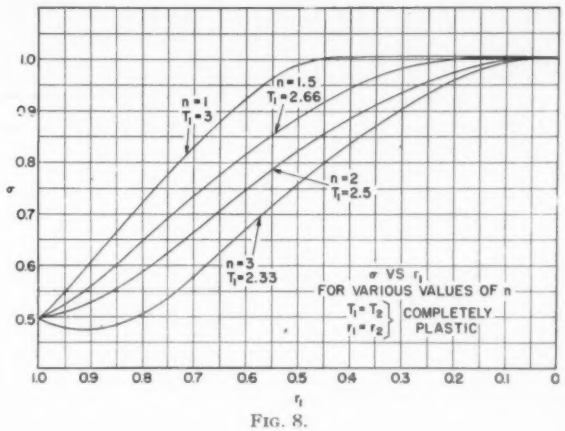

FIG. 8.

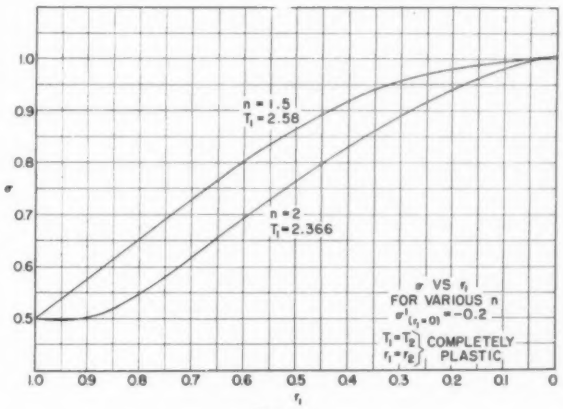

FIG. 9.

(IV) Solution for Strains

In order to solve for strains, it is necessary first to solve Eq. (13) for the modified plastic elastic coefficient H. The solution is

$$He^{\int P_1\,dr} = \int Q_2 e^{\int P_1\,dr}dr + c$$

which is generally too complicated to evaluate.

A second method is to use the same technique as in Case (2) for stresses. From Eq. (13), together with Eq. (17), we obtain

$$\left(\sigma_t - \frac{\sigma_r}{2}\right)H' + \left(\sigma_t' + \sigma_r' + \frac{3}{2}T_1r_1\right)H = T_1r_1\left(\frac{1}{2} - \nu\right) \tag{33a}$$

$$\left(\sigma_t - \frac{\sigma_r}{2}\right)H'' + \left(2\sigma_t' + \frac{\sigma_r'}{2} + \frac{3}{2}T_1r_1\right)H' + \left(\sigma_t'' + \sigma_r'' + \frac{3}{2}T_1\right)H = T_1\left(\frac{1}{2} - \nu\right) \tag{33b}$$

$$\left(\sigma_t - \frac{\sigma_r}{2}\right)H''' + \left(3\sigma_t' + \frac{3}{2}T_1r_1\right)H'' + \left(3\sigma_t'' + \frac{3}{2}\sigma_r'' + 3T_1\right)H' + (\sigma_t''' + \sigma_r''')H = 0 \tag{33c}$$

$$\left(\sigma_t - \frac{\sigma_r}{2}\right)H'''' + \left(4\sigma_t' - \frac{\sigma_r'}{2} + \frac{3}{2}T_1r_1\right)H''' + \left(6\sigma_t'' + \frac{3}{2}\sigma_r'' + \frac{9}{2}T_1\right)H'' + \left(4\sigma_t''' + \frac{5}{2}\sigma_r'''\right)H' + (\sigma_t'''' + \sigma_r'''')H = 0 \tag{33d}$$

and all higher derivatives as required. From Eqs. (33a)–(33d) it is seen that, having the stresses and their derivatives at a point, H can be expanded about that point. This is,

$$H(r_1) = H(d) - \frac{d - r_1}{1!}H'(d) + \frac{(d - r_1)^2}{2!}H''(d) - \dots \tag{34}$$

where usually $d = 1$. At $d = 1$, it is easy to see that $H = 1$, since this is the plastic boundary. Now Eq. (34) will converge within a sufficiently small rgion, and it is possible, although not necessary, that this region will include the entire disc. However, to calculate the required derivatives for Eq. (34) is much too tedious a job. To simplify this procedure, it is neces-

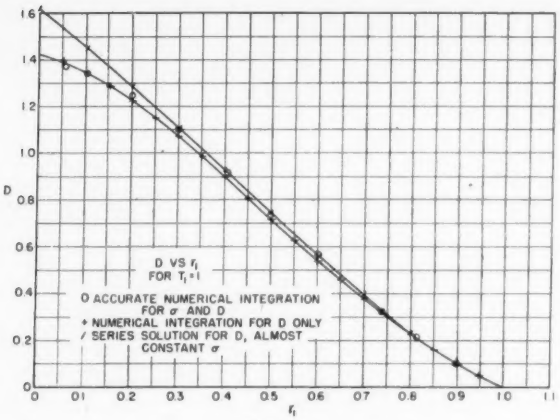
D VS r_1
FOR T_1=1
O ACCURATE NUMERICAL INTEGRATION FOR σ AND D
+ NUMERICAL INTEGRATION FOR D ONLY
/ SERIES SOLUTION FOR D, ALMOST CONSTANT σ
D
r_1

FIG. 10.

sary only to calculate the first few derivatives and values at a new point, where the convergence is sufficiently rapid. Using these values, derivatives are found about the new point, and in this way the solution is continued over the entire disc.

The solution can be divided into two main groups.

Group (I).—Constant and almost constant σ: The case of constant and almost constant σ has been shown to have, for any degree of accuracy, the same σ_r, σ_t, and σ. Because of this fact, it is apparent that they will have this same correspondence in strains. Hence, we will take, from Eqs. (23) and (24),

$$\sigma_r = Ar_1^n - (1/2)T_1r_1^2 + C \quad (35a)$$
$$\sigma_r' = nAr_1^{n-1} - T_1r_1 \quad (35b)$$
$$\sigma_r'' = n(n-1)Ar_1^{n-2} - T_1 \quad (35c)$$
$$\sigma_r^K = n(n-1)\ldots(n-K+1)\,Ar_1^{n-K} \quad (35d)$$

$$\sigma_t = Gr_1^n - (1/2)T_1r_1^2 + C \quad (36a)$$
$$\sigma_t' = nGr_1^{n-1} - T_1r_1 \quad (36b)$$
$$\sigma_t'' = n(n-1)\,Gr_1^{n-2} - T_1 \quad (36c)$$
$$\sigma_t^K = n(n-1)\ldots(n-K+1)\,Gr_1^{n-K} \quad (36d)$$

Group (II).—Variable σ: We obtain the values of the stress and derivatives from Eqs. (29) and (30); they are:

$$\sigma_r = A_1r_1^n - (1/2)T_1r_1^2 + Fr_1 + C \quad (37a)$$
$$\sigma_r' = nA_1r_1^{n-1} - T_1r_1 + F \quad (37b)$$
$$\sigma_r'' = n(n-1)A_1r_1^{n-2} - T_1 \quad (37c)$$
$$\sigma_r^K = n(n-1)\ldots(n-K+1)\,A_1r_1^{n-K} \quad (37d)$$

$$\sigma_t = G_1r_1^n - (1/2)T_1r_1^2 + E_1r_1 + C \quad (38a)$$
$$\sigma_t' = nG_1r_1^{n-1} - T_1r_1 + E_1 \quad (38b)$$
$$\sigma_t'' = n(n-1)\,G_1r_1^{n-2} - T_1 \quad (38c)$$
$$\sigma_t^K = n(n-1)\ldots(n-K+1)\,G_1r_1^{n-K} \quad (38d)$$

Thus, H can be found by use of Eqs. (35) and (36) or (37) and (38), together with Eqs. (33) and (34). From Eqs. (6) to (9) inclusive, the strains are computed, and, in the case of variable σ, the σ-ϵ curve can be established.

Fig. 10 compares D obtained by numerical integration and by series expansion for constant and almost constant σ, $T_1 = 1$. The series expansion is about $d = 1$, which is sufficiently accurate for this case. If higher accuracy were desired, an expansion about $d = 0.2$ would be sufficient.

Fig. 11 shows results of a series expansion for $T = 3.55$ and almost constant σ. Here, we see that for accurate results it was necessary to expand a second time about $d_1 = 1/2$. By expanding back to $r_1 = 1$, the error at $r_1 = 0$ can be estimated. If the results are used for the expansion about $d = 1$ for $1/2 \leq r_1 \leq 1$ and that about $d_1 = 1/2$ for $0 \leq r_1 \leq 1/2$, a maximum error of about 4 per cent at $r_1 = 0$ will result.

Fig. 12 shows a comparison of the strains for two individual numerical integrations with constant σ for the series expansion based on approximately constant σ and for the theory of maximum shear neglecting elastic strains in the plastic region. Here, the discontinuities of the latter theory become apparent. The strains, especially that of ϵ_z, are greatly in error. We also note that the results of the series expansion agree with the numerical integrations.

Typical solutions for a strain-hardening material are presented in Figs. 13 to 16, inclusive. They were only investigated for $\sigma_{inside} = 2\sigma_{outside}$. A comparison with Figs. 8 and 9 will lead to the conclusion that the more easily obtained stress-radius diagram can be of great

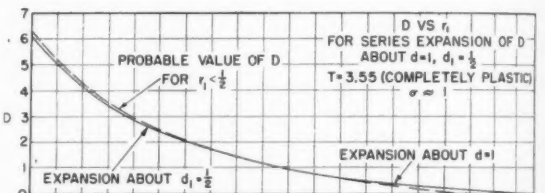

FIG. 11.

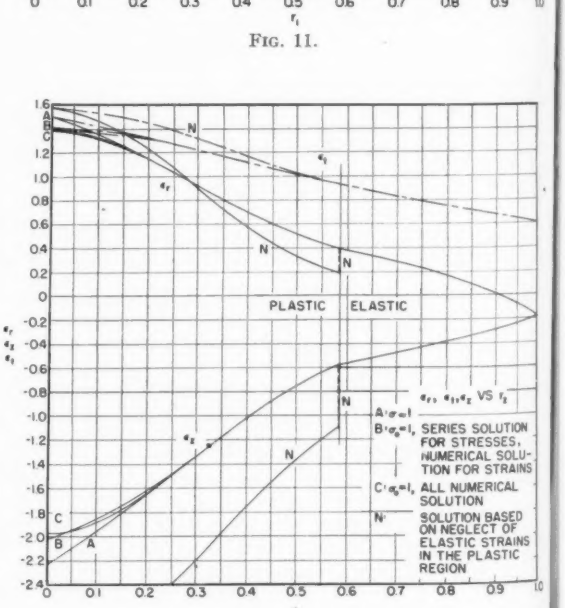
PLASTIC
ELASTIC
A: σ=1
B: σ_0=1, SERIES SOLUTION FOR STRESSES, NUMERICAL SOLUTION FOR STRAINS
C: σ_0=1, ALL NUMERICAL SOLUTION
N: SOLUTION BASED ON NEGLECT OF ELASTIC STRAINS IN THE PLASTIC REGION
r_2

FIG. 12.

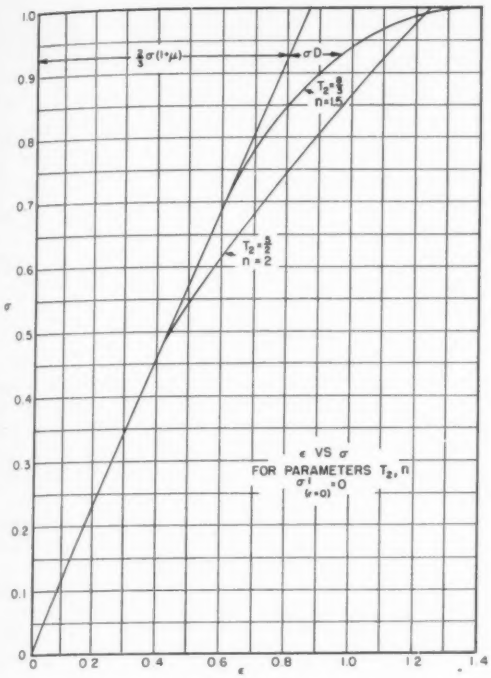

FIG. 13.

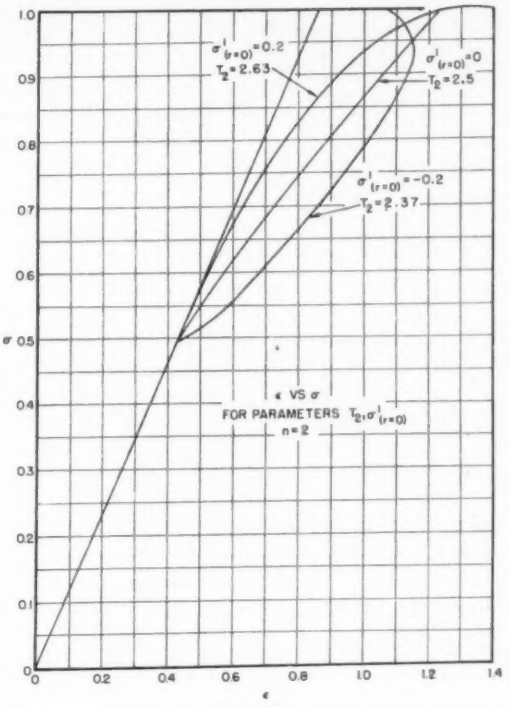

FIG. 14.

value in determining a good approximation to the required stress-strain curve.

(V) EXAMPLE

Given: Disc; (1) 24 in. radius, flat; (2) steel ($\gamma = 0.283$); and (3) yield stress (s_0) = 50×10^3.

Required: (1) Speed necessary to cause a plastic region of 28-in. diameter. (2) Speed necessary to cause the plastic region to extend throughout the disc. (3) Stress distribution in the disc with a plastic region of 28-in. diameter. (4) Strain distribution in the disc with a plastic region of 28-in. diameter.

Solution: (1) $a = 28/2 = 14$ in. and $b = 24$ in.; therefore $a/b = 0.5833$. From Fig. 3 we find $T_2 = 2.94$. Since

$$T_2 = (\gamma/g)\ (\omega^2/s_0)\ b^2$$

we have $\omega = 590$ rad./sec. or $\omega = 5{,}640$ r.p.m. to cause a penetration of 14-in. radius.

(2) For full penetration, $a = b$ and $a/b = 1$. From Fig. 3, $T_2 = 3.35$ and, as above,

$$\omega = 635 \text{ rad./sec.} = 6{,}030 \text{ r.p.m.}$$

(3) $T_1 = (a^2/b^2)T_2$, or for 14-in. penetration $a/b = 0.5833$, $T_1 = 1$. From Fig. 4, $A = 0.228$, $n = 1.82$, and using these values in Eq. (25) leads to $G = 0.642$. Returning to Eqs. (23) and (24) for the plastic region, we have

$$s_r/s_0 = 0.228 r_1^{1.82} - (1/2)\ (1)\ r_1^2 + 1 \quad \text{(Ex 1)}$$

$$s_t/s_0 = 0.642 r_1^{1.82} - (1/2)\ (1)\ r_1^2 + 1 \quad \text{(Ex 2)}$$

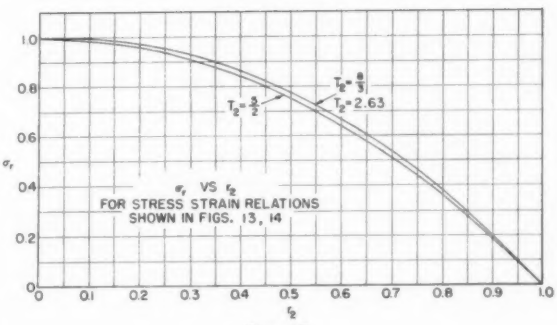

FIG. 15.

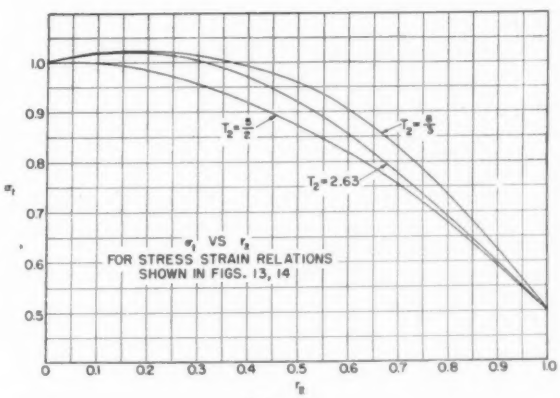

FIG. 16.

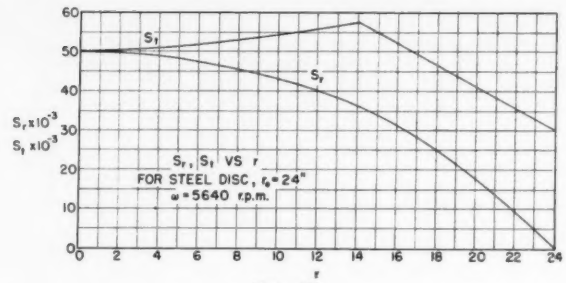

FIG. 17.

$0 \leq r_1 \leq 1$. For the elastic region we use Eqs. (14) and (15), which give

$$s_r/s_0 = C_1 - C_2 r_2^{-2} - (2.94/8)(3.3) r_2^2 \quad \text{(Ex 3)}$$

$$s_t/s_0 = C_1 + C_2 r_2^{-2} - (2.94/8)(1.9) r_2^2 \quad \text{(Ex 4)}$$

$0.583 \leq r_2 \leq 1$. Now, at $r_1 = 1$, $r_2 = 0.583$, we have

$$(s_r/s_0)_{\text{plastic}} = (s_r/s_0)_{\text{elastic}}$$
$$(s_t/s_0)_{\text{plastic}} = (s_t/s_0)_{\text{elastic}}$$

using these facts in the above equations results in $C_1 = 1.259$ and $C_2 = 0.041$. Thus,

$$s_r/s_0 = 1.259 - 0.041 r_2^{-2} - 1.21 r_2^2 \quad \text{(Ex 5)}$$

$$s_t/s_0 = 1.259 + 0.041 r_2^{-2} - 0.699 r_2^2 \quad \text{(Ex 6)}$$

We can check Eq. (Ex 5) by the fact that, at $r_2 = 1$, $s_r = 0.008 s_0$, but we expect $s_r = 0$. Considering that the values of T_2, n, and A are read from graphs, the accuracy is high. Recalling that $r_1 = r/a$, $r_2 = r/b$, we use Eqs. (Ex 1), (Ex 2), (Ex 5), and (Ex 6) to find s_r, s_t vs. r as shown in Fig. 17.

(4) The strains can be obtained from Fig. 12 in terms of ϵ_r, ϵ_t, ϵ_z, vs. r.

REFERENCES

[1] Nadai, A., and Donnell, L. H., *Stress Distribution in Rotating Disks of Ductile Material After the Yield Point Has Been Reached*, Transactions, A.S.M.E., APM-51-16, 1929.

[2] Nadai, A., *Theory of Flow and Fracture of Solids*, Vol. 1, Engineering Societies Monographs; McGraw-Hill Book Company, Inc., New York, 1950.

[3] Fisher, J. C., *Plasticity Problems for General Examination of Mr. J. C. Fisher*, unpublished work done while at M.I.T., June, 1946.

[4] Courant, R., and Hilbert, D., *Mathematische Physik II*; Julius Springer, Berlin, 1937.

A Second-Order Solution for an Oscillating Two-Dimensional Supersonic Airfoil

(*Concluded from page 696*)

Hence, the theoretical second-order solution for the airfoil rotating about its midchord ($x_0 = 1/2$) is found to be

$$M_\alpha = \frac{1}{3\beta^3}\left(2 - M^2 - \frac{0.15D}{\beta} - 0.075B\beta\right) \tag{45}$$

The damping coefficients as given by the experimental investigations, linearized theory, and the present paper [Eq. (45)] are presented on Fig. 9 as a function of Mach Number. As may be seen, the second-order† solution reproduces the trends of, but is somewhat lower in magnitude than, the experimental data. Some of the discrepancy is probably due to the effects of flexure in the model which would tend toward increasing the magnitude of M_α.

REFERENCES

[1] Wylly, A., *A Second-Order Solution for an Oscillating, Two-Dimensional Supersonic Airfoil*, Thesis, California Institute of Technology, Pasadena, Calif., 1951.

[2] Possio, Camillo, *L'Azione Aerodinamica sul Profilo Oscillante alle Velocita Ultrasonore, Acta Pontif. Acad. Sci.*, Vol. 1, No. II, 1937. (Available as Cornell Aeronautical Laboratory Translation: *The Aerodynamic Action on an Oscillating Profile at Supersonic Velocities.*)

[3] von Borbély, S., *Über die Luftkräfte die auf einen harmonisch schwingenden zweidimensionalen Flügel bei Überschallgeschwindigkeit wirken*, ZWB FB 1701, 1942. (Also available as British RTP-2019.)

[4] Stewart, H. J., and Ting-Yi Li, *Periodic Motions of a Rectangular Wing Moving at Supersonic Speed, Journal of the Aeronautical Sciences*, Vol. 17, No. 9, p. 549, 1950.

[5] Miles, J. W., *Transient Loading of Wide Delta Airfoils at Supersonic Speeds*, U.S. Naval Ordnance Test Station Tech. Memo. RRB-37, 1950.

[6] Miles, J. W., *The Oscillating Rectangular Airfoil at Supersonic Speeds*, U.S. Naval Ordnance Test Station Report 1170, 1949.

[7] Hipsch, H. M., *Harmonic Oscillations of a Narrow Delta Wing in Supersonic Flow*, Thesis, California Institute of Technology, Pasadena, Calif., 1951.

[8] Froelich, J. E., *Non-Stationary Motion of Purely Supersonic Wings*, Thesis, California Institute of Technology, Pasadena, Calif. 1950.

[9] Parkinson, G. V., *Non-Uniform Motion of a Wide Delta Wing*, Thesis, California Institute of Technology, Pasadena, Calif. 1951.

[10] Guderley, G., *The Lift of a Two-Dimensional Flat Plate Oscillating with a Small Frequency*, unpublished note, December, 1947.

[11] Watkins, C. E., *Effect of Aspect Ratio on the Air Forces and Moments of Harmonically Oscillating Thin Rectangular Wings in Supersonic Potential Flow*, N.A.C.A. T.N. No. 2064, 1950.

[12] Van Dyke, Milton D., *A Study of Second-Order Supersonic Flow*, Thesis, California Institute of Technology, Pasadena, Calif., 1948. (Also available as N.A.C.A. T.N. No. 2200, 1951.)

[13] Courant, R., and Friedrichs, K. O., *Supersonic Flow and Shock Waves*, p. 365; Interscience, New York, 1948.

[14] Garrick, I. E., and Rubinow, S. I., *Flutter and Oscillating Air Force Calculations for an Airfoil in a Two-Dimensional Supersonic Flow*, N.A.C.A. T.N. No. 1158, 1946.

[15] Beavan, J. A., and Holder, D. W., *Recent Developments in High Speed Research, The Journal of the Royal Aeronautical Society*, Vol. 54, No. 477, September, 1950.

† The angular frequency of the experimental tests was extremely low so that $\bar{\omega} \simeq 0$; thus, the higher-order terms in frequency are certainly negligible.

On Heat Transfer over a Sweat-Cooled Surface in Laminar Compressible Flow with a Pressure Gradient*

MORRIS MORDUCHOW†

Polytechnic Institute of Brooklyn

SUMMARY

A simple expression is derived for the normal injection velocity distribution theoretically required to maintain a given uniform temperature along a porous surface in the laminar boundary-layer region of a compressible flow with a given velocity distribution outside of the boundary layer. This expression is valid for any given free-stream Mach Number but is based on a Prandtl Number of unity and on the assumption that the viscosity coefficient varies linearly with the temperature. By using the Dorodnitsyn type of transformation, the variation of fluid properties even in the case of zero Mach Number is taken into account. This study is of particular practical interest in connection with the sweat-cooling of turbine blades and of airfoil surfaces in high-speed flow. The method of analysis consists of applying the Kármán-Pohlhausen method to both the momentum and energy boundary-layer equations and of using an additional heat balance equation, involving the coolant temperature. A closed-form approximate solution of the equations is then derived. Numerical examples for flow in the immediate vicinity of a stagnation point and for a typical type of flow over a turbine blade are given.

INTRODUCTION

A PROBLEM OF PARTICULAR INTEREST in connection with the sweat-cooling of turbine blades or of airfoil surfaces in high-speed flow is that of maintaining a given uniform wall temperature. This can be done by designing the porosity of the surfaces so as to obtain a certain distribution, along the walls, of normal mass flow of the coolant. The main purpose of the present analysis is to derive this required distribution theoretically for the general case of laminar flow. The required mass flow distribution will, in general, be a function of the coolant temperature, the desired uniform wall temperature, the free-stream Mach Number, and the velocity distribution outside of the boundary layer, which depends on the shape of the surface profile. All of these factors are here taken into account. The coolant will be assumed to be the same as the external gas flowing over the surface. Radiation effects are neglected, while the temperature of the coolant is assumed as constant along the surface. Centrifugal and Coriolis effects due to possible rotation of the airfoil surfaces will not be considered. In view of the results of Fogarty,[1] this may not cause any serious errors in actual application of the theory to rotating blades.

Heat-transfer analyses have already been carried out for a number of special cases. Yuan[2,3] has investigated in detail the heat-transfer characteristics for incompressible and compressible flow over a sweat-cooled flat plate, using the Kármán-Pohlhausen method. Klunker and Ivey[4] have also investigated this case. They used various simplifying assumptions but included, in their heat-transfer calculations, effects of radiation and (if the coolant is a liquid) of vaporization. Eckert,[5] using the transformation methods of Schlichting[6] and of Falkner and Skan[7] has analyzed the case in which the velocity outside of the boundary layer is proportional to a power (especially the first) of distance along the wall from the stagnation point. Eckert's analysis was based on incompressible flow and constant fluid properties.

The method to be used in the present investigation is essentially the same as that of references 8 and 9 and is based on an application of the Kármán-Pohlhausen method to both the energy and momentum boundary-layer equations for compressible flow. In reference 8, however, a normal velocity at the wall was not considered. In reference 9, a normal velocity at the wall was considered, but a heat balance involving the coolant temperature was not taken into account. Hence, in reference 9 the coolant injection velocity and the wall temperature were considered as independent parameters, instead of as being related through the temperature of the coolant; the separate effects of the injection parameter and the wall temperature parameter on the boundary-layer characteristics could then be investigated there in some detail for general cases. In the present analysis, a heat balance equation is added to the boundary-layer equations, and the primary emphasis is now not on the boundary-layer characteristics as such but on the heat-transfer properties at the wall and on the injection velocity distribution required to maintain a given uniform wall temperature.

By making use of the Dorodnitsyn type of transformation for compressible boundary-layer flow and by making the approximating assumption that the ratio of dynamical to thermal boundary-layer thickness is

Received November 15, 1951.

* This research was conducted under the auspices of Project Squid, jointly sponsored by the Office of Naval Research and the Office of Air Research under contract N6-ORI-98, Task Order NR-220-039. The author hereby expresses his thanks to Drs. S. W. Yuan and P. A. Libby for their valuable suggestions.

† Assistant Professor of Applied Mathematics.

constant along the flow, it is possible to obtain a simple approximate solution to the ordinary differential equations developed here. For any given main-stream velocity distribution and Mach Number, this solution permits a rapid determination of any pertinent heat-transfer characteristics and of the injection velocity distribution required for a given uniform wall temperature.

The results obtained here are based on laminar flow, which is the type to be expected at least near the leading edge of a surface where the pressure gradient is favorable. The results are also based on a Prandtl Number of unity and on the assumption that the viscosity coefficient is proportional to the absolute temperature.

As numerical examples, results for the flow near a forward stagnation point are given in some detail, since this is the type of flow which may be expected in the immediate vicinity of the leading edge of a round-nosed object in subsonic flow. Numerical results are also given for what might represent the flow over the suction side and over the pressure side of an actual turbine blade.

Symbols

a_1 = coefficient of η_1 in velocity profile
$\bar{a}_1$, $\bar{a_1^2}$ = constant "average" values of a_1 and a_1^2
b_1 = coefficient of η_2 in stagnation enthalpy profile
C = coolant-temperature parameter, defined by Eq. (16b)
c_p = specific heat of gas at constant pressure
g = ratio of dynamical to thermal boundary-layer thickness in (x, t) plane ($g \equiv \delta_{t1}/\delta_{t2} \equiv \kappa/\lambda$)
H = stagnation enthalpy, defined as the quantity $[(u^2/2) + c_pT]$
h = H_0/H_1; for a Prandtl Number of 1, $h = T_0/T_e$ (ratio of actual wall temperature to equilibrium zero-heat-transfer wall temperature)
k = coefficient of heat conductivity of gas
l = characteristic length
M = Mach Number
Re = Reynolds Number $(\rho_\infty u_\infty l/\mu_\infty)$
T = absolute temperature
T_e = temperature of the coolant
t = variable defined by Eq. (7)
u = velocity of flow along surface
v = velocity of flow normal to surface
x, y = distance along and normal to surface, respectively
γ = ratio of specific heats (c_p/c_v); $\gamma = 1.4$ for air here
δ_{t1}, δ_{t2} = dynamical and thermal boundary-layer thicknesses, respectively, in (x, t) plane
η_1, η_2 = (t/δ_{t1}) and (t/δ_{t2}), respectively
κ = $(\delta_{t1}/l)Re^{1/2}$
λ = $(\delta_{t2}/l)Re^{1/2}$
ν = kinematic viscosity (μ/ρ)
ξ = x/l
φ = $[(\rho_0 v_0/\rho_\infty u_\infty)Re^{1/2}]$, injection parameter

Subscripts

0 = values at wall—e.g., T_0, v_0, ρ_0
1 = values at local outer edge of boundary layer—e.g., M_1, T_1, u_1
∞ = values at a convenient reference point outside of boundary layer—e.g., in undisturbed flow at infinity in absence of shock waves

A prime (′) denotes differentiation with respect to ξ.

Basic Equations

The momentum and energy equations for compressible two-dimensional flow in the laminar boundary layer of a gas with a Prandtl Number $(\mu c_p/k)$ of unity can be expressed in the form

$$\rho u \frac{\partial u}{\partial x} + \rho v \frac{\partial u}{\partial y} = \rho_1 u_1 \frac{du_1}{dx} + \frac{\partial}{\partial y}\left(\mu \frac{\partial u}{\partial y}\right) \tag{1}$$

$$\rho u \frac{\partial H}{\partial x} + \rho v \frac{\partial H}{\partial y} = \frac{\partial}{\partial y}\left(\mu \frac{\partial H}{\partial y}\right) \tag{2}$$

The continuity equation is

$$[\partial(\rho u)/\partial x] + [\partial(\rho v)/\partial y] = 0 \tag{3}$$

Since the pressure is assumed as constant across the boundary-layer thickness, the ideal gas law implies

$$\rho/\rho_1 = T_1/T \tag{4}$$

It will be assumed here that the coefficient of viscosity is proportional to the temperature—i.e.,

$$\mu/\mu_1 = T/T_1 \tag{5}$$

The heat-balance equation, stating that the heat transferred by the hot gas to the wall is absorbed by the coolant, can be written as (cf. references 2, 3, 4, and 5)*

$$[k(\partial T/\partial y)]_0 = \rho_0 v_0 c_p (T_0 - T_e) \tag{6}$$

Introducing the Dorodnitsyn variable t defined by

$$y = \int_0^t (T/T_1)\, dt \tag{7}$$

integrating both Eqs. (1) and (2) with respect to t from $t = 0$ to $t = \delta_{t1}$ or δ_{t2}, whichever is larger, and using Eqs. (3), (4), and (5), the following equations expressed in nondimensional form, are obtained, under the boundary conditions of $u = 0, v = v_0(x)$ at the wall and smooth transition of the velocity and stagnation enthalpy profiles to the local main-stream values at the outer edges of the boundary layer:

$$F_1 \kappa \kappa' + \kappa^2 \left[F_1 \frac{\rho_1'}{\rho_1} + F_1' + F_2 \frac{u_1'}{u_1}\right] = \frac{u_\infty}{u_1} \times \left[\kappa\varphi \frac{\rho_\infty}{\rho_1} + F_3 \frac{\nu_1}{\nu_\infty}\right] \tag{8}$$

$$F_4 \lambda \lambda' + \lambda^2 \left[F_4' + F_4\left(\frac{u_1'}{u_1} + \frac{\rho_1'}{\rho_1}\right)\right] = \frac{u_\infty}{u_1}\left[\lambda\varphi(1-h)\frac{\rho_\infty}{\rho_1} + F_5 \frac{\nu_1}{\nu_\infty}\right] \tag{9}$$

* In references 2 and 3, Eq. (6) was used in integrated form over the length of the plate, so that the heat balance was satisfied there only in the average rather than at each point along the plate. Consequently, the constant surface temperature appearing in references 2 and 3 must be interpreted as a kind of average temperature over the length of the plate, since according to Eq. (6) in the present form the surface temperature will actually vary along the plate if the injection velocity is uniform.

where

$$
\left.
\begin{aligned}
F_1 &= \int_0^1 \left(\frac{u}{u_1}\right)\left(1 - \frac{u}{u_1}\right) d\eta_1 \\
F_3 &= [(\partial/\partial\eta_1)\ (u/u_1)]_0 \\
F_5 &= [(\partial/\partial\eta_2)\ (H/H_1)]_0 \\
F_2 &= 2F_1 + \frac{1}{g}\int_0^1 \left(\frac{T}{T_1} - \frac{u}{u_1}\right) d\eta_2 + \\
&\quad \int_{1/g}^1 \left(\frac{T}{T_1} - \frac{u}{u_1}\right)_{H/H_1=1} d\eta_1 \quad (g \geq 1) \\
F_2 &= 2F_1 + \int_0^1 \left(\frac{T}{T_1} - \frac{u}{u_1}\right) d\eta_1 + \\
&\quad \frac{1}{g}\int_g^1 \left(\frac{T}{T_1} - \frac{u}{u_1}\right)_{u/u_1=1} d\eta_2 \quad (g \leq 1) \\
F_4 &= \int_0^1 \left(\frac{u}{u_1}\right)\left(1 - \frac{H}{H_1}\right) d\eta_2 \quad (g \geq 1) \\
F_4 &= \int_0^g \left(\frac{u}{u_1}\right)\left(1 - \frac{H}{H_1}\right) d\eta_2 + \\
&\quad \int_g^1 \left(1 - \frac{H}{H_1}\right) d\eta_2 \quad (g \leq 1)
\end{aligned}
\right\} \tag{10a}
$$

From the definition of the stagnation enthalpy H, it follows that

$$
\frac{T}{T_1} = \left(\frac{H}{H_1}\right)\left(1 + \frac{\gamma - 1}{2} M_1^2\right) - \left(\frac{u}{u_1}\right)^2 \left(\frac{\gamma - 1}{2}\right) M_1^2 \tag{10}
$$

Eqs. (8) and (9) are essentially extensions of the von Kármán integral equation to the momentum and energy laminar boundary-layer equations in compressible flow.

The following fourth-degree profiles in η_1 and η_2 are now assumed for the velocity and the stagnation enthalpy:

$$
u/u_1 = a_1\eta_1 + (6 - 3a_1)\eta_1^2 + (3a_1 - 8)\eta_1^3 + (3 - a_1)\eta_1^4 \tag{11}
$$

$$
H/H_1 = h + b_1\eta_2 + (6 - 6h - 3b_1)\eta_2^2 + (8h - 8 + 3b_1)\eta_2^3 + (3 - 3h - b_1)\eta_2^4 \tag{12}
$$

where

$$
a_1 = \frac{2 + \frac{1}{6}\frac{u_1'}{u_\infty} h \left(1 + \frac{\gamma - 1}{2} M_1^2\right) \frac{\nu_\infty}{\nu_1} \kappa^2}{1 + (1/6)\kappa\varphi(T_\infty/T_1)}
$$

$$
b_1 = 2(1 - h)/[1 + (1/6)\lambda\varphi(T_\infty/T_1)] \tag{14}
$$

These profiles have been chosen to satisfy the following boundary conditions at the wall in the physical (x, y) plane: At $y = 0$,

$$
u/u_1 = 0, \qquad H/H_1 = h
$$

$$
\rho_0 v_0 \left(\frac{\partial u}{\partial y}\right)_0 = \rho_1 u_1 \frac{du_1}{dx} + \left[\frac{\partial}{\partial y}\left(\mu \frac{\partial u}{\partial y}\right)\right]_0
$$

$$
\rho_0 v_0 \left(\frac{\partial H}{\partial y}\right)_0 = \left[\frac{\partial}{\partial y}\left(\mu \frac{\partial H}{\partial y}\right)\right]_0
$$

The last two conditions above follow from the original partial differential Eqs. (1) and (2).

At the outer edge of the boundary layer, the following conditions are satisfied by the profiles (11) and (12): At $t = \delta_{t1}$ $(\eta_1 = 1)$,

$$
\frac{u}{u_1} = 1, \quad \frac{\partial(u/u_1)}{\partial\eta_1} = \frac{\partial^2(u/u_1)}{\partial\eta_1^2} = 0
$$

At $t = \delta_{t2}$ $(\eta_2 = 1)$,

$$
\frac{H}{H_1} = 1, \quad \frac{\partial(H/H_1)}{\partial\eta_2} = \frac{\partial^2(H/H_1)}{\partial\eta_2^2} = 0
$$

Since the Prandtl Number has been assumed as unity, the equilibrium wall temperature T_e for zero heat transfer $(b_1 = 0)$ will be

$$
T_e = T_1\left(1 + \frac{\gamma - 1}{2} M_1^2\right) = T_\infty\left(1 + \frac{\gamma - 1}{2} M_\infty^2\right) \tag{15a}
$$

Moreover,

$$
h \equiv \frac{H_0}{H_1} \equiv \frac{c_p T_0}{(u_1^2/2) + c_p T_1} = T_0/T_e \tag{15b}
$$

Thus, for a Prandtl Number of unity, h is the ratio of actual wall temperature to the equilibrium zero-heat-transfer wall temperature. The case $h = 1$ is that of a heat-insulated wall, while the cases $h < 1$ and $h > 1$ are, respectively, those of an artificially cooled and an artificially heated wall.

Eq. (6), with the use of Eqs. (10b), (12), (14), (15a), and (15b) and with the relation $\lambda = \kappa/g$, can be written in nondimensional form as a quadratic in $(\varphi\kappa)$. Solving this equation for $(\varphi\kappa)$ yields

$$
\varphi\kappa = Cg(T_1/T_\infty) \tag{16a}
$$

where C is a constant defined as

$$
C = 3\left(\left\{1 + \frac{4}{3}\left[\frac{1 - h}{h - (T_e/T_\infty)}\right]\right\}^{1/2} - 1\right) \tag{16b}
$$

Thus the required injection parameter $\varphi(\xi)$ varies inversely as the dimensionless boundary-layer thickness κ in the (x, t) plane.

With the profiles (11) and (12), the expressions for the F_i will be

$$
\begin{aligned}
F_1 &= 0.1143 + 0.00953a_1 - 0.00397a_1^2 \\
F_3 &= a_1 \\
F_5 &= b_1 \\
F_2 &= 2F_1 + 0.4\left(1 - \frac{1}{g}\right) + \left(\frac{0.4}{g}\right)h + 0.05\left(\frac{b_1}{g} - a_1\right) + \left(\frac{\gamma - 1}{2}\right)M_1^2 \times \\
&\quad \left[0.514 - \frac{0.4}{g} + \left(\frac{0.4}{g}\right)h + \left(\frac{0.05}{g}\right)b_1 - 0.0405a_1 - 0.00397a_1^2\right] \\
F_4 &= (1 - h)\,[0.4 - (0.4g) + 0.2286g^3 - 0.1429g^4 + 0.0286g^5] + a_1(1 - h)\,(0.05g - 0.0429g^3 + \\
&\quad 0.0286g^4 - 0.00596g^5) + b_1(-0.05 + 0.1g^2 - 0.1143g^3 + 0.0536g^4 - 0.00953g^5) + \\
&\quad a_1b_1\,(-0.01667g^2 + 0.0214g^3 - 0.0107g^4 + 0.00199g^5) \quad (g \leq 1) \\
F_4 &= (1 - h)\left(\frac{0.2286}{g^2} - \frac{0.1429}{g^3} + \frac{0.0286}{g^4}\right) + a_1(1 - h)\left(\frac{0.1}{g} - \frac{0.1143}{g^2} + \frac{0.0536}{g^3} - \frac{0.00953}{g^4}\right) + \\
&\quad b_1\left(-\frac{0.0429}{g^2} + \frac{0.0286}{g^3} - \frac{0.00595}{g^4}\right) + a_1b_1\left(-\frac{0.01667}{g} + \frac{0.0214}{g^2} - \frac{0.0107}{g^3} + \frac{0.00199}{g^4}\right) \quad (g \geq 1)
\end{aligned}
\tag{17}
$$

With Eq. (16a), the expressions (13) and (14) for a_1 and b_1 become

$$a_1 = \frac{2 + \frac{1}{6}\frac{u_1'}{u_\infty}h\left(1 + \frac{\gamma - 1}{2}M_1^2\right)\frac{\nu_\infty}{\nu_1}\kappa^2}{1 + 1/6\,Cg} \tag{18}$$

$$b_1 = 2(1 - h)/[1 + (1/6)C] \tag{19}$$

From the relation $(u^2/2) + c_pT =$ constant, and the assumption of isentropic flow, the following relations can be derived for the flow outside of the boundary layer:*

$$T_1/T_\infty = 1 + [(\gamma - 1)/2]M_\infty^2[1 - (u_1/u_\infty)^2] \tag{20a}$$

$$M_1^2 = M_\infty^2(u_1/u_\infty)^2\,(T_1/T_\infty)^{-1} \tag{20b}$$

$$\rho_1/\rho_\infty = (T_1/T_\infty)^{1/(\gamma-1)} \tag{20c}$$

The problem in this investigation can now be formulated thus. For a given constant ratio (h) of wall temperature to equilibrium temperature, a given value of the coolant-temperature parameter (C), a given Mach Number (M_∞), and a given velocity distribution $(u_1/u_\infty)(\xi)$, it is required to solve Eqs. (8), (9), and (16a) for $\kappa(\xi)$, $\lambda(\xi)$, and $\varphi(\xi)$. A simple approximate solution of these equations will be derived in the next section.

It should be noted that in the present analysis the case of zero Mach Number is not equivalent to incompressible flow, since when $h \neq 1$ (i.e., $T_0 \neq T_1$) the density ρ, as well as the temperature and viscosity coefficient, will still vary across the boundary-layer thickness in accordance with Eqs. (4), (5), (10b), (12), and (14).

* In the case of a shock-wave at the leading edge, the quantities with subscript "∞" refer to a convenient reference point behind the wave.

General Approximate Solution

To solve Eqs. (8), (9), and (16a) in a simple manner, the following two approximating assumptions are made:

(a) The ratio (g) of velocity (dynamical) to stagnation enthalpy (thermal) boundary-layer thickness in the (x, t) plane is constant along the flow (although it may be different for different types of flow).

(b) In the expressions for F_1 and F_2 (and only there), the quantities a_1 and a_1^2 may be replaced by constant "average" values $\overline{a_1}$ and $\overline{a_1^2}$.

Assumption (a), aside from the fact that it may appear reasonable physically, is based on noting that it is exactly valid for the flow over a flat plate ($u_1/u_\infty = 1$) with a uniform wall temperature, regardless of the Mach Number and of the injection velocity distribution. In that case, in fact, Eqs. (8) and (9) imply that $g = 1$ everywhere. Moreover, as will be shown subsequently, this assumption is also exactly valid for flow at zero Mach Number near a stagnation point.

Assumption (b) is justified by the fact that the a_1 terms appearing in F_1 and F_2 [Eqs. (17)] are relatively small and that, consequently, errors made in evaluating these terms will have only a relatively small effect there. As a check on the accuracy of assumptions (a) and (b), the cases $u_1/u_\infty = 1 + \xi$ and $u_1/u_\infty = 1 - \xi$ were solved numerically and also by the use of these assumptions. The details are shown in reference 9; satisfactory agreement between the two sets of solutions was obtained.

By substituting for φ, as given by Eq. (16a), into Eq. (8),* using the expression (18) for a_1 in the right side of Eq. (8), and making use of assumptions (a) and (b), as well as of relations (20*a*), (20*b*), and (20*c*), Eq. (8) becomes the following linear differential equation in κ^2:

$$(\kappa^2)' + \frac{u_1'}{u_1}(J_1 - J_2 M_1^2)\kappa^2 = \frac{2}{F_1}\frac{u_\infty}{u_1}\left(\frac{T_1}{T_\infty}\right)^{(\gamma-2)/(\gamma-1)}\left[Cg + \frac{2}{1 + (Cg/6)}\right] \tag{21}$$

where F_1, J_1, and J_2 are constants given by

$$\left.\begin{aligned} F_1 &= 0.1143 + 0.00953\bar{a}_1 - 0.00397\bar{a}_1^2 \\ J_1 &= 4 + \frac{2}{F_1}\left(0.4\left(1 - \frac{1}{g}\right) + \frac{0.1}{g[1 + (C/6)]} + h\left\{\frac{0.4}{g} - \frac{1/6}{1 + (Cg/6)} - \frac{0.1}{g[1 + (C/6)]}\right\} - 0.05\bar{a}_1\right) \\ J_2 &= 2 - \left(\frac{\gamma - 1}{F_1}\right)\left(0.514 - \frac{0.4}{g} + \frac{0.1}{g[1 + (C/6)]} - 0.0405\bar{a}_1 - \right. \\ &\qquad \left. 0.00397\,\bar{a}_1^2 + h\left\{\frac{0.4}{g} - \frac{1/6}{1 + (Cg/6)} - \frac{0.1}{g[1 + (C/6)]}\right\}\right) \end{aligned}\right\} \tag{22}$$

An integrating factor I of Eq. (21) is, by the use of relations (20a) and (20b), found to be

$$I = (u_1/u_\infty)^{J_1}(T_1/T_\infty)^{J_2/(\gamma-1)}$$

The solution of Eq. (21), satisfying the condition of zero or finite† boundary-layer thickness at the leading edge ($\xi = 0$), is, then:

$$\kappa^2 = \frac{2}{F_1}\left[Cg + \frac{2}{1 + (Cg/6)}\right]\frac{\int_0^\xi (u_1/u_\infty)^{J_1-1}(T_1/T_\infty)^{(J_2+\gamma-1)/(\gamma-1)}\,d\xi}{(u_1/u_\infty)^{J_1}(T_1/T_\infty)^{J_2/(\gamma-1)}} \tag{23}$$

The distribution of the injection parameter φ required to maintain a uniform wall temperature will, according to Eq. (16a), be

$$\varphi(\xi) = Cg[(T_1/T_\infty)/\kappa] \tag{24}$$

where $\kappa(\xi)$ is given by Eq. (23). The magnitude of the required injection parameter φ is evidently proportional to

$$Cg(Cg + \{2/[1 + (Cg/6)]\})^{-1/2}$$

and thus will increase as (Cg) increases.

For a given velocity distribution $(u_1/u_\infty)(\xi)$ and a given ratio (h) of wall temperature to adiabatic equilibrium temperature,‡ the effect of Mach Number is given simply by the (T_1/T_∞) terms in Eqs. (23) and (24). From Eqs. (23) and (24) it follows that, whereas in the flow over a flat plate $(u_1/u_\infty = T_1/T_\infty = 1)$ the injection parameter $\varphi(\xi)$ required to maintain a uniform wall temperature ratio h will depend only on the parameter C and not on h itself, nor on the Mach Number M_∞, the required injection parameter in the case of flow with a pressure gradient will depend on the value of h (which appears in J_1 and J_2) and of M_∞, as well as on C.

In cases in which $\kappa = 0$ at the leading edge ($\xi = 0$), κ will increase with ξ, and $\varphi(\xi)$ according to Eq. (24) will then diminish along the wall from an infinite value at $\xi = 0$. Such is the case for flow over a flat plate or for supersonic flow over a thin sharp-edged airfoil. In the case of a blunt-nosed object in subsonic flow, however, the leading edge will be a stagnation point, and κ will then have a finite value there. In that case, Eq. (24), with application of L'Hôpital's Rule to Eq. (23), implies that

$$\varphi_{\xi=0} = (F_1 J_1/2)^{1/2}\frac{Cg}{\left[Cg + \frac{2}{1 + (Cg/6)}\right]^{1/2}}\left(\frac{T_1}{T_\infty}\right)_{\xi=0}^{\gamma/2(\gamma-1)}\left(\frac{u_1'}{u_\infty}\right)_{\xi=0}^{1/2} \tag{25}$$

Thus, for flow near a forward stagnation point, φ will be finite at the leading edge and will be proportional to the square root of the velocity gradient $(u_1/u_\infty)'$ there.

---

* The use of Eq. (16a) by means of this substitution actually simplifies Eq. (8) [and would also simplify Eq. (9)] considerably.

† In case $u_1/u_\infty = 0$ at $\xi = 0$.

‡ For a given ratio (T_0/T_∞) of wall temperature to *free-stream* temperature, a Mach Number effect will also appear in the value of h, since, for a given value of (T_0/T_∞), h diminishes with increasing Mach Number.

By means of Eqs. (23) and (24), the injection velocity distribution required to maintain a given uniform wall temperature ratio h with a given value of the coolant-temperature parameter C can be quickly calculated for any flow with a given velocity distribution $(u_1/u_\infty)(\xi)$ and given Mach Number M_∞. The calculations will involve, at most, numerical integration (e.g., Simpson's Rule). The present results can be used for the case of heat transfer with zero injection velocity by putting $C = 0$ in Eqs. (22) and (23) and by keeping h arbitrary.

A value of g in any given case can usually be obtained from leading-edge conditions. Thus, if $\kappa = \lambda = 0$ at the leading edge* while $u_1 \neq 0$ and u_1' is finite there, Eqs. (8), (9), and (16a) will be found to imply $g = 1$ there; this value may then be assumed for the entire flow (cf. reference 9). On the other hand, if the leading edge is a stagnation point, the value of g to be chosen is usually less than 1 and can be obtained in the manner shown in the first numerical example below.

The Nusselt Number Nu, which is a measure of the local rate of heat transfer at the wall, can be calculated by means of the expressions

$$Nu \equiv \frac{[k(\partial T/\partial y)]_0}{k_\infty(T_e - T_0)} = 2\left(\frac{T_1}{T_\infty}\right)_\kappa \frac{g}{[1 + (C/6)]} Re^{1/2} \quad (26)$$

From Eqs. (26) and (23) it will be found that an increase in the parameter C—i.e., an increase in the value of $(1 - h)/[h - (T_e/T_e)]$—causes a decrease in the Nusselt Number.

Eqs. (24) and (26) imply the following simple relation between the local Nusselt Number Nu (ξ) and the injection parameter φ (ξ) required to maintain a given uniform wall temperature:

$$Nu\ (\xi)\ Re^{-1/2}/\varphi\ (\xi) = 2/C[1 + (C/6)] \quad (27)$$

Eq. (27) states that, in general, the Nusselt Number at any station ξ will be proportional to the injection parameter there, the proportionality factor being a constant dependent only on the coolant-temperature parameter C. This relation will be valid for any Mach Number and any main-stream velocity distribution (u_1/u_∞) (ξ). Thus, the Nusselt Number distribution and the injection parameter distribution along the wall will, in general, be exactly similar if the wall temperature is uniform.

The local skin-friction coefficient C_f follows readily from the expressions

$$C_f \equiv \frac{(\mu\partial u/\partial y)_0}{\rho_\infty {u_\infty}^2} = \left(\frac{u_1}{u_\infty}\right)\left(\frac{T_1}{T_\infty}\right)\frac{a_1}{\kappa} Re^{-1/2} \quad (28)$$

where a_1 (ξ) is given by Eq. (18). Because of the κ^2 term in the numerator of a_1, it will be found that the value of the parameter C has a smaller effect on the value of C_f than on the value of Nu. On the other hand, for a fixed C, a decrease of the wall temperature ratio h will tend to lower the skin friction in a favorable pressure gradient $(u_1' > 0)$ but will have only a small effect on the Nusselt Number.

Velocity profiles can be calculated by means of Eq. (11) in conjunction with the transformation (7) to the physical (x, y) plane. The temperature field can be similarly obtained from Eqs. (10b) and (12).

Numerical Examples

Example (1) Flow Near a Stagnation Point.—The case $(u_1/u_\infty)(\xi) = m\xi$, where m is a positive constant, represents the flow in the immediate vicinity of a forward stagnation point, such as at the leading edge of a round-nosed object in subsonic flow. It may be of particular practical importance to analyze such a flow, since, thereby, leading-edge conditions for the subsonic flow over most blunt-nosed objects can be obtained. In particular, as will be illustrated by the second example, the value of g can thus be determined.

For $u_1/u_\infty = m\xi$, the change of variables

$$\xi_1 = m\xi, \quad \kappa_1 = \kappa m^{1/2}, \quad \lambda_1 = \lambda m^{1/2}, \quad \varphi_1 = \varphi m^{-1/2} \quad (29)$$

will leave Eqs. (8), (9), and (16a) unchanged, except that ξ is now replaced by ξ_1, κ by κ_1, λ by λ_1, and φ by φ_1. However, $u_1/u_\infty = \xi_1$ now, while the constant m no longer appears in the equations. For $u_1/u_\infty = \xi_1$ and $M_\infty = 0$, it can be easily verified that Eqs. (8), (9), and (16a), or Eq. (23) with $\bar{a}_1 = a_1$ and $\overline{a_1}^2 = a_1^2$, will be satisfied exactly by the simple type of solution κ, λ, and φ = constant. In this case, in fact, the following simultaneous algebraic equations in κ_1 and λ_1 result from Eqs. (8), (9), and (16a):

$$F_2{\kappa_1}^2 = Cg + a_1 \quad (30)$$

$$F_4{\lambda_1}^2 = [(1 - h)C] + b_1 \quad (31)$$

where F_2, F_4, a_1 (which contain the unknowns κ_1 and λ_1), and b_1 are given by Eqs. (17), (18), and (19).

Eqs. (30) and (31) can be solved numerically for given values of C and h. The values of φ are then calculated from Eq. (24). Solutions for κ_1, g, φ_1, and Nusselt Number are given in Figs. 1 and 2. From Eqs. (29) and (26) it is evident, as would also follow from Eq. (25), that φ and Nu are each proportional to $m^{1/2}$. Thus, the velocity gradient m plays an important role here.

Example (2) Flow over a Turbine Blade.—Fig. 3 represents, at least qualitatively, the velocity distribution $(u_1/u_\infty)(\xi)$ over the forward part of a turbine blade airfoil in subsonic flow. Both the pressure and suction sides of the airfoil are represented, and the length l is here taken to be the chord length of the blade profile. The dimensionless distance ξ is measured along the surface from the forward stagnation point. In this example, the value $M_\infty = 0$ will be assumed.

* Such will be the case, for example, if

$$u_1/u_\infty = c_0 + c_1\xi + c_2\xi^2 + \ldots (c_0 \neq 0).$$

For this example, Eq. (23) can be used. Since $M_\infty = 0$ here, $T_e = T_1 = T_\infty$. Let h ($\equiv T_0/T_e$) = $1/3$ and $T_e/T_1 = 0.2$; then, $C = 5.31$. A value for g can be obtained from conditions at the leading edge (stagnation point here) by noting that $(u_1/u_\infty)(\xi)$ behaves like $(m\xi)$ as $\xi \to 0$. Consequently, the results of the first example can be used. From Fig. 1, for $h = 1/3$ and $C = 5.31$, one finds $g = 0.81$, and this is the value that will be used here. From Figs. 1 and 2, one also finds $(\kappa)_{\xi=0} = 4.96m^{-1/2}$ and $(\varphi)_{\xi=0} = 0.86m^{1/2}$. Here the value of m, which is equal to $(u_1'/u_\infty)_{\xi=0}$, has been taken as 34.0 for the suction side and as 9.50 for the pressure side.* From Eqs. (22), with $\overline{a_1} = 1.95$ and $\overline{a_1^2} = 3.80$, it is found that $F_1 = 0.1178$ and $J_1 = 3.80$. These values can be used for both the suction and pressure sides, since at $\xi = 0$ they are independent of m. $\kappa^2(\xi)$ can now be obtained from Eq. (23) by numerical integration. Simpson's Rule was used for the present calculations, and the results for $\varphi(\xi)$ [$= Cg/\kappa(\xi)$] are shown in Fig. 4.

Conclusions

The main results of this analysis for a sweat-cooled surface with a uniform wall temperature in laminar compressible flow with a Prandtl Number of unity can be summarized as follows:

(1) For any given velocity distribution outside of the boundary layer and free-stream Mach Number, the normal injection velocity distribution of the coolant required to maintain a given uniform wall temperature can be readily calculated by means of the equations [Eqs. (23) and (24)] developed here. The Nusselt Number and the skin-friction coefficient can also be rapidly calculated by means of the equations derived here. The equations can, moreover, be used for the case of heat transfer with zero injection.

* In cases where actual accurate data for $(u_1/u_\infty)(\xi)$ are given, $(u_1'/u_\infty)_{\xi=0}$ can be evaluated by fitting a polynomial to several points near $\xi = 0$ and differentiating (cf., e.g., reference 10). It may be noted that, in applying Eq. (23), it is not only sufficient but actually convenient to have $(u_1/u_\infty)(\xi)$ given as a set of numerical values.

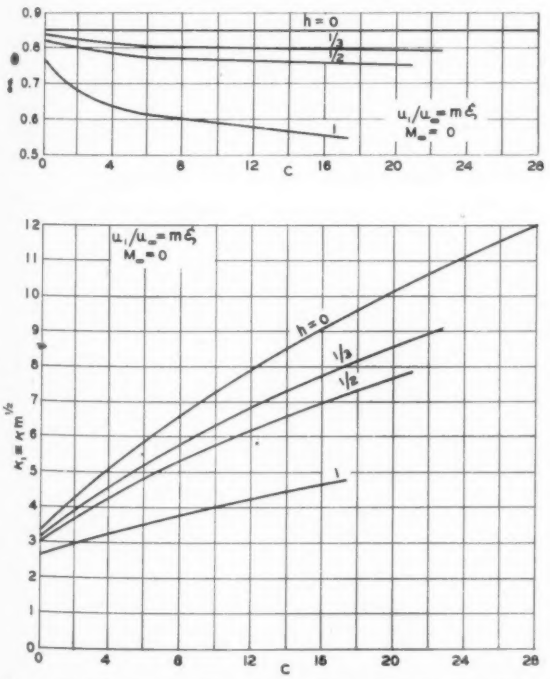

FIG. 1 VALUES OF κ_1 AND g VS C AND h FOR FLOW NEAR STAGNATION POINT

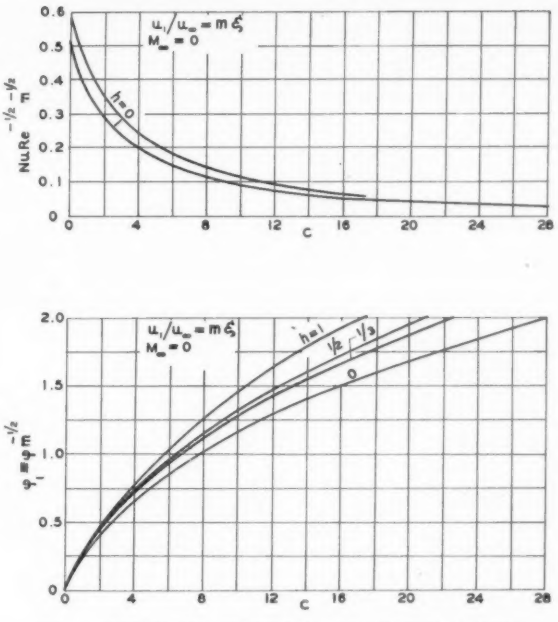

FIG. 2 VALUES OF INJECTION PARAMETER (φ) AND NUSSELT NUMBER (Nu) VS C AND h FOR FLOW NEAR STAGNATION POINT

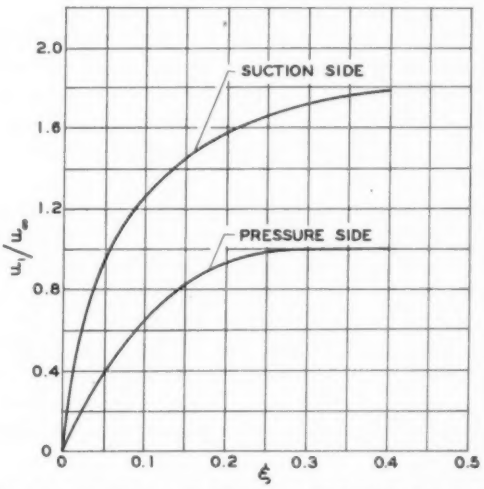

FIG. 3 TYPICAL VELOCITY DISTRIBUTION OF SUBSONIC FLOW OVER FORWARD PART OF A TURBINE BLADE

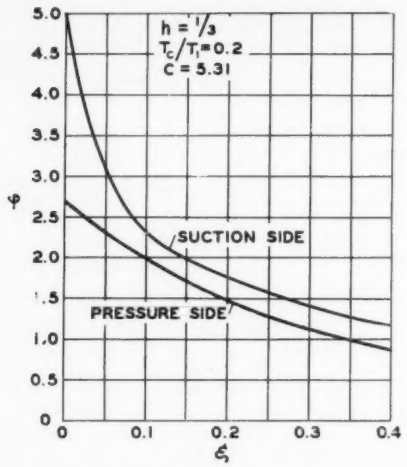

FIG. 4 INJECTION PARAMETER DISTRIBUTION REQUIRED TO MAINTAIN A UNIFORM WALL-TEMPERATURE RATIO h OF 1/3 FOR EXAMPLE OF FIG. 3

(2) For flow over a flat plate, the required normal injection velocity distribution depends only on a single parameter (C), which is a function of the ratio of the difference between the equilibrium wall temperature and the actual wall temperature to the difference between the actual wall temperature and the coolant temperature. For flow with an axial pressure gradient, however, the required injection velocity also depends on the ratio of actual wall temperature to adiabatic equilibrium temperature.

(3) A simple relation exists [Eq. (27)] between the local Nusselt Number distribution (Nu) and injection parameter distribution (φ) required for a uniform wall temperature. This relation, which is valid for any mainstream velocity distribution and any Mach Number, states that Nu is proportional to φ, the proportionality factor being a constant dependent only on the coolant-temperature parameter C. The distribution of the Nusselt Number along the wall will thus, in general, be exactly similar to the distribution of the required normal injection velocity.

(4) For objects in a flow with a forward stagnation point, the required injection parameter at that point will be proportional to the square root of the mainstream velocity gradient there.

(5) As the value of the coolant-temperature parameter C is increased, the required injection velocity is increased while the Nusselt Number is decreased. For a fixed value of C, decreasing the ratio (h) of wall temperature to equilibrium zero-heat-transfer, temperature will decrease the skin friction in a favorable pressure gradient but will have relatively little effect on the Nusselt Number.

References

[1] Fogarty, L. E., *The Laminar Boundary Layer on a Rotating Blade*, Journal of the Aeronautical Sciences, Vol. 18, No. 4, p. 247, April, 1951.

[2] Yuan, S. W., *A Theoretical Investigation of the Temperature Field in the Laminar Boundary Layer on a Porous Flat Plate with Fluid Injection*, Project Squid, Tech. Rep. No. 4, September 5, 1947.

[3] Yuan, S. W., *Heat Transfer in Laminar Compressible Boundary Layer on a Porous Flat Plate with Fluid Imjection*, Journal the of Aeronautical Sciences, Vol. 16, No. 12, p. 741, December, 1949.

[4] Klunker, E. B., and Ivey, H. Reese, *An Analysis of Supersonic Aerodynamic Heating with Continuous Fluid Injection*, N.A.C.A. T.N. No. 1987, December, 1949.

[5] Eckert, E. R. G., *Heat Transfer and Temperature Profiles in Laminar Boundary Layers on a Sweat-Cooled Wall*, A.A.F. Tech. Rep. 5646, Air Materiel Command, November, 1947.

[6] Schichting, H., and Bussmann, K., *Schriften der Deutschen Akademie der Luftfahrtforschung*, Vol. 7B, Nr. 2, 1943.

[7] Falkner, V. M., and Skan, S. W., *Some Approximate Solutions of the Boundary Layer Equations*, R. & M. No. 1314, British A.R.C., 1930.

[8] Kalikhman, L. E., *Heat Transmission in the Boundary Layer*, N.A.C.A. T.M. No. 1229, April, 1949.

[9] Morduchow, M., and Galowin, L., *On the Compressible Laminar Boundary Layer in an Axial Pressure Gradient over a Surface Cooled by Fluid Injection*, Project Squid Report, to be submitted for publication.

[10] Scarborough, J. B., *Numerical Mathematical Analysis*, 2nd Ed.; Johns Hopkins Press, 1950.

Readers' Forum

BRIEF REPORTS of investigations in the aeronautical sciences and discussions of papers published in the JOURNAL are presented in this special department. The publication will be completed as soon as possible after receipt of the material. The Editorial Committee does not hold itself responsible for the opinions expressed by the correspondents. Contributions should not exceed 800 words in length.

On the Lift and Circulation of Airfoils in Some Unsteady-Flow Problems

Nelson H. Kemp
Graduate School of Aeronautical Engineering, Cornell University, Ithaca, N.Y.
June 13, 1952

IN CONNECTION WITH SOME INVESTIGATIONS of unsteady flow in compressor cascades, it has been found useful to apply certain results of von Kármán and Sears[1, 2] and to extend these results in two directions—(1) to calculate the circulation of airfoils in sinusoidal motion and (2) to generalize Sears'[2] results for an airfoil flying through a sinusoidal gust in a manner described below.

(1) If an airfoil in two-dimensional incompressible flow is subjected to steady periodic variations of angle of attack or of vertical velocity, the "quasi-steady" circulation can be written as

$$\Gamma_0 = G_0 e^{i\nu t}$$

where G_0 is a constant and ν is the circular frequency. The "quasi-steady" circulation is that produced by the instantaneous motion of the airfoil relative to the air without regard to the effects of the wake of trailing vortices produced by the nonsteady motion and is calculated from ordinary thin-airfoil theory. Using the results of von Kármán and Sears[1] for this case, it is easy to show that the total circulation $\Gamma(t)$ is given by

$$\Gamma(t) = \Gamma_0 e^{-i\omega} S(\omega) \tag{1}$$

where

$$S(\omega) = 1/i\omega[K_0(i\omega) + K_1(i\omega)]$$

with the reduced frequency $\omega \equiv \nu c/2U$, c and U being the airfoil chord and forward speed, respectively. K_0 and K_1 are modified Bessel functions of the second kind.

Eq. (1) shows that $S(\omega)$ bears somewhat the same relation to the circulation as the well-known Theodorsen function bears to the lift. (It must, of course, be remembered that the Kutta-Joukowski relation between lift and circulation does not hold in unsteady motion.)

Now $S(\omega)$ has never been calculated, although it is useful for determination of the energy in the wake. In fact, it is easily shown that, if x is measured rearward from the center of the airfoil, then the jump in the velocity potential ϕ across the wake is given by

$$\phi_{top} - \phi_{bottom} = \Gamma_0 e^{-i\nu x/U} S(\omega)$$

However, Professor Sears has called my attention to an interesting reciprocal relationship; he showed[2] that the *lift* on an airfoil entering a sharp-edged gust is proportional to the *circulation* in the "Wagner problem"—that is, the total circulation due to a sudden unit change in the quasi-steady circulation. Now it is well known that the steady-state response of any linear system to an input of the form $e^{i\nu t}$ is found from the Laplace transform of its response to a unit step-function input by replacing the variable of the Laplace transform by $i\nu$, dividing by $i\nu$, and multiplying by the input function. Applying this rule to the above-mentioned reciprocal relationship, we immediately see that the *lift* due to an infinitely long sinusoidal gust must be proportional to the *circulation* of an airfoil in sinusoidal motion and, thus, proportional to $S(\omega)$.

The lift on an airfoil in such a sinusoidal gust was calculated by Sears[2] and found to be

$$L(t) = \pi\rho c U W e^{i\nu t}\left[\frac{J_0(\omega)K_1(i\omega) + iJ_1(\omega)K_0(i\omega)}{K_1(i\omega) + K_0(i\omega)}\right] \tag{2}$$

where W is the amplitude of the gust velocity, J_0 and J_1 are the usual Bessel functions, and ρ is the air density.

The following identities regarding Bessel functions can be deduced:*

$$K_0(i\omega) = -(\pi/2)i[J_0(\omega) - iY_0(\omega)]$$
$$K_1(i\omega) = -(\pi/2)[J_1(\omega) - iY_1(\omega)]$$

Thus,

$$J_0(\omega)K_1(i\omega) + iJ_1(\omega)K_0(i\omega) = (\pi/2)i[J_0(\omega)Y_1((\omega) - J_1(\omega)Y_0(\omega)]$$

But*

$$J_n(\omega)Y_{n+1}(\omega) - J_{n+1}(\omega)Y_n(\omega) = -(2/\pi\omega)$$

so that, finally, the expression in brackets in Eq. (2) is seen to be just $S(\omega)$, and

$$L(t) = \pi\rho c U W e^{i\nu t} S(\omega) \tag{3}$$

is the result we expected.

Sears[2] has plotted $S(\omega)$ in his Fig. 3, and $S_r(\omega)$ and $S_i(\omega)$, where $S(\omega) = S_r(\omega) + iS_i(\omega)$, is given in Table 1 of the present note.

(2) The result given in Eq. (3) is the lift due to a gust velocity of the form

$$v(x, t) = We^{i\nu[t - (x/U)]}$$

In connection with the effect of the wakes of stator blades on a rotor blade moving through them, it is necessary to calculate the lift due to a gust of the form

$$V(x, t) = We^{i\nu t} e^{-i\mu x/U}$$

with $\nu \neq \mu$. This is easily done by a generalization of the development given by Sears,[2] and the result is

$$L(t) = \pi\rho c U W e^{i\nu t} K(\omega, \lambda) \tag{4}$$

where $\lambda = \mu c/2U$, with

$$K(\omega, \lambda) = [J_0(\lambda) - iJ_1(\lambda)]C(\omega) + i(\omega/\lambda)J_1(\lambda) \tag{5}$$

Here, $C(\omega)$ is the Theodorsen function, defined as

$$C(\omega) = K_1(i\omega)/[K_0(i\omega) + K_1(i\omega)]$$

* See pages 78, 75, 73, and 77 of Reference 4.

TABLE 1

ω	S_r	S_i	ω	S_r	S_i
0	1.000	0	2.5	−0.048	0.247
0.02	0.963	−0.075	3.0	−0.145	0.178
0.04	0.924	−0.114	3.5	−0.197	0.081
0.06	0.887	−0.139	4.0	−0.198	−0.021
0.08	0.852	−0.154	4.5	−0.155	−0.106
0.10	0.821	−0.164	5.0	−0.081	−0.159
0.20	0.702	−0.160	6.0	+0.081	−0.141
0.30	0.624	−0.126	7.0	0.150	−0.008
0.40	0.568	−0.085	8.0	0.082	+0.114
0.50	0.525	−0.044	9.0	−0.049	0.124
0.60	0.488	−0.005	10.0	−0.124	0.002
0.70	0.456	+0.032	11.0	−0.084	−0.086
0.80	0.426	0.066	12.0	+0.026	−0.112
0.90	0.397	0.097	13.0	0.104	−0.037
1.0	0.369	0.126	14.0	0.084	+0.065
1.2	0.312	0.176	15.0	−0.009	0.103
1.4	0.255	0.215	∞	0	0
1.6	0.196	0.242			
1.8	0.138	0.260			
2.0	0.082	0.268			

While ν is a real number, it should be noted that μ (and therefore λ) can be an arbitrary complex number.

It is readily seen that $K(\omega, \omega) = S(\omega)$, so that Eq. (4) reduces to Eq. (3) if $\mu = \nu$. If, on the other hand, $\mu = 0$, $K(\omega, 0) = C(\omega) + (1/2)i\omega$, and the lift from Eq. (4) agrees with that given in Eq. (20) of Reference 1 (where $W = A_0U$, $c = 2$). Thus, $K(\omega, \lambda)$ is seen to be a generalized function, which connects the familiar Theodorsen function for oscillating airfoils with the Sears function for a sinusoidal gust.

The circulation in this case can be easily found using Eqs. (4), and (5), and (1). The result is

$$\Gamma = \pi cWe^{i\nu t}e^{-i\omega}[J_0(\lambda) - iJ_1(\lambda)]S(\omega)$$

The application of these results to the unsteady flow through a compressor stage will be published in the near future.

REFERENCES

[1] von Kármán, Th., and Sears, W. R., *Airfoil Theory for Non-Uniform Motion*, Journal of the Aeronautical Sciences, Vol. 5, No. 10, 1938.

[2] Sears, W. R., *Some Aspects of Non-Stationary Airfoil Theory and Its Practical Application*, Journal of the Aeronautical Sciences, Vol. 8, No. 3, 1941.

[3] Sears, W. R., *Operational Methods in the Theory of Airfoils in Non-Uniform Motion*, J. Franklin Institute, Vol. 230, No. 1, 1940.

[4] Watson, G. N., *Theory of Bessel Functions*, 2nd Ed.; The Macmillan Company, New York, 1945.

Note on Creep Buckling of Columns

George Gerard
College of Engineering, New York University, New York

June 30, 1952

IT APPEARS FROM LIBROVE'S INTERESTING ANALYSIS[1] that, for the case of creep buckling of columns, the initial imperfections contained in ordinary columns provide the mechanism by which failure due to creep occurs after a period of time. In fact, it can be concluded from this analysis that a theoretically perfect column that is initially loaded below the time-independent critical load will not buckle at all. This is an interesting contrast to the case of static buckling where small initial imperfections play an insignificant role, since the failing load of an initially imperfect column is substantially the same as that of a theoretically perfect column. It is of interest, therefore, to conjecture whether there is any possible mechanism by which a column containing no initial imperfections can fail as a result of creep when the initial load is less than the theoretical buckling load.

First, it is pertinent to consider a column of a viscoelastic material. Such a model demonstrates rather vividly the significance of initial imperfections in creep buckling. For a perfect column, the application of an infinitesimal lateral disturbance to determine the point where an exchange of equilibrium configurations occurs merely results in a temporary increase in stress on the concave side and decrease on the convex side of the column if the application and removal of the disturbance is instantaneous. Since the path of disturbance follows a line of slope E, the instantaneous bending rigidity is the same for all values of E in the time-dependent phase, and, consequently, creep buckling cannot occur.

For the imperfect column, a small amount of bending is present as a result of the initial loading. Consequently, in the time-dependent stage of deformation a stress reversal occurs, with an increase in lateral deflection of the column. After some time this deflection may become excessive, essentially constituting failure in a restricted sense.

Instead of considering a viscoelastic material, the creep law used by Libove appears to be more realistic for aircraft materials

$$\epsilon = (\sigma/E) + Ae^{B\sigma}t^k \tag{1}$$

If a mechanical equation of state concept is applied to the creep law used by Libove, Eq. (1), then a series of "stress-strain" curves under conditions of constant strain rate can be found. If the lateral disturbance is applied instantaneously, then the concave side would follow a loading path of slope E, and therefore the local bending stiffness would always have a value of E, thus precluding creep buckling for the theoretically perfect column. However, if it is now assumed that a lateral disturbance is applied at a strain rate corresponding to the local strain rate of the stress-strain curve, then the loading path on the concave side would follow the local tangent modulus and the bending stiffness would then be a function of the local tangent modulus. Since, with this assumption, the local bending stiffness would decrease with time, creep buckling would be possible after a "critical time."

The assumption that the lateral disturbance is applied at the local strain rate is based on the room temperature behavior associated with plastic buckling of a column. For such a column there is an implicit assumption that the loading on the convex side follows the stress-strain curve pertinent to the strain rate at which the axial loading is applied. If this assumption were not implied but, instead, an instantaneous lateral disturbance were assumed, then at room temperature, as well as at elevated temperature, the local bending stiffness would have a value of E and buckling would not occur. Thus the assumption concerning the strain rate of the disturbance appears to have a somewhat realistic basis.

With use of this assumption, the solution for creep buckling of a theoretically perfect H-section column reduces to determining the "critical time" at which the following equilibrium equation is satisfied

$$E_r(t)I(d^2w/dx^2) + \bar{\sigma}Aw = 0 \tag{2}$$

In this case $\bar{\sigma}$ is the applied stress and is constant, and the lateral disturbance produces a deflection w essentially independent of time t. Hence, when $E_r(t)$ has reduced sufficiently to satisfy Eq. (2), the critical time is reached. The solution of Eq. (2) is the usual column equation

$$\bar{\sigma} = \pi^2E_r(t)/(L'/\rho)^2 \tag{3}$$

Since the average stress $\bar{\sigma}$ is held constant, the buckling process must occur with a strain reversal, and therefore the correct value of the effective modulus is the reduced modulus, E_r. With this suggested mechanism, a finite critical time is predicted for creep buckling of a theoretically perfect column.

REFERENCE

[1] Libove, C., *Creep Buckling of Columns*, Journal of the Aeronautical Sciences, Vol. 19, No. 7, p. 459, July, 1952.

Transonic Flow Past a Wedge with Detached Shock Wave

A. H. Armstrong, M. Holt, and C. K. Thornhill
Armament Research Establishment, Fort Halstead, Kent, England
May 6, 1952

RECENT PAPERS BY GUDERLEY AND YOSHIHARA[1] and by Vincenti and Wagoner[2] present approximate treatments of transonic flow past a finite wedge (Fig. 1), using Tricomi's equation. In both cases treated ($M = 1$ and $M > 1$, respectively), consideration is restricted to wedges such that flow downstream of the shoulder does not influence the subsonic region of flow upstream of the sonic line CF so that a Tricomi-Frankl[3] boundary-value problem can be formulated. In this note the condition is determined for this to be true.

The condition clearly depends on the extent of the expansion at the shoulder. Provided $\phi \leq (1/2)(\theta + \alpha)$, then, in the hodograph plane (Fig. 2), the backward characteristic CD defining the centered wave at the shoulder, will extend far enough to meet the forward characteristic through F at some point G; FG will, in fact, then be one of the forward characteristics of the centered wave. A Tricomi-Frankl boundary-value problem can then be formulated in the hodograph plane, bounded by FABCG.

If, however, $\phi > (1/2)(\theta + \alpha)$, the forward characteristic through F begins on the wedge surface downstream of the shoulder and the last forward characteristic of the centered wave is DE. In this case the boundary FABCD is not complete, and, to render the problem determinate, the conditions on the portion of the sonic line EF must be known. These are evidently determined by the wedge contour downstream of the shoulder.

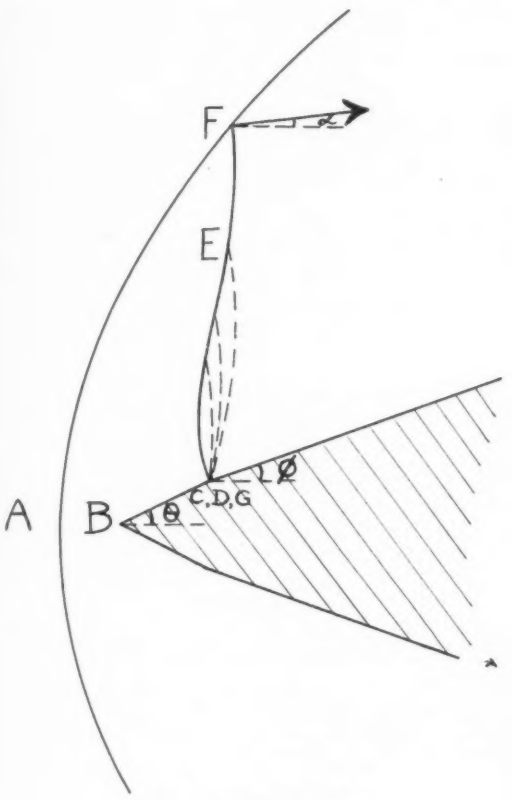

FIG. 1. Physical plane.

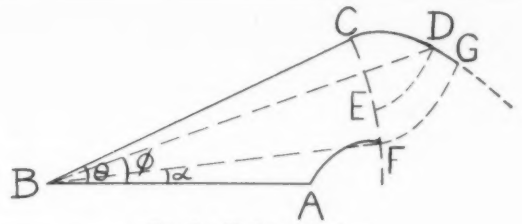

FIG. 2. Hodograph plane.

Acknowledgment is made to the Chief Scientist, Ministry of Supply, for permission to publish this note.

REFERENCES

[1] Guderley, G., and Yoshihara, H., Journal of the Aeronautical Sciences, Vol. 17, No. 11, November, 1950.
[2] Vincenti, W. G., and Wagoner, C. B., N.A.C.A. T.N. Nos. 2339 and 2588, December, 1951.
[3] Frankl, F., N.A.C.A. T.M. No. 1155, June, 1947.

Remarks on "An Analytical Approach to the Fuel Sloshing and Buffeting Problems of Aircraft"

M. Z. Krzywoblocki
Professor of Gas Dynamics and Theoretical Aerodynamics, Department of Aeronautical Engineering, University of Illinois, Urbana, Ill.
June 15, 1952

THE AUTHORS OF THE PAPER (see reference 1) wrote, on page 227: "Some new ideas on buffeting were recently reported by Liepmann." And next: "The central points in Liepmann's suggestions are that (1) the wake of a stalled body is turbulent and is described mathematically by mean values. . . ." The writer takes the liberty to mention that the idea of a turbulent wake is probably as old as the concept of Bénard-Kármán vortex street. Previous investigations were concerned mainly with the measurements of characteristic dimensions and frequencies of a Bénard-Kármán vortex street, as well as with the stability of its configuration. But here and there one may trace some indications that Bénard-Kármán vortex street is in some relation to a turbulent wake. In the Fage and Johansen experiments,[2] the variations of the spacing ratio in the wake was thoroughly investigated. In a Bénard-Kármán vortex range, the fluctuations have definite frequencies. Further downstream, the existing vorticity appears as "isotropic turbulence" (see references 3 and 4) "in which discreet vortex frequencies cannot be detected but a more or less continuous spectrum of eddy frequencies of much smaller scale and intensity than the Bénard-Kármán vortexes exists."[4] An analysis by Hooker[5] attributes the downstream variation in the spacing ratio principally to the viscosity. The change in the configuration of the wake in the vicinity of the critical Reynolds Number from a distinct periodic motion to a motion in which definite periods are lacking (i.e., random motion, remark of the writer of the present note) was discussed by Goldstein (*Modern Developments in Fluid Dynamics*, 1938) and others.[6] But for a certain length of the wake with no distinct Bénard-Kármán vortex street, the frequencies of the most prominent disturbances in the wake could be recorded. Krzywoblocki,[6] following the opinion that to obtain a better review of this phenomenon one has to look for a solution in the theory of turbulence, applied certain results of Schlichting's calculations of the flow in the boundary layer along a flat plate (1935) and obtained the values of the Strouhal Number in the turbulent wake which agree with the

results cited previously by Goldstein (Vol. II, p. 419, Fig. 149). The idea of Professor Liepmann to apply some results of the theory of isotropic turbulence to buffeting calculations seems to be interesting, but for the time being, at least, it is not known exactly how far behind a body the turbulence in the wake is fully isotropic. It seems that the transition from a distinct Bénard-Kármán vortex street to an isotropic turbulence is a gradual one. This would mean that in the turbulent part of the wake between the Bénard-Kármán vortex street and fully developed isotropic turbulence there are some recordable frequencies of the most prominent disturbances signalized by Goldstein and others long ago. It may be that the wake in its entire length is a Kolmogoroff's system of locally isotropic turbulence.

The recent investigations and hypotheses of the structure of a turbulent wake with no distinct vortices by Townsend, Kovasznay, and Batchelor seem to be of great interest to both theoreticians and designers.

References

[1] Luskin, Harold, and Lapin, Ellis, *An Analytical Approach to the Fuel Sloshing and Buffeting Problems of Aircraft*, Journal of the Aeronautical Sciences, Vol. 19, No. 4, pp. 217–228, April, 1952.

[2] Fage and Johansen, Proc. Roy. Soc. London, A, 116, pp. 170–197, 1927.

[3] Dryden, Hugh L., Journal of the Aeronautical Sciences, Vol. 3, No. 3, p. 173, 1936.

[4] Spivack, Journal of the Aeronautical Sciences, Vol. 13, No. 6, p. 289, 1946.

[5] Hooker, Proc. Roy. Soc. London, A, 154, p. 67, 1938.

[6] Krzywoblocki, Journal of the Aeronautical Sciences, Vol. 12, No. 1, p. 51, 1945.

Supersonic Nozzles with Continuous Wall Curvature

R. C. Frost and H. P. Liepman

Aerodynamic Engineer, Consolidated Vultee Aircraft Corporation, Fort Worth, Tex., and Director, Supersonic Wind Tunnel, Engineering Research Institute, University of Michigan, respectively

June 15, 1952

CROWN[1] DEVELOPED A METHOD for designing a perfect fluid nozzle with continuous wall curvature, since the elastic contour of a flexible wall nozzle will admit only this type of curvature. His analysis further assumes that the point of inflection at the wall lies on the "patching" Mach line, which divides the region of curved intersecting characteristics from the simple wave region with straight nonintersecting characteristics.

The requirements of continuous wall curvature can also be shown to exist on the basis of a physically desirable Mach Number distribution along the centerline of the nozzle. In this case, however, the point of inflection must be upstream of the end point of the patching Mach line.

The existence of this requirement was discovered in 1950 by Frost, then a Research Assistant at the Engineering Research Institute, during the design of a Mach 2.5 nozzle for the 8- by 13-in. supersonic wind tunnel of the University of Michigan.[2] In this design the Nilson method[3] was modified to eliminate discontinuities in the first derivative of the assumed Mach Number distribution along the nozzle centerline. Evvard and Marcus, of the N.A.C.A., have recently given the same relations between continuous wall curvature, axial Mach Number gradient, and location of inflection point with respect to patching Mach line.[4]

Since the discussion of reference 2 has not been published and is based on physical reasoning instead of on equations as done by Evvard and Marcus, an abbreviated version may be of interest.

The nozzle contour shown in Fig. 1 was calculated from an assumed Mach Number distribution along the centerline. A sinusoidal distribution was chosen to assure continuity of dM/dx along the nozzle with a final value of $dM/dx = 0$ at point P' (Fig. 1). It was reasoned that, if the nozzle were designed for continuous changes in flow, its actual performance would be least affected by manufacturing errors and variations in stagnation conditions.

Referring to Fig. 1, the flow in the nozzle can be discussed in terms of the strength of the two families of characteristics, the strength of a characteristic being proportional to the change of expansion angle or Mach Number. Since dM/dx is made to go to zero at point P' continuously, the strength of the reflected or right running family of characteristics R must do the same. In the initial portion of the nozzle starting at point T', dM/dx is nearly constant, and thus the strength of the incident or left running characteristics L must be nearly constant there and subsequently decrease continuously to zero also at point P'.

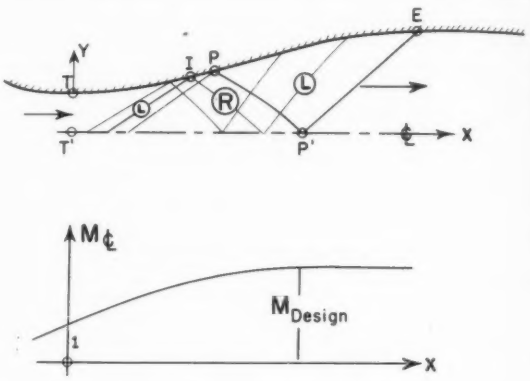

Figure 1. Typical Characteristics and Mach Number Distribution on Nozzle Center Line.

Along the wall, between points T and P, the change in slope of the contour—i.e., the curvature—is proportional to the difference in strength between reflected and incident characteristics, since the flow must be tangent to the wall. To provide the required expansion, the slope of the contour increases downstream of T and, hence, the strength of family R must be greater than that of family L. Since the strength of family R is continuously decreasing, it will be equal to the strength of family L at some point I, the point of inflection, where the curvature is zero. Downstream of this point I, the strength of family R continues to decrease smoothly until it is zero at the patching Mach line, point P.

Downstream of the patching Mach line, the contour between points P and E is entirely determined by the continuously decreasing strength of family L which vanishes at E, thus ensuring continuous curvature at E also.

Thus, since all changes in slope of the wall contour between points T and E have been accomplished continuously, the curvature is continuous along the wall, and it has been shown that the point of inflection must be upstream of the patching Mach line.

References

[1] Crown, J. C., *Design of Nozzles Having Continuous Wall Curvature*, Readers' Forum, Journal of the Aeronautical Sciences, Vol. 19, No. 5, p. 358, May, 1952.

[2] Frost, R. C., *Nozzle Design Considerations*, University of Michigan, Supersonic Wind Tunnel Report WTM-188 (unpublished) October, 1950.

[3] Nilson, E., *Design of an Inlet for a Two-Dimensional Supersonic Nozzle*, Meteor Report UAC-13, December, 1947.

[4] Evvard, J. C., and Marcus, L. E., *Achievement of Continuous Wall Curvature in Design of Two-Dimensional Symmetric Supersonic Nozzles*, N.A.C.A. T.N. No. 2616, January, 1952.

Direct Measurement of Supersonic Skin Friction

Donald Coles
Research Engineer, Jet Propulsion Laboratory, California Institute of Technology, Pasadena, Calif.
July 2, 1952

RECENT EXPERIMENTS AT THE Jet Propulsion Laboratory have established the effect of compressibility on local skin friction for Mach Numbers up to 4.5. Friction coefficients were obtained simultaneously at three stations on a flat plate, for both laminar and turbulent boundary-layer flow, for Reynolds Numbers from 4×10^5 to 1×10^7. The floating element technique used is similar to that of Liepmann and Dhawan.[1]

Figs. 1 and 2 show typical measurements with a clean leading edge and with a tripping device. The Reynolds Numbers in the figures are based on the distance from the leading edge and on the free-stream velocity and kinematic viscosity. No corrections for local pressure gradient or Mach Number variation have been made.

Fig. 3 shows the dependence of turbulent local friction on Mach Number at a Reynolds Number of 8×10^6. It is believed that these data will remain substantially unchanged by any corrections to be applied during the analysis of the experiments.

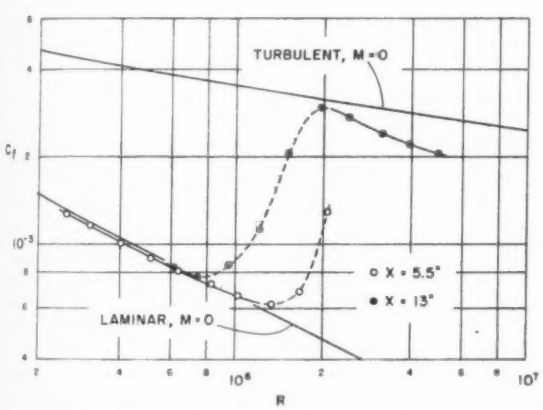

FIG. 1. Local friction on a smooth flat plate at a Mach Number of 2.6; no tripping device.

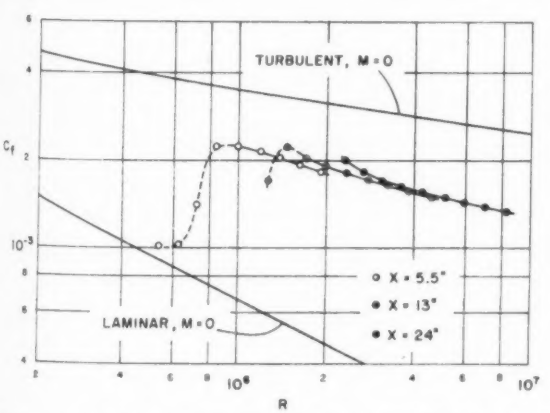

FIG. 2. Local friction on a smooth flat plate at a Mach Number of 3.7 with tripping device.

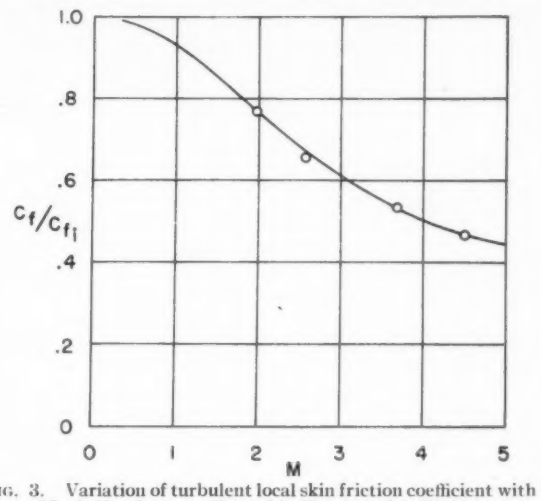

FIG. 3. Variation of turbulent local skin friction coefficient with Mach Number at a Reynolds Number of 8,000,000.

The boundary-layer research summarized here was discussed in detail at the Annual Summer Meeting of the Institute of the Aeronautical Sciences in Los Angeles in July, 1952.

REFERENCE

[1] Liepmann, H., and Dhawan, S., *Direct Measurements of Local Skin Friction in Low-Speed and High-Speed Flow*, Proc., 1st U. S. National Congress of Applied Mechanics, Illinois Institute of Technology, 1951; see also Dhawan, S., *Direct Measurements of Skin Friction*, N.A.C.A. T.N. No. 2567, January, 1952.

On Theodorsen Function in Incompressible Flow and C-Function in Supersonic Flow

Chieh-Chien Chang
Research Contract Director, The Johns Hopkins University, and Consultant, Air Research and Development Command, U.S.A.F.
June 6, 1952

FOUR INTERESTING PAPERS[1-4] in the Reader's Forum of the March JOURNAL discuss the validity of generalizing the Theodorsen function to the stable airfoil oscillation. To readers not too familiar with flutter problems, it should be emphasized that these discussions are not on the validity of the original Theodorsen[5] function. The current confusion lies entirely in the extension of the Theodorsen function to stable oscillations.

In the notation of reference 1, $k = k_0 + ik_1$ (where k_0 is real, positive and k_1 is real). The references[1-4] take $k_1 \lessgtr 0$, respectively for unstable, harmonic, and stable oscillations. A sketch shows airfoils in flight at constant velocity $-V$, leaving wake vortex sheets corresponding to the three cases, $k_1 \lessgtr 0$. It is assumed that all the airfoils started from *rest* at past time $-s/V$ and produced wakes of equal finite length s. Observe that the maximum magnitude of vortex strength $U(s)$* in the wake sheet exponentially decreases with s for $k_1 < 0$, is constant for $k_1 = 0$, and exponentially increases with s for $k_1 > 0$. The limit of case (b) as $s \to \infty$ is the Theodorsen function $c(k)$. Actually,

$$c(k) = \int_1^\infty \frac{s}{\sqrt{s^2 - 1}} e^{iks}\, ds \Big/ \int_1^\infty \frac{s+1}{\sqrt{s^2 - 1}} e^{iks}\, ds$$

* The author is fully aware that for a finite wake the vortex strength also depends on the time. $U(s)$ is purely for demonstration.

which is neither finite nor unique in value unless we first impose $k_1 < 0$ and then let $k_1 \to 0$. From the sketch for $k_1 > 0$ (bottom, Fig. 1), it is obvious that the maximum magnitude of $U(s)$ goes to infinity exponentially as $s \to \infty$. From the physical point of view, it is not surprising that $c(k)$ is divergent for $k_1 > 0$ as pointed out,[1-3] because the vortex strengths at the extremely large values of s contribute more to the value of the integral.

Furthermore, the Theodorsen function generalized to the stable airfoil oscillation has no physical reality. The primary aim of flutter analysis is to determine the critical frequency at which airfoil oscillations occur. The theory was developed for vanishingly small oscillations. To apply the generalized Theodorsen function to calculate the aerodynamic behavior of an airfoil, a few limitations must be considered.

(a) The amplitude of the airfoil oscillation present or past as shown in the wake vortex strength must be small in order to satisfy the original assumption of Theodorsen.

(b) In incompressible flow, time derivatives do not enter into the differential equation. However, the transient effect appears in the vortex and source strengths determined from the boundary conditions. Judged in this sense, the vorticity shed by the oscillating airfoil during the whole past history of flight will influence the present flow. Since the viscosity in the fluid takes time to dissipate the kinetic energy into heat energy, the vortex strength in the wake must deteriorate progressively with the past time interval or s. Even if exponentially increasing vorticity with s could be produced, the viscosity will dissipate all the vorticity at ∞ into heat in the infinite time interval.

It is impossible physically that vorticity produced a long time ago still maintains its strength and influences the flow now. The Theodorsen model of constant oscillation magnitude must deteriorate in wake vortex strength with s. This suggests that $k_1 < 0$ may be assumed to take care of the viscosity dissipation in the Theodorsen model. It is worth while to investigate what value of k_1 is equivalent to the viscosity dissipation. This also offers a physical justification for the method of evaluating $c(k)$.

A finite length wake has physical meaning in all three cases $k_1 \gtrless 0$, because the magnitude of $U(s)$ is always bounded. If the time interval is very small, the dissipation may be unimportant. Unfortunately, the Wagner function cannot be expressed in a closed form. R. T. Jones' approximation for the Wagner function should be applied cautiously and should be compared against exact solutions wherever possible.

In supersonic flow, the corresponding Wagner function has been found. By means of a convolution integral, the effects of the transient and quasi-steady harmonic oscillation have been found and expressed as incomplete and complete C-functions, respectively.[6] The incomplete C-function takes into account the transient effect of abrupt oscillation. It corresponds to van der Vooren's results of finite wake in incompressible flow. Recently, Miles[7] identified the complete C-function with the Schwartz function. Fortunately, the supersonic wake has no influence on the aerodynamic behavior of the airfoil, and, consequently, the viscosity dissipation in the wake negligibly influences the airfoil pressure. Thus the aerodynamic load is valid for any oscillation, stable ($k_1 > 0$) or unstable ($k_1 < 0$). Although only the case $k_1 = 0$ has been investigated,[6] the corresponding functions for $k_1 \neq 0$ can be deduced easily with the same principles.

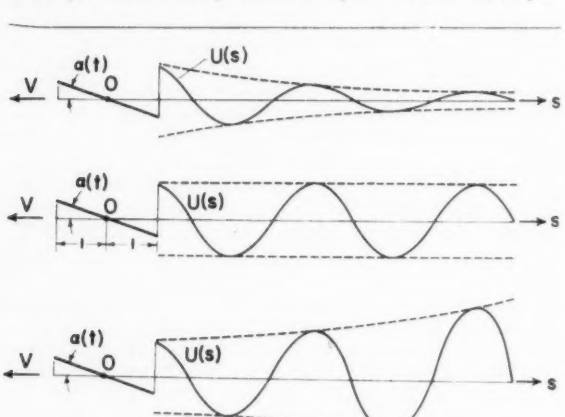

FIG. 1. (*Top*) Unstable oscillating airfoil, $k_1 < 0$. (*Center*) Harmonically oscillating airfoil, $k_1 = 0$ (Theodorsen's case, $s \to \infty$). (*Bottom*) Stable oscillating airfoil, $k_1 > 0$.

REFERENCES

[1] van der Vooren, A. I., *Generalization of the Theodorsen Function to Stable Oscillations*, Readers' Forum, Journal of the Aeronautical Sciences, Vol. 19, No. 3, pp. 209–211, March, 1952.

[2] Laitone, E. V., *Theodorsen's Circulation Function for Generalized Motion*, Readers' Forum, Journal of the Aeronautical Sciences, Vol. 19, No. 3, pp. 211–213, March, 1952.

[3] Jones, W. P., *The Generalized Theodorsen Function*, Readers' Forum, Journal of the Aeronautical Sciences, Vol. 19, No. 3, p. 213, March, 1952.

[4] Dengler, M. A., Goland, M., and Luke, Y. L., *Notes on the Calculation of the Response of Stable Aerodynamic Systems*, Readers' Forum, Journal of the Aeronautical Sciences, Vol. 19, No. 3, pp. 213–214, March, 1952.

[5] Theodorsen, Th., *General Theory of Aerodynamic Instability and the Mechanism of Flutter*, N.A.C.A. T.R. No. 496, 1935.

[6] Chang, Chieh-Chien, *Transient Aerodynamic Behavior of an Airfoil Due to Different Arbitrary Modes of Non-stationary Motion in a Supersonic Flow*, N.A.C.A. T.N. No. 2333, April, 1951.

[7] Miles, John W., *On Chang's Function for Nonstationary Flow*, Readers' Forum, Journal of the Aeronautical Sciences, Vol. 19, No. 2, p. 138, February, 1952.

Radii of Gyration of Aircraft

J. P. Chawla

Aerodynamics Department, Hughes Aircraft Company, Culver City, Calif.

June 9, 1952

MOMENTS OF INERTIA OF AIRPLANES are needed in the preliminary design stages of an aircraft in order to estimate dynamic loads on various components of its primary structure and to evaluate its dynamic stability characteristics. Various authors have put forth simple formulas for the radii of gyration of aircraft, about the body (or principal) axes through its center of gravity, expressed in terms of its overall dimensions of height, length, and span. These studies have invariably been from a statistical point of view, using data on airplanes built and successfully flown, and they have proved valuable to the preliminary design engineer. This note is intended to report significant results of an analysis recently made at Hughes Aircraft Company[1] in which the same basic approach was used.

Data on 101 airplanes, 73 of American design and 28 of British design, were analyzed. The airplanes were subdivided into four main functional categories—namely, (1) fighter, (2) bomber, (3) cargo transport, and (4) flying boat. Thirty-three of the airplanes analyzed were fighters, 22 bombers, 26 cargo transports, and 20 flying boats. The fighters range in design gross weight from 5,000 to 40,000 lbs.; the bombers, from 6,000 to 400,000 lbs.; the cargo transports, from 24,000 to 300,000 lbs.; and the flying boats, from 8,000 to 400,000 lbs.

Radii of gyration about the three axes were nondimensionalized in the following manner:

$$r_x = k_x/b, \quad r_y = k_y/L, \quad r_z = k_z/e$$

where k_x, k_y, and k_z are the radii of gyration in roll, pitch, and yaw, respectively; b is the span, L is the overall length, and e is the arithmetic mean of b and L—that is,

$$e = (1/2)(b + L)$$

The criterion used for obtaining a mean value for these nondimensional ratios was to find a number, M, which would give the greatest number of points in the band between $0.95M$ and $1.05M$. The results indicated that only unconventional designs may be expected to yield more than 10 per cent deviations from the mean.

Mean values of r_x, r_y, and r_z for each category are listed in Table 1. Mean values of r_z and r_z for flying boats are not included because of paucity of data. We note that values of r_y and r_z for different functional categories of aircraft lie in a narrow band, while the values of r_x extend over a wide range. A single mean value of $r_y = 0.165$ confirms a previous study[2] in which the airplanes were not subdivided into different categories.

TABLE 1

Mean Values of Nondimensional Radius of Gyration Ratios

Type of Aircraft	r_x	r_y	r_z
Fighter	0.120	0.165	0.200
Bomber	0.155	0.160	0.208
Cargo Transport	0.145	0.165	0.211
Flying Boat	...	0.165	...

A detailed analysis of the radii of gyration in roll showed that, with the mean values of r_x chosen for each category, 35 per cent of the airplanes analyzed gave a deviation of less than 5 per cent and 45 per cent gave a deviation of less than 10 per cent. This bears out the fact that the radius of gyration in roll varies considerably with the design of the airplane—in particular, the type and spanwise location of power plant, wing taper (both in plan and elevation), and the presence of tip pods, if any.

The selected mean values of r_y put 48 per cent of the airplanes in the 0 to ± 5 per cent band of deviation and 74 per cent in the 0 to ± 10 per cent band. It may be inferred that the value of $(k_y \div L)$ is fairly constant.

From analysis of the radii of gyration in yaw, it was found that 56 per cent of the airplanes had less than 5 per cent deviation and 83 per cent had less than 10 per cent deviation from the mean value. Constancy is again manifest in the value of the parameter (k_z/e).

In closing, it may be remarked that statistical studies have to be revised from time to time as design trends undergo significant changes.

REFERENCES

[1] Chawla, J. P., *Empirical Formulae for Radii of Gyration of Aircraft*, paper presented to the Society of Aeronautical Weight Engineers, Inc., at their Eleventh National Conference in Buffalo, N.Y., from May 5 to 8, 1952.

[2] Anon., *Empirical Formulae for Moments of Inertia of Aircraft*, Royal Aircraft Establishment, Structures Report No. 28, 1948.

On Folds Occurring in the Mapping from the Physical Plane to the Hodograph Plane

Keith C. Harder and E. B. Klunker
Langley Aeronautical Laboratory, N.A.C.A., Langley Field, Va.
June 20, 1952

IN THE QUALITATIVE study of two-dimensional transonic flow problems, it is often enlightening to consider sketches of the flow in the physical and hodograph planes simultaneously. Such considerations yield considerably more information than studies restricted to either plane alone. The starting point of such studies is usually the physical plane. One troublesome point in sketching the corresponding hodograph is locating the folds in the hodograph plane. The following rule has proved useful in this regard:

Rule.—A line in the physical plane, separating expansion and compression waves of the same family, corresponds to a fold in the hodograph plane.

Proof.—A characteristic ABC (see Fig. 1) in the physical plane maps into a unique line in the hodograph plane. Traversing this characteristic from A to C, at first only expansion waves are crossed, and the velocity increases until point B is reached. From point B to C, the velocity decreases, since only compression waves are crossed. Since we must stay on the same characteristic in the hodograph plane, part of this characteristic is covered twice in the hodograph plane. The locus of points in the hodograph plane (such as B), where we first start to retrace our path, is termed a fold. Such a retracing always occurs as we move from an expansion field to a compression field (or vice versa).

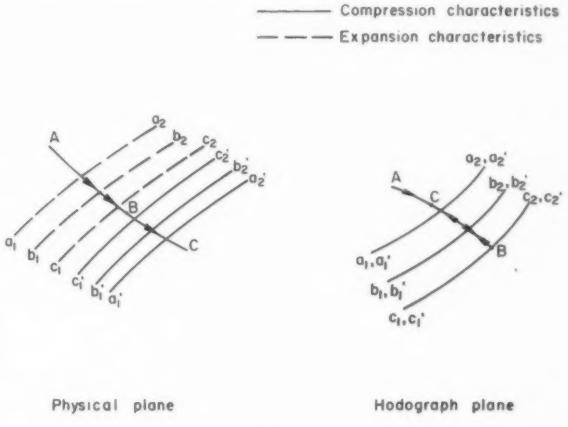

FIG. 1.

The rule gives the following information concerning the mapping of flows with shock waves:

(a) Flows with a shock wave in an expansion field will have one fold along the initial conditions of the shock and one along the final conditions.

(b) Flows with an expansion field immediately upstream of the shock followed by a compression field immediately downstream of the shock will have a fold along the initial conditions of the shock.

(c) Flows with a compression field immediately upstream of the shock followed by an expansion field immediately downstream of the shock will have a fold along the final conditions of the shock.

Determination of Modes and Frequencies Above the Fundamental by Matrix Iteration

P. Cicala
Professor of the Politecnico di Torino. Now at the E.S.A. and University of Cordoba, Cordoba, Argentina
July 2, 1952

MATRIX ITERATION PROCEDURES may be used to calculate the second mode and frequency if the dynamical matrix is postmultiplied by a factor eliminating the first mode component from input deformations. A general expression for this factor is here indicated, from which the sweeping matrix of references 1 and 2 is deduced as a particular case. It is shown that, in general, inaccuracies in the first modes markedly influence sub-

sequent results, the errors being magnified by factors containing the square ratios of higher to lower frequencies. By a particular matrix factor, sweeping out the first mode component from the rows of the dynamical matrix, the effects of first mode errors are considerably reduced.

These concepts lead to general formulas for the calculation of the rth mode which reduce the influence of the errors affecting the previously calculated $r-1$ lower frequency modes to second-order effects.

The dynamical equations for the free vibrations of a system with n degrees of freedom may be written in matrix form

$$D\{q\} = \lambda\{q\} \tag{1}$$

where D is the dynamical matrix, product of the flexibility influence matrix by the inertia matrix M; $\{q\}$ is the column of parameter amplitudes; and $\lambda = 1/\omega^2$ (ω = natural frequency). Let Q be the matrix of modal columns whose jth column $\{q_j\}$ is formed by the parameter values representing the jth mode, appropriate to the eigenvalue $\lambda = \lambda_j$. Let P be the transpose of MQ; its ith row $[p_i]$ is the characteristic row appropriate to λ_i. Let the modal values be normalized so that $PQ = I$, where I is the unit matrix of order n.

It can be shown that the matrix D may be expanded as follows:*

$$D = \sum_{k=1}^{n} \lambda_k\{q_k\}\{p_k\} \tag{2}$$

Any system of n values, in particular the column $\{q\}$, may be expanded in the series of normal modes; thus we write

$$\{q\} = Q\{A\} \tag{3}$$

The ith element A_i of the last column is the coefficient of the ith term in this modal expansion.

Iterative solution of Eq. (1) yields approximate values for the first mode which we denote by symbols with superposed bars; these are expressed as follows:

$$\{\bar{q}_1\} = Q\{\delta_i + e_1\} \tag{4}$$

$$[\bar{p}_1] = [\delta_1 + e_1]P \tag{5}$$

with $\delta_1 = 1$ for the first element and $\delta_i = 0$ elsewhere; the (small) coefficients in the column $\{e_1\}$ and its transposed $[e_1]$ represent in modal expansions the errors by which the calculated mode is affected. We denote by ϵ_1 the square root of the quantity $[e_1]\{e_1\}$.

According to Eqs. (3) and (5) we get

$$[\bar{p}_1]\{q\} = A_1 + s_1 \tag{6}$$

where $s_1 = [e_1]\{A\}$. We put

$$S = I - \{b\}[\bar{p}_1] \tag{7}$$

where $\{b\}$ is a column of arbitrary coefficients which may be expressed by

$$\{b\} = Q\{B\} \tag{8}$$

in terms of the new coefficients $B_1, \ldots, B_n$. Thus, from Eqs. (3), (6), (7), and (8), we obtain

$$S\{q\} = Q\{A'\} \tag{9}$$

The ith element of the column $\{A'\}$ is given by

$$A_i' = A_i - B_iA_1 - B_is_1 \tag{10}$$

If error terms are neglected and the following condition is satisfied

$$B_1 = [\bar{p}_1]\{b\} = 1 \tag{11}$$

then $A_1' = 0$—i.e., premultiplication by S sweeps out from the column $\{q\}$ the first component in the modal expansion. Therefore, if the matrix D in Eq. (1) is replaced by the product DS, the new equation gives, through iteration, the second mode, whatever the values of $B_2, \ldots, B_n$ are.

The above equations yield, for S, the expression of the sweeping matrix indicated in references 1 and 2 if we give zero values to all the coefficients b but one, which, according to Eq. (11), must be equated to the reciprocal of the corresponding $\bar{p}_1$ factor. In this case, B_i is represented by the ratio $p_i/\bar{p}_1$ at this same station.

In order to evidence the effects of errors in the first calculated mode, the asymptotic relations between the coefficients A, after infinite iteration cycles, are considered, neglecting terms of the order of ϵ_1^2. Denoting by ρ_2 the ratio of the values of A_2 in two successive steps of iteration, from Eqs. (2), (9), and (10), with $B_1 = 1$, we get

$$\rho_2/\lambda_2 = 1 + e_{12}B_2(\lambda_1 - \lambda_2)/\lambda_2 \tag{12}$$

where e_{12} is the second element in the row $[e_1]$. The error term is considerably magnified by the factor $(\lambda_1 - \lambda_2)/\lambda_2$; it affects the frequency calculation. This and similar errors appearing in the mode shape would be nullified if we could make $B_2 = \ldots = B_n = 0$. The best possible approach to this ideal condition is attained by taking $\{b\} = \{\bar{q}_1\}$ and, consequently,

$$DS = D - \lambda_1\{\bar{q}_1\}[\bar{p}_1] \tag{13}$$

having replaced $\lambda_1\{\bar{q}_1\}$ for $D\{\bar{q}_1\}$. Thus the error in Eq. (12) reduces to the order of ϵ_1^2.

In more general terms, for the calculation of the rth mode, after the preceding $r-1$ have been determined with certain error ϵ, we replace the matrix D by

$$D^{(r)} = D - \sum_{k=1}^{r-1} \lambda_k\{\bar{q}_k\}[\bar{p}_k] \tag{14}$$

With this matrix, the iteration process gives in the limit an rth mode $\{\bar{q}_r\}$ which contains errors of the order of ϵ^2 in the coefficient A_r. Consequently, from it the rth eigenvalue can be calculated exactly up to ϵ^2 terms. The calculated mode contains impurities of the order of ϵ; these can be eliminated by evaluating $\{q_r\}$ as follows:†

$$\{q_r\} = \{\bar{q}_r\} - \sum_{k=1}^{r-1} \frac{\lambda_k}{\lambda_k - \lambda_r}[\bar{p}_k]\{\bar{q}_r\}\{\bar{q}_k\} \tag{15}$$

If main interest is placed upon certain overtones, for other frequencies the iteration process can be less accurate and the correction by Eq. (15) can be omitted, since only squares of mode errors enter in subsequent calculations.

References

[1] Flomenhoft, H. I., *A Method for Determining Mode Shapes and Frequencies Above the Fundamental by Matrix Iteration*, Journal of Applied Mechanics, Vol. 17, No. 3, pp. 249–256, September, 1950.

[2] Scanlan, R. H., and Rosenbaum, R., *Introduction to the Study of Aircraft Vibration and Flutter*, p. 182; The Macmillan Company, New York, 1951.

* This equation shows an interesting analogy with the expansion for the kernel of the corresponding integral equation.

† If the modes are not normalized, the kth term of the summations in Eqs. (14) and (15) must be divided by $[\bar{p}_k]\{q_k\}$.